

Ethylene binding in mono- and binuclear Cu^I complexes with tetradentate pyridinophane ligands

Ayumu Karimata,^a Tatiana Gridneva,^a Pradnya H. Patil,^a Robert R. Fayzullin,^a Eugene Khaskin,^a Sébastien Lapointe,^a Alèria Garcia-Roca^a and Julia R. Khusnutdinova*^a

^aOkinawa Institute of Science and Technology Graduate University, Coordination Chemistry and Catalysis Unit, 1919-1 Tancha, Onna-son, Okinawa, Japan, 904-0495.

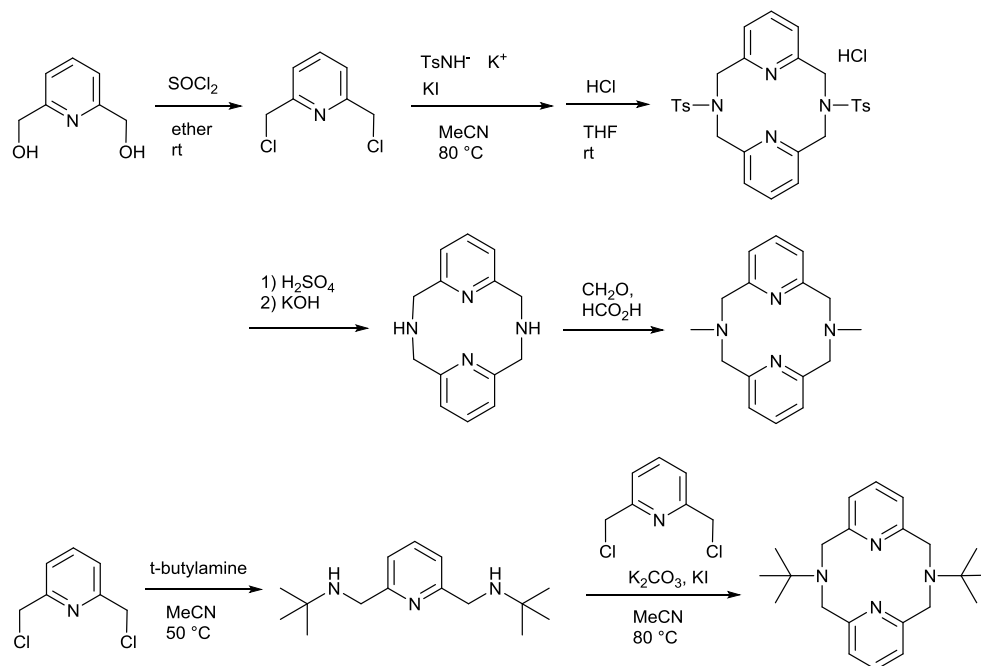
^bArbuzov Institute of Organic and Physical Chemistry, FCR Kazan Scientific Center, Russian Academy of Sciences, 8 Arbuzov Street, Kazan 420088, Russian Federation.

Email: juliak@oist.jp

Table of Contents

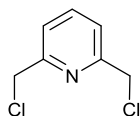
Synthesis and characterization of ligands and complexes	S3
2,6-Bis(chloromethyl)pyridine	S3
<i>N,N'</i>-ditosyl-2,11-diaza[3,3](2,6)pyridinophane hydrochloride salt (¹⁵N4*HCl)	S5
2,11-diaza[3,3](2,6)pyridinophane (¹N4)	S8
<i>N,N'</i>-dimethyl-2,11-diaza[3,3](2,6)pyridinophane (^{Me}N4)	S9
2,6-Bis[<i>t</i>-butylamino)methyl]pyridine	S11
<i>N,N'</i>-di-<i>t</i>-butyl-2,11-diaza[3,3](2,6)pyridinophane (^{Bu}N4)	S12
Synthesis of 2	S14
Characterization of 4	S18
Characterization of 5	S21
Characterization of 6	S25
Characterization of 7	S29
NMR spectra comparison before and after reaction with ethylene or MeCN	S30
NMR spectra of 1 and 3 in acetone-<i>d</i>₆ before and after bubbling ethylene	S30
NMR spectra of 1–3 in acetonitrile-<i>d</i>₃ before and after exposure to ethylene	S31
NMR spectra of 4–6 in acetonitrile-<i>d</i>₃	S32
NMR spectra of free ethylene	S32
NMR spectra of 4-6 in the presence of variable amounts of MeCN	S33
Cyclic voltammograms	S37
UV-vis spectra	S39
Photoluminescent properties	S40
Summary of representative reported mononuclear Cu–ethylene complexes	S42
X-ray structure determination details	S43
Computational details	S49
QTAIM analysis	S50
NBO analysis	S56
NBO analysis of Cu-ethylene binding in selected complexes with N-donor ligands reported in the literature	S67
References	S97

Synthesis and characterization of ligands and complexes



Scheme S1. Synthesis of ligands.

2,6-Bis(chloromethyl)pyridine



2,6-bis(chloromethyl)pyridine was synthesized following reported procedure with some modifications.¹ 2,6-pyridinedimethanol (28.0 g, 0.201 mol) and diethyl ether (200 mL) were added to a 500 mL round bottom flask equipped with a gas outlet adapter. The mixture was stirred and cooled down in ice water bath. The use of efficient magnetic stirring bar is important in the following steps. Thionyl chloride (32 mL) was added slowly using syringe over 3 min time period, then the reaction mixture was warmed up to room temperature slowly and stirred overnight. White precipitate was collected by filtration and washed with ether. The collected powder was added slowly to an aqueous solution of sodium hydroxide (8.00 g, 0.200 mol) in water (200 mL) in a 500 mL beaker while keeping low temperature using ice water bath and stirred for 10 min, then diethyl ether (200 mL) was added, and the reaction mixture was stirred further for 10 min. The aqueous layer was confirmed to be basic by pH paper, then separated and extracted with diethyl ether (ca. 50 mL \times 3). The all diethyl ether solutions were combined and dried over MgSO_4 , filtered off, then evaporated under reduced pressure to give a white powder (31.2 g, 88%).

2,6-bis(chloromethyl)pyridine: ^1H NMR (400 MHz, CDCl_3): 7.77 (t, $^3J_{\text{HH}} = 7.8$ Hz, $p\text{-H}_{\text{Py}}$, 1H), 7.44 (d, $^3J_{\text{HH}} = 7.8$ Hz, $m\text{-H}_{\text{Ts}}$, 2H), 4.67 (s, 4H, $-\text{CH}_2-$). $^{13}\text{C}\{^1\text{H}\}$ NMR (100MHz, CDCl_3): 156.5 ($o\text{-C}_{\text{Py}}$), 138.3 ($p\text{-C}_{\text{Py}}$), 122.2 ($m\text{-C}_{\text{Py}}$), 46.5 ($-\text{CH}_2-$).

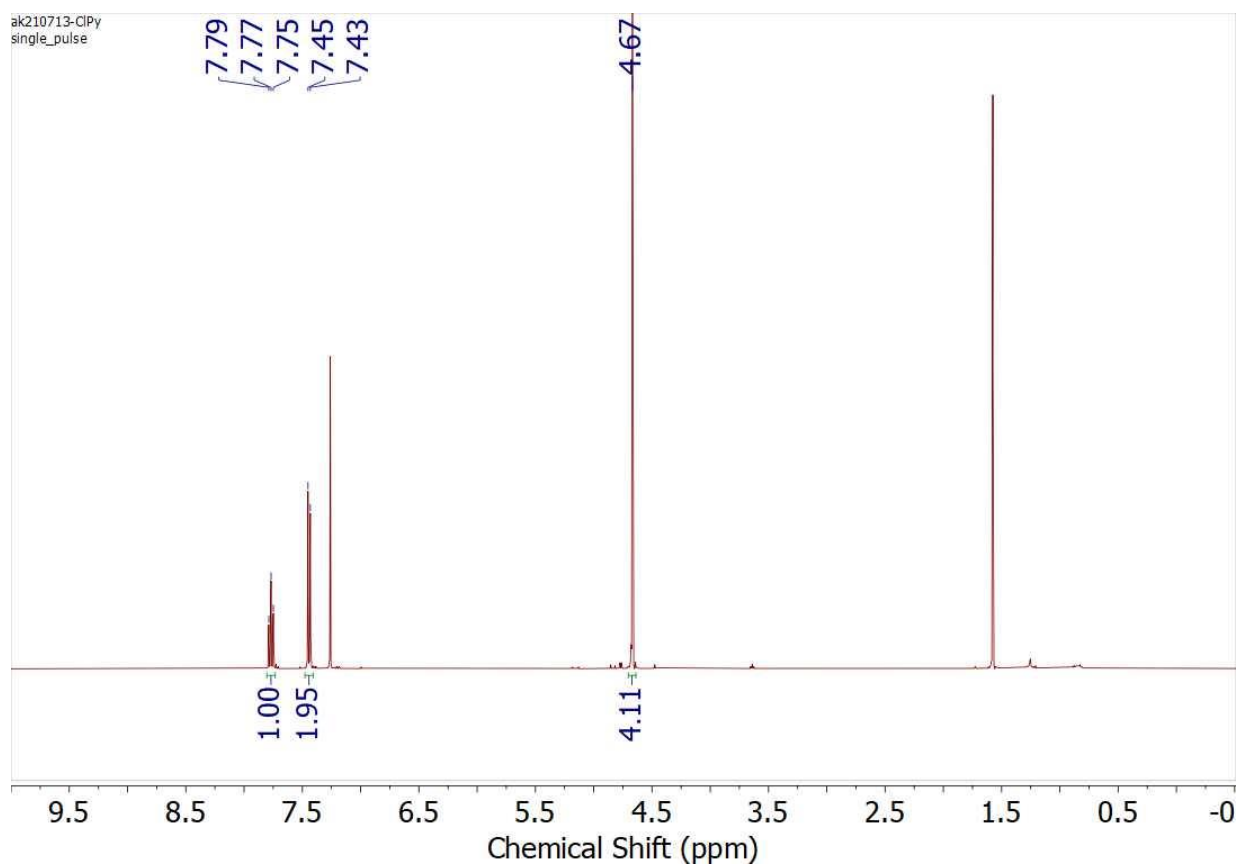


Figure S1. ^1H NMR spectrum of 2,6-bis(chloromethyl)pyridine in CDCl_3 .

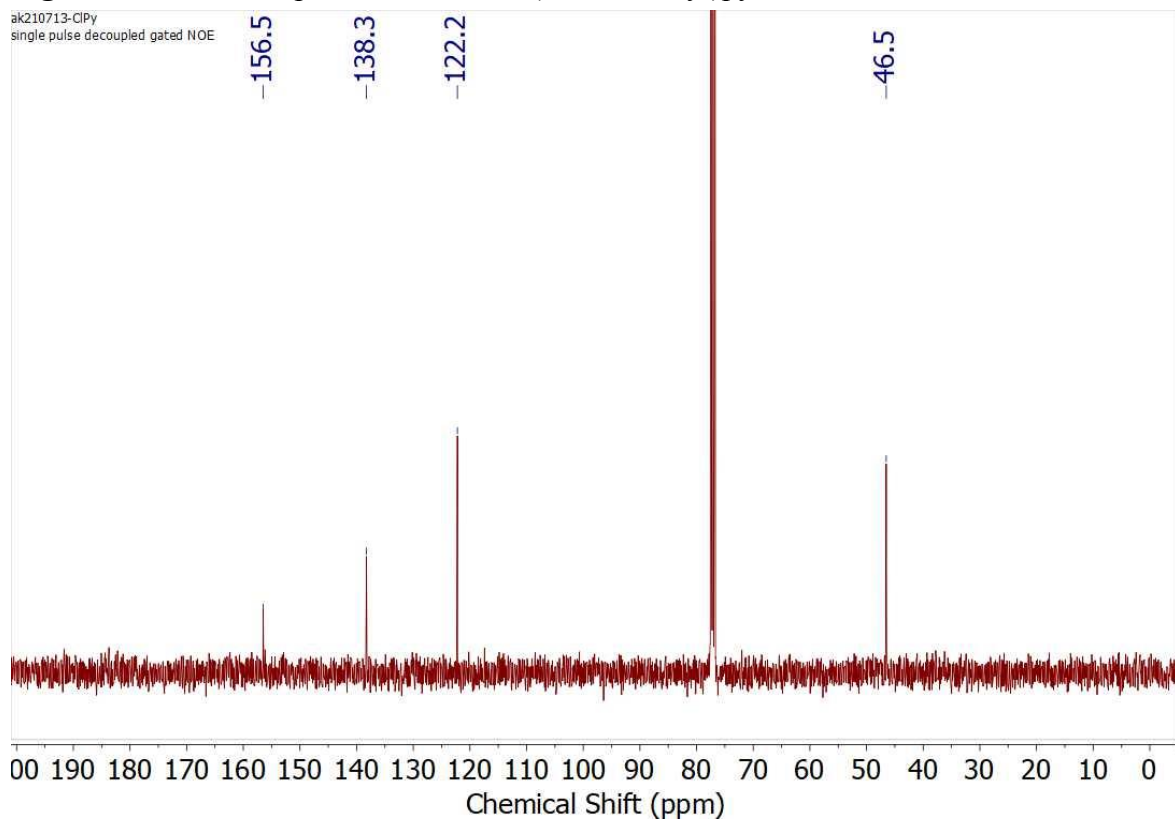
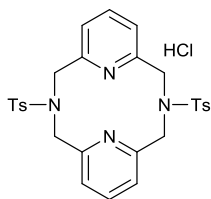


Figure S2. $^{13}\text{C}\{^1\text{H}\}$ NMR spectrum of 2,6-bis(chloromethyl)pyridine in CDCl_3 .

N,N'-ditosyl-2,11-diaza[3,3](2,6)pyridinophane hydrochloride salt (¹⁵N₄*HCl)



N,N'-ditosyl-2,11-diaza[3,3](2,6)pyridinophane hydrochloride salt was prepared by following reported procedure with some modifications.²⁻³

Potassium hydroxide (3.61 g, 64.3 mmol) was added to methanol (40 mL) in a 500 mL round flask and dissolved by stirring at room temperature. After addition of a powder of *p*-toluenesulfonamide (11.0 g, 64.2 mmol), the mixture was stirred for 10 min, then evaporated under reduced pressure in the 500 mL round flask to remove solvents. The obtained white powder was further dried under vacuum for 2 hours. Acetonitrile (320 mL), and potassium iodide (2.66 g, 16.0 mmol) were added to the mixture and stirred at room temperature, then warmed up to 80 °C. After addition of 2,6-bis(chloromethyl)pyridine (5.64 g, 32.0 mmol), the reaction mixture was stirred at 80 °C for 1 day. The reaction mixture was concentrated under reduced pressure, then methanol (40 mL) was added and stirred at 50 °C to dissolve byproducts for 30 min. After cooling down to room temperature, white precipitate was collected by filtration, washed with water (ca. 10 mL), then with methanol (ca. 5 mL). The collected white solid was added to THF (120 mL) and stirred at 60 °C to dissolve target product for 30 min. The hot mixture was filtered off to remove insoluble solid.

Due to difficulty in the further purification of the target product by crystallization and precipitation, the target product was protonated and precipitated, then further purified as follows. Hydrochloric acid [35%] (0.5 mL) was added slowly to the THF filtrate solution while stirring intensely. After stirring the mixture for 10 min, white solid was collected by filtration, washed with ether (ca. 10 mL), and dried under vacuum to give the target product of ¹⁵N₄ as a hydrochloric acid salt (2.26 g, 23%). The solution sample for NMR spectrum of ¹⁵N₄ was prepared by stirring a mixture of ¹⁵N₄ hydrochloric acid salt and potassium carbonate in CDCl₃ for 10 minutes.

(Use of sodium hydroxide and sodium iodide instead of potassium hydroxide and potassium iodide also gave similar product yield.)

¹⁵N₄ hydrochloric acid salt: ¹H NMR (400 MHz, DMSO-*d*₆): 8.28 (t, ³*J*_{HH} = 7.8 Hz, *p*-**H**_{Py}, 2H), 7.85 (d, ³*J*_{HH} = 8.2 Hz, *m*-**H**_{Ts}, 4H), 7.78 (d, ³*J*_{HH} = 7.8 Hz, *m*-**H**_{Py}, 4H), 7.48 (d, ³*J*_{HH} = 8.2 Hz, *o*-**H**_{Ts}, 4H), 4.94 (s, 8H, -**CH**₂-), 2.44 (s, 6H, **CH**₃). ¹³C {¹H} NMR (100MHz, DMSO-*d*₆): 155.8 (S-**C**-C), 144.5 (*o*-**C**_{Py}), 142.9 (*p*-**C**_{Py}), 133.9 (*p*-**C**_{Ts}), 130.2 (*o*-**C**_{Ts}), 127.6 (*m*-**C**_{Ts}), 122.7 (*m*-**C**_{Py}), 52.9 (-**CH**₂-), 21.1 (**CH**₃).

¹⁵N₄: ¹H NMR (400 MHz, CDCl₃): 7.78 (d, ³*J*_{HH} = 8.3 Hz, *o*-**H**_{Ts}, 4H), 7.37 (d, ³*J*_{HH} = 8.3 Hz, *m*-**H**_{Ts}, 4H), 7.32 (t, ³*J*_{HH} = 7.6 Hz, *p*-**H**_{Py}, 2H), 7.15 (d, ³*J*_{HH} = 7.6 Hz, *m*-**H**_{Py}, 4H), 4.46 (s, 8H, -**CH**₂-), 2.46 (s, 6H, **CH**₃). ¹³C {¹H} NMR (100 MHz, CDCl₃): 154.9 (S-**C**-C), 143.9 (*o*-**C**_{Py}), 137.4 (*p*-**C**_{Py}), 136.1 (*p*-**C**_{Ts}), 130.1 (*o*-**C**_{Ts}), 127.1 (*m*-**C**_{Ts}), 123.3 (*m*-**C**_{Py}), 56.7 (-**CH**₂-), 21.7 (**CH**₃).

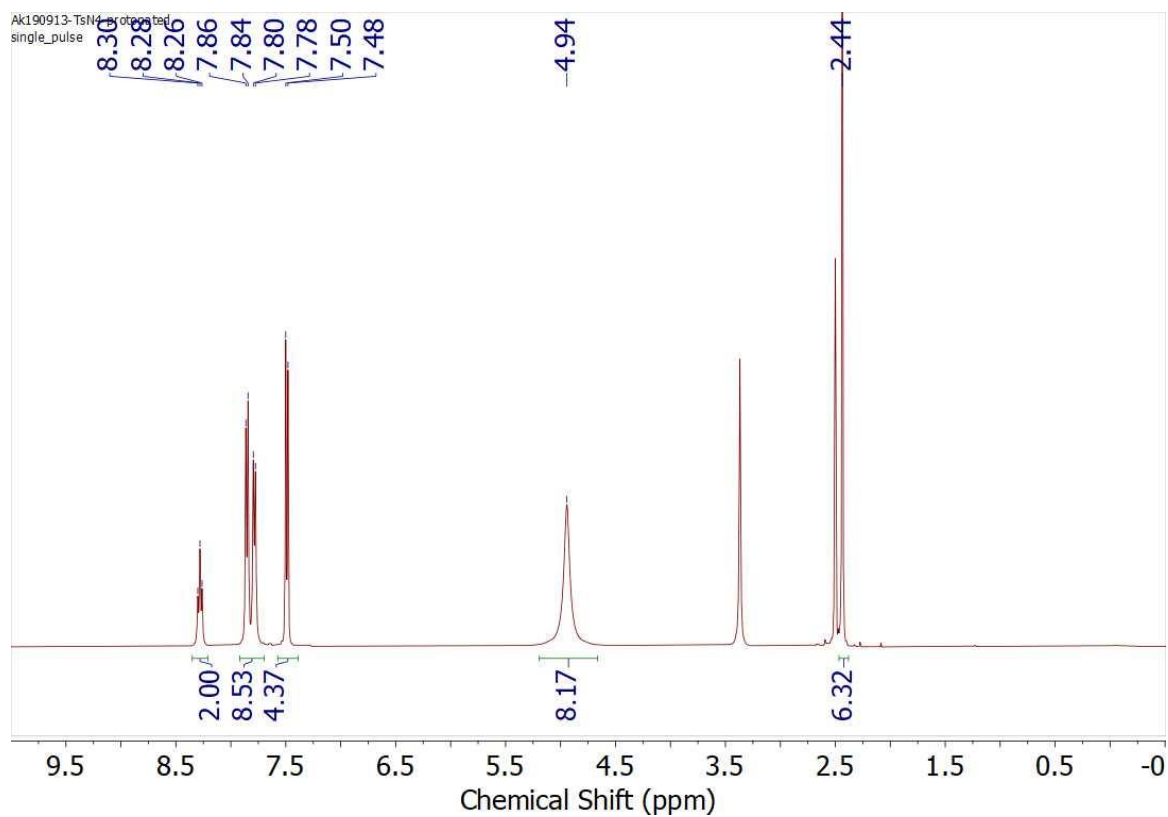


Figure S3. ^1H NMR spectrum of $\text{TsN4}\cdot\text{HCl}$ in $\text{DMSO-}d_6$ at RT (400 MHz).

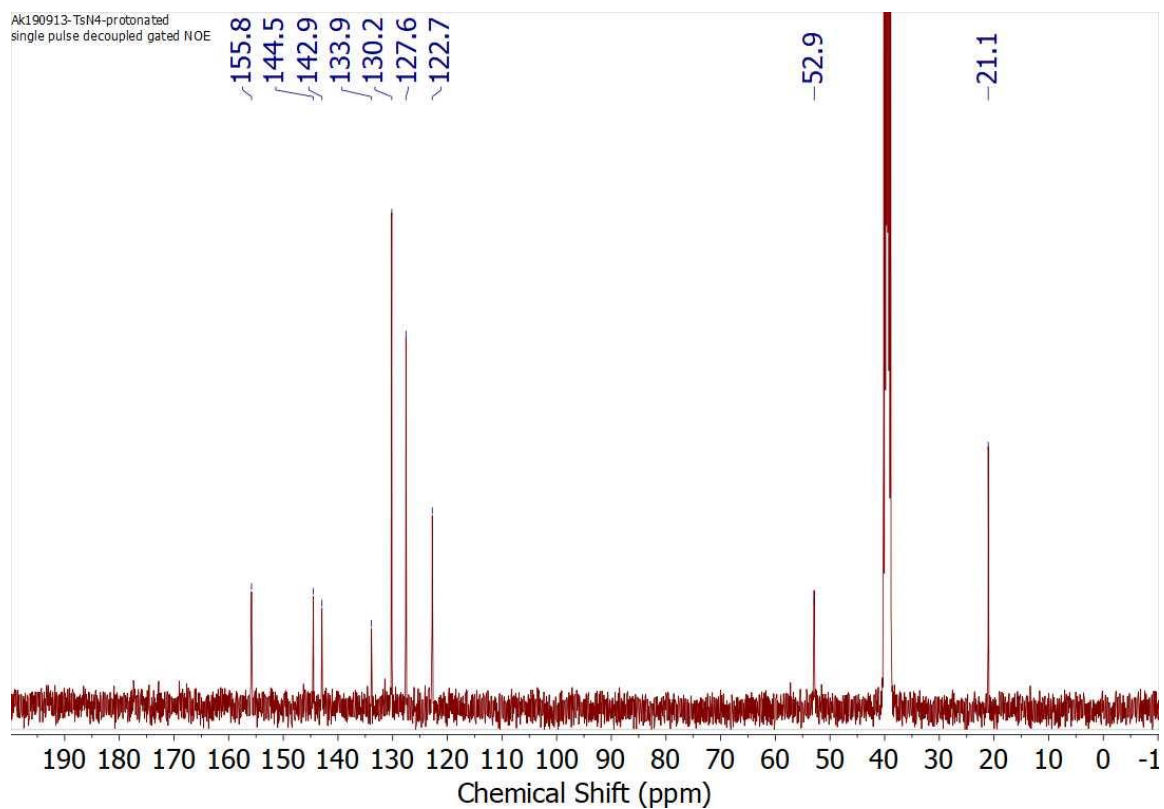


Figure S4. $^{13}\text{C}\{^1\text{H}\}$ NMR spectrum of $\text{TsN4}\cdot\text{HCl}$ in $\text{DMSO-}d_6$ at RT (100 MHz).

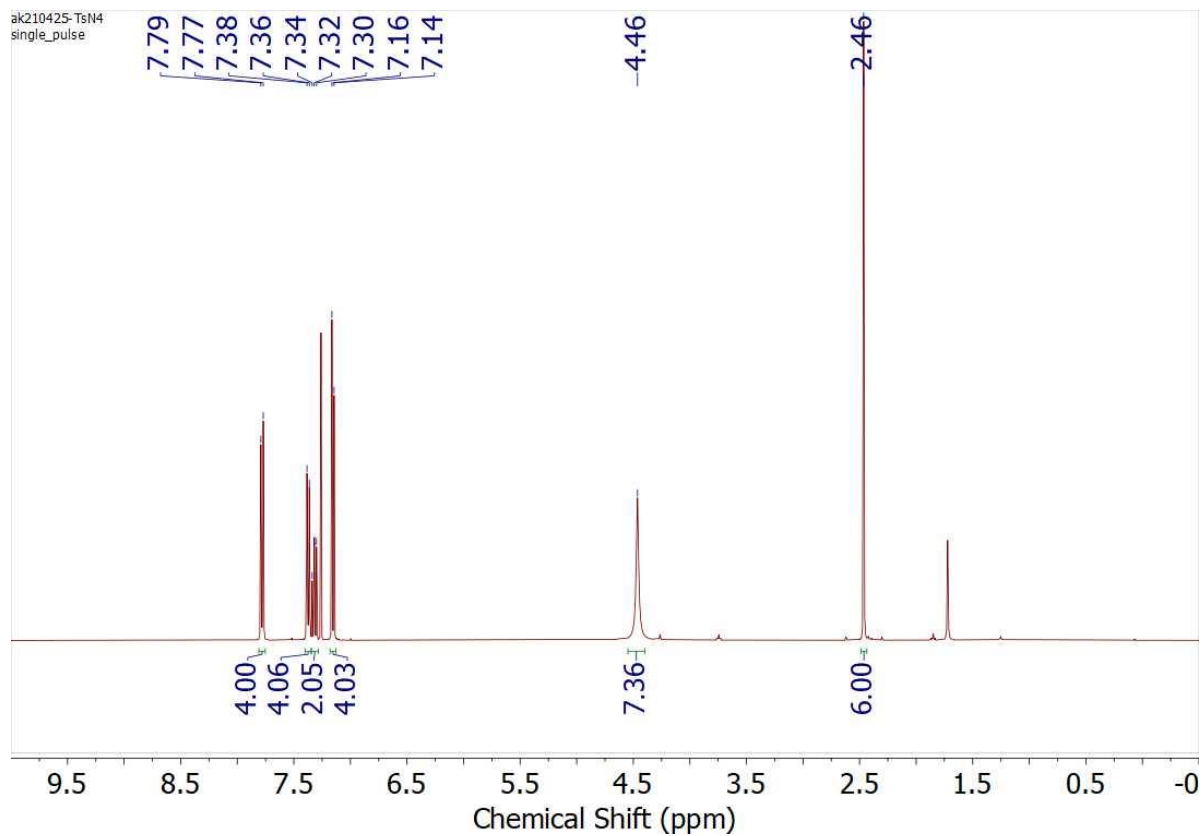


Figure S5. ^1H NMR spectrum of TsN4 in CDCl_3 at room temperature (400 MHz).

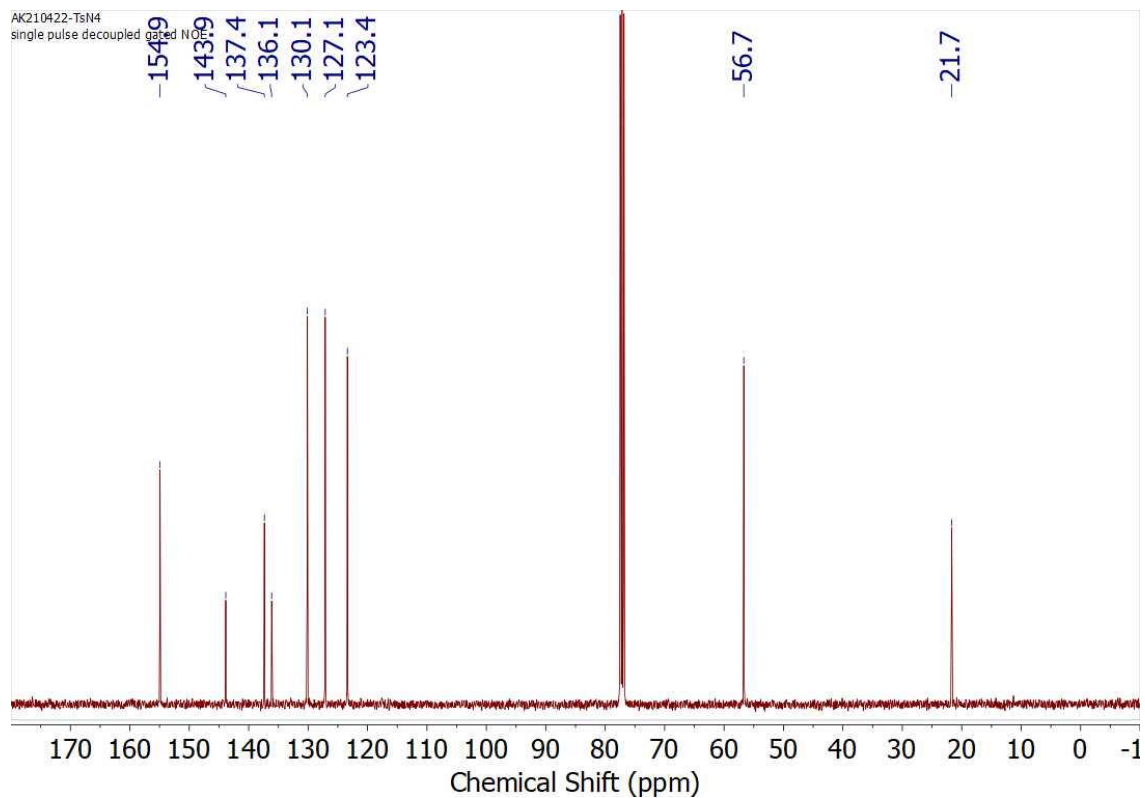
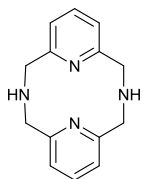


Figure S6. $^{13}\text{C}\{^1\text{H}\}$ NMR spectrum of TsN4 in CDCl_3 at room temperature (100 MHz).

2,11-diaza[3,3](2,6)pyridinophane (¹H_{N4})



2,11-diaza[3,3](2,6)pyridinophane was synthesized by following reported procedure with some modifications.²

¹⁵N₄·HCl (3.00 g, 5.13 mmol) was added to 3 mL of 97% sulfuric acid in round flask and stirred at 100 °C for 3 h. (The powder dissolved slowly over 10 min to give a homogeneous solution. The use of efficient magnetic stirring is important) After cooling down to room temperature, the mixture was added slowly to water (80 mL) cooled with ice water bath. Potassium hydroxide (7.20 g, 128 mmol) was dissolved in cooled water (20 mL), then added to the mixture slowly. Small portion of potassium hydroxide was further added to the solution until the pH was confirmed to be around 12–13. (Basic solution is important for extraction) The aqueous layer was extracted with dichloromethane (ca. 100 mL ×5) and dried over mixture of K₂CO₃ and MgSO₄, filtered off and concentrated under reduced pressure to give a white powder of target product (938 mg, 76%).

¹H NMR (400MHz, CDCl₃): 7.06 (t, ³J_{HH} = 7.2 Hz, *p*-**H**_{Py}, 2H), 6.48 (d, ³J_{HH} = 7.2 Hz, *m*-**H**_{Py}, 4H), 3.93 (s, 8H, -**CH**₂-). ¹³C {¹H} NMR (100MHz, CDCl₃): 159.6 (*o*-**C**_{Py}), 135.9 (*p*-**C**_{Py}), 119.9 (*m*-**C**_{Py}), 56.1 (Py-**CH**₂-N).

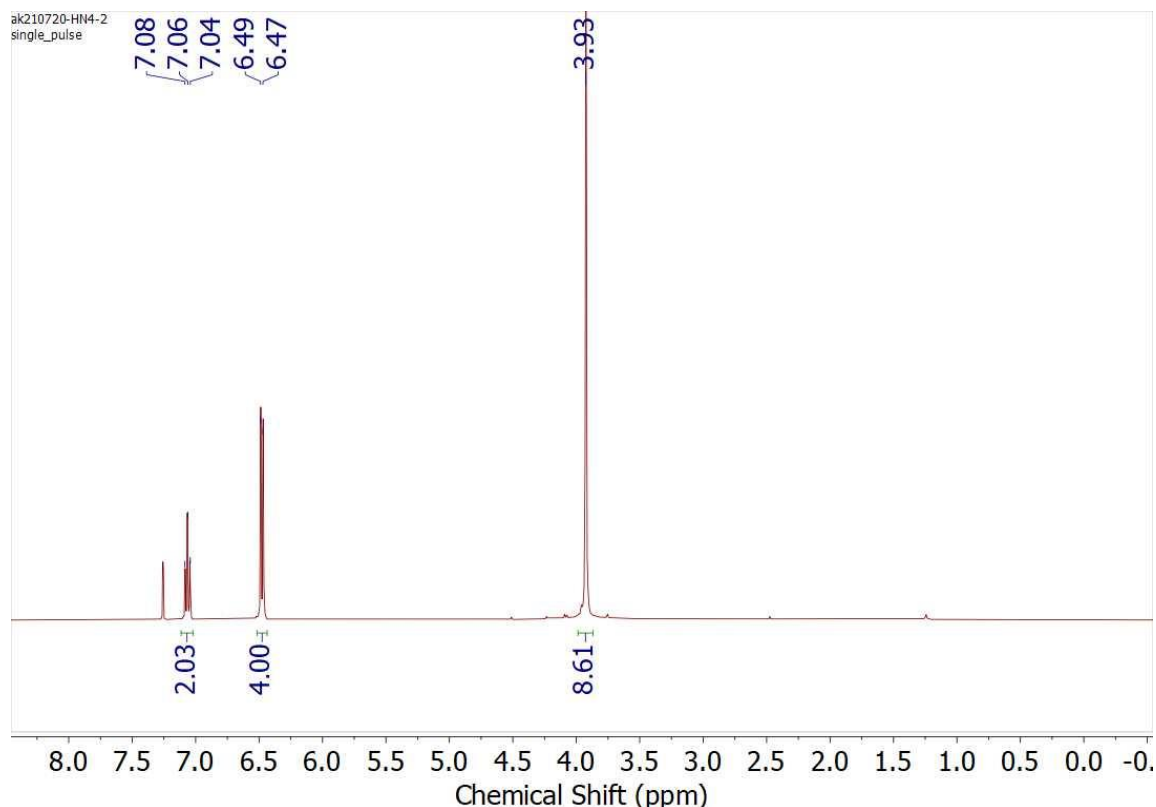


Figure S7. ¹H NMR spectrum of ¹H_{N4} in CDCl₃ at RT (400 MHz).

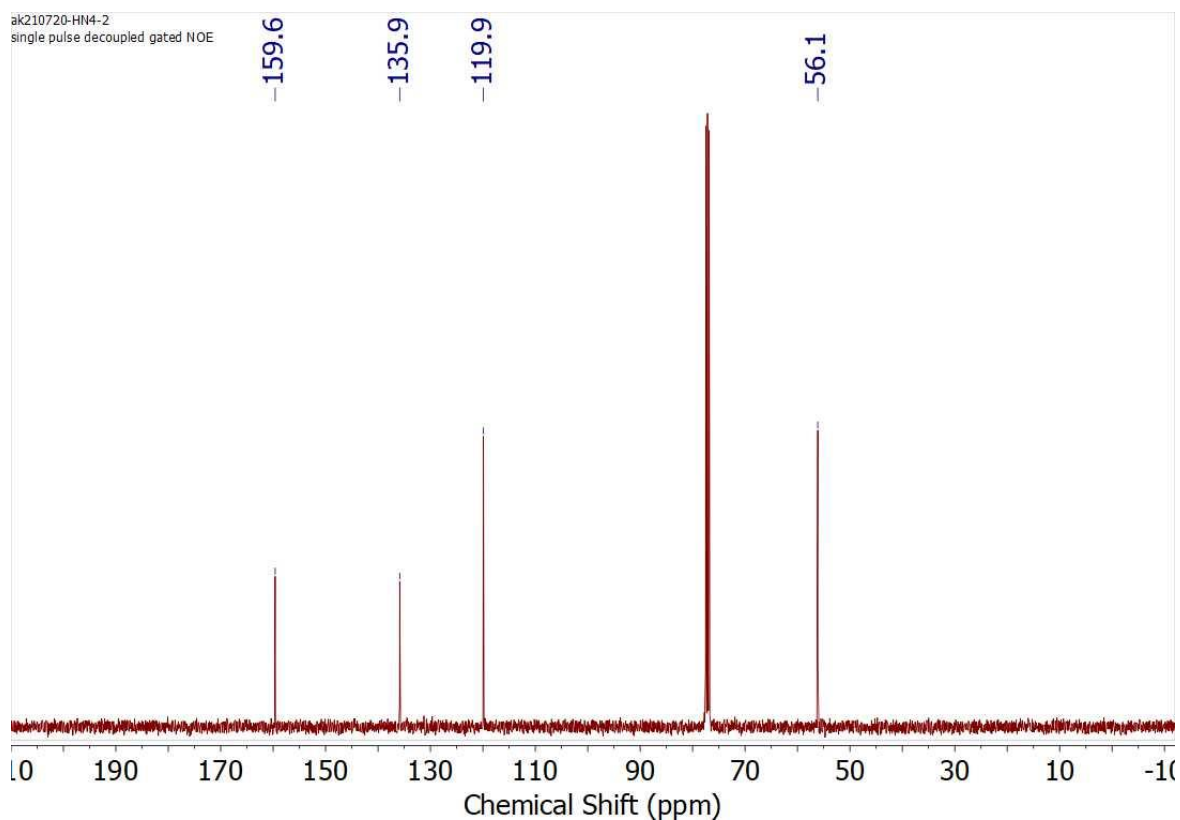
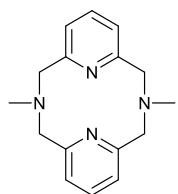


Figure S8. $^{13}\text{C}\{^1\text{H}\}$ NMR spectrum of $^{\text{H}}\text{N4}$ in CDCl_3 at RT (100 MHz).

***N,N'*-dimethyl-2,11-diaza[3,3](2,6)pyridinophane ($^{\text{Me}}\text{N4}$)**



N,N'-dimethyl-2,11-diaza[3,3](2,6)pyridinophane was synthesized by following reported procedure with some modifications.²

A solution of 2,11-diaza[3,3](2,6)pyridinophane (400 mg, 1.66 mmol), formic acid (5 mL), and 37% formaldehyde in methanol (5 mL) was stirred at 80 °C under air for 18 h. The mixture was evaporated under reduced pressure, then basified with saturated K_2CO_3 aqueous solution (3 mL) and extracted with dichloromethane (ca. 10 mL \times 5). The organic layer was dried over MgSO_4 , filtered off and concentrated under reduced pressure. Acetonitrile (5 mL) was added to the crude mixture and extracted with hexane (ca. 10 mL \times 5) and concentrated under reduced pressure to give the target product (370 mg, 83%).

^1H NMR (400 MHz, CDCl_3): 7.14 (t, $^3J_{\text{HH}} = 7.8$ Hz, *p*- H_{Py} , 2H), 6.79 (d, $^3J_{\text{HH}} = 7.8$ Hz, *m*- H_{Py} , 4H), 3.86 (s, 8H, $-\text{CH}_2-$), 2.74 (s, 6H, $-\text{CH}_3$). $^{13}\text{C}\{^1\text{H}\}$ NMR (100 MHz, CDCl_3): 157.3 (*o*- C_{Py}), 135.7 (*p*- C_{Py}), 122.7 (*m*- C_{Py}), 66.3 ($-\text{CH}_2-$), 49.3 ($-\text{CH}_3$).

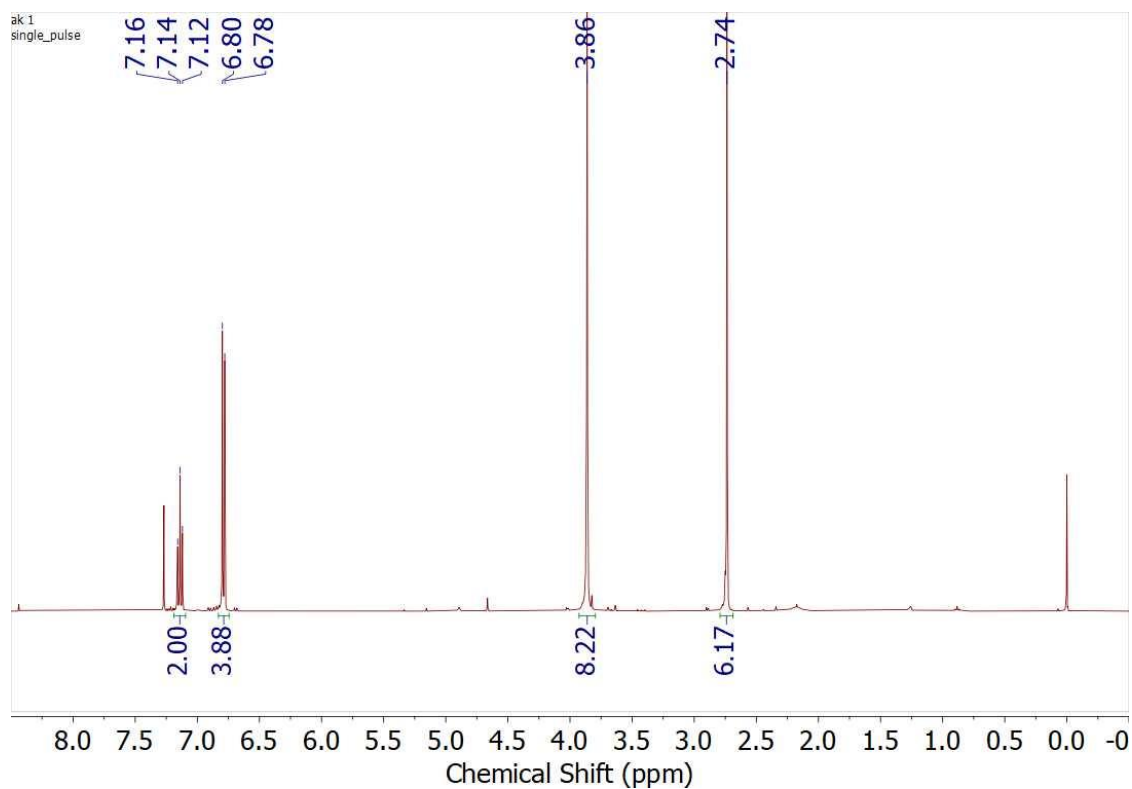


Figure S9. ^1H NMR spectrum of $^{\text{Me}}\text{N4}$ in CDCl_3 at RT (400 MHz).

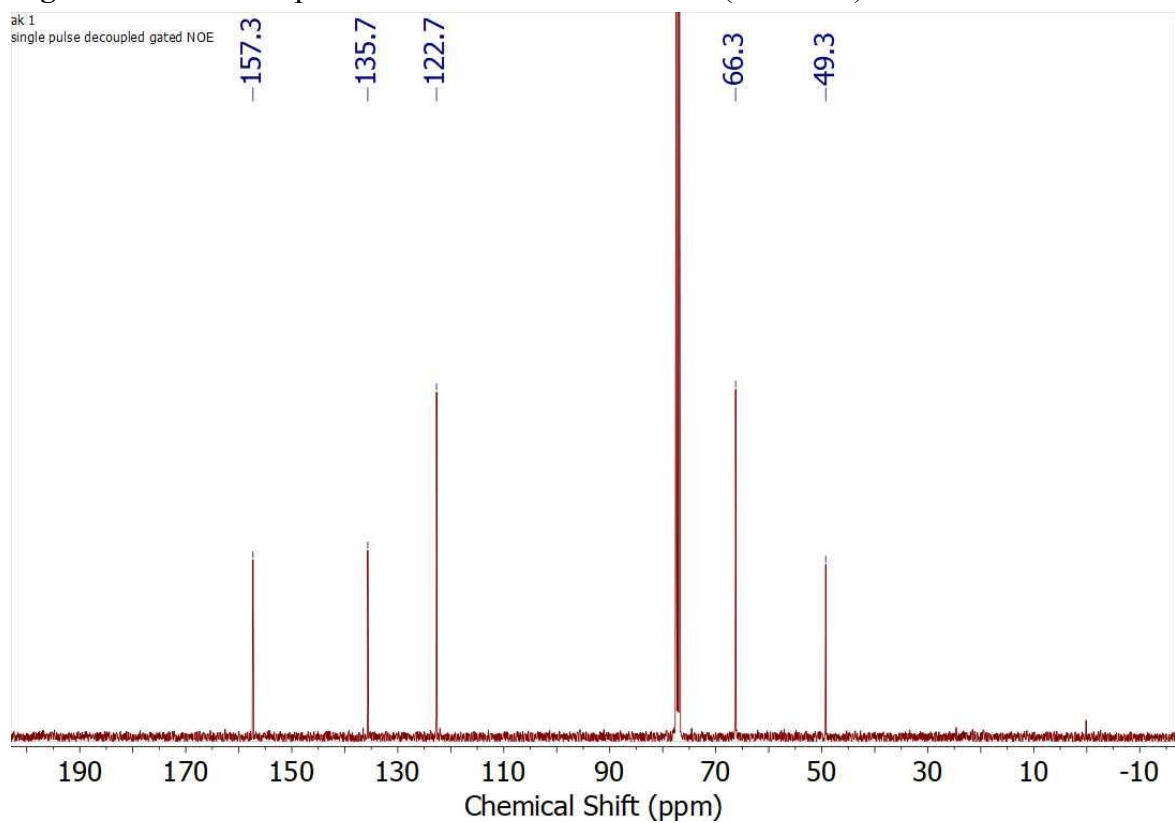
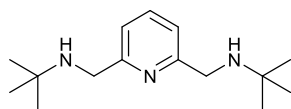


Figure S10. $^{13}\text{C}\{^1\text{H}\}$ NMR spectrum of $^{\text{Me}}\text{N4}$ in CDCl_3 at RT (100 MHz).

2,6-Bis[(*t*-butylamino)methyl]pyridine



t-Butylamine (23.4 g, 320 mmol) was added to a solution of 2,6-bis(chloromethyl)pyridine (1.41 g, 8.01 mmol) in acetonitrile (32 mL), and the solution was stirred at 50 °C under air for 6 h. The solvents were removed under reduced pressure. After the addition of saturated K₂CO₃ aqueous solution (20 mL), the mixture was extracted with diethyl ether (ca. 50 mL ×3), dried over a mixture of MgSO₄ and K₂CO₃, filtered off, and concentrated under reduced pressure to provide colorless oil (1.95 g, 98%).

¹H NMR (400 MHz, CDCl₃), δ (ppm): 7.55 (t, *J*_{HH} = 7.5 Hz, *p*-**H**_{Py} 1H), 7.16 (d, *J*_{HH} = 7.5 Hz, *m*-**H**_{Py}, 2H), 3.85 (s, 4H), 1.18 (s, 18H, *t*Bu). ¹³C{¹H} NMR (100 MHz, CDCl₃), δ(ppm): 159.9 (*o*-C_{Py}), 136.9 (*p*-C_{Py}), 120.3 (*m*-C_{Py}), 50.6 (-CH₂-), 48.6 (CCH₃), 29.3 (CH₃).

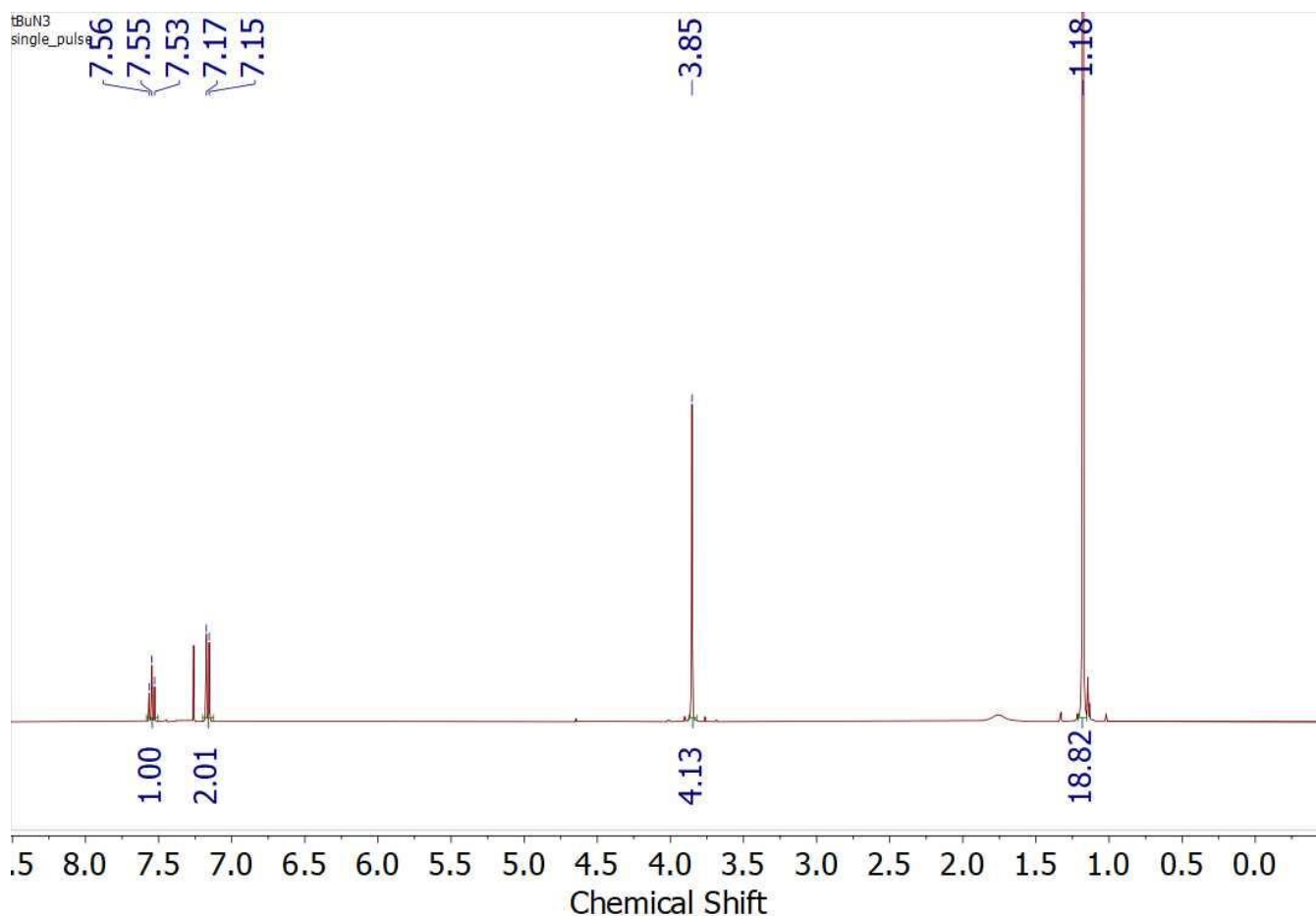


Figure S11. ¹H NMR spectrum of 2,6-bis[(*N*-*t*-butylamino)methyl]pyridine in CDCl₃ at room temperature (400 MHz).

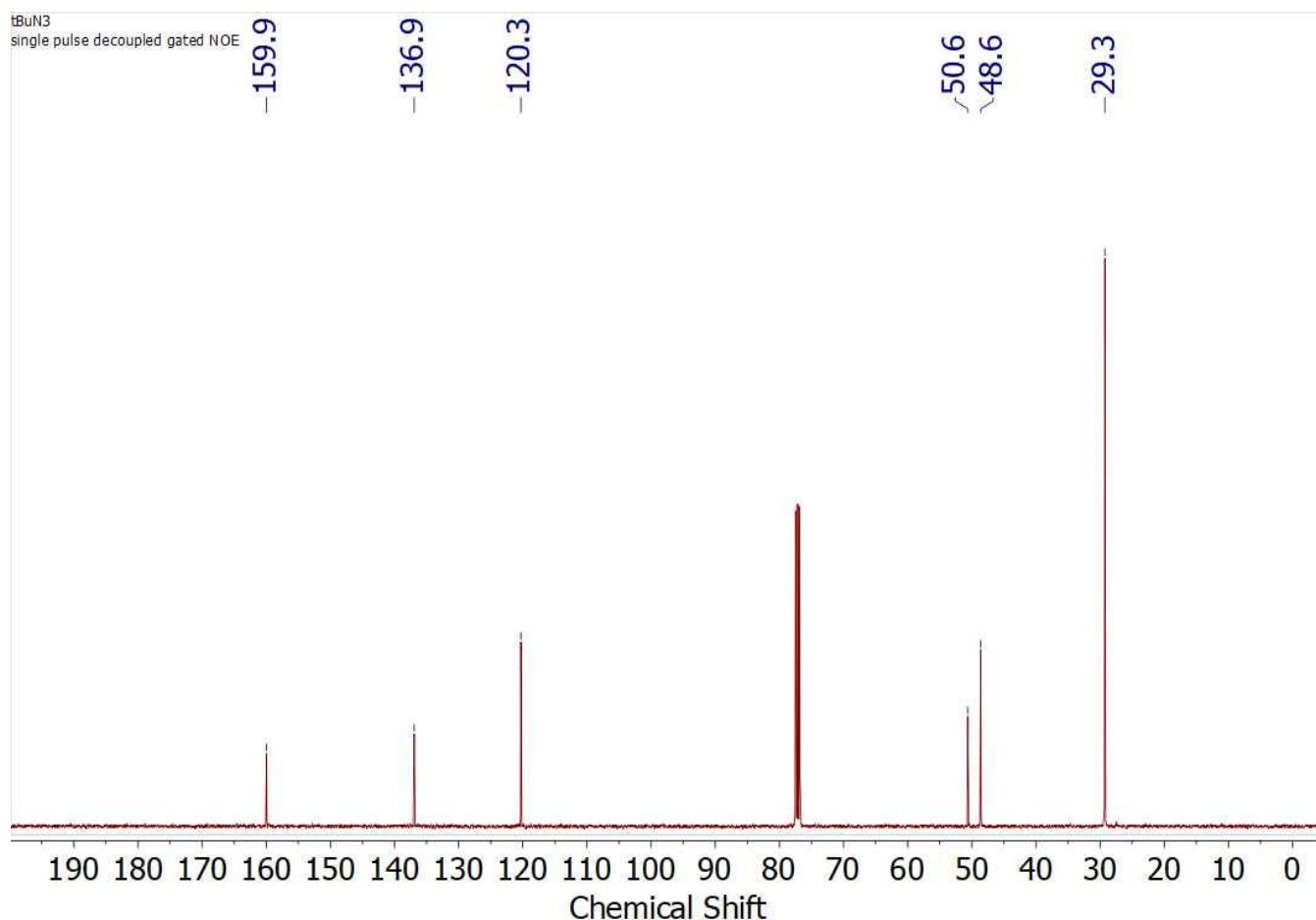
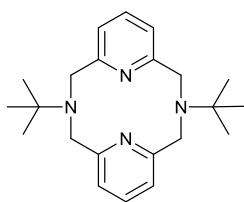


Figure S12. $^{13}\text{C}\{^1\text{H}\}$ NMR spectrum of 2,6-bis[(*N*-*t*-butylamino)methyl]pyridine in CDCl_3 at room temperature (100 MHz).

***N,N'*-di-*t*-butyl-2,11-diaza[3,3](2,6)pyridinophane ($^t\text{BuN4}$)**



N,N'-di-*t*-butyl-2,11-diaza[3,3](2,6)pyridinophane⁴ was prepared by following reported procedure with some modifications.⁵

A mixture of 2,6-bis[(*t*-butylamino)methyl]pyridine (1.50 g, 6.00 mmol), 2,6-bis(chloromethyl)pyridine (1.06 g, 6.02 mmol), potassium iodide (500 mg, 3.01 mmol), and potassium carbonate (8.30 g, 60.1 mmol) in acetonitrile (210 mL) was stirred at 80 °C for 16 h under air. After removing the solvent under reduced pressure, toluene (150 mL) was added to the mixture. The mixture was stirred at 80 °C for 30 minutes to dissolve the target product. The hot toluene mixture was filtered off to remove inorganic salts. [The hot mixture need to be filtered off quickly by vacuum filtration using larger filtration paper to avoid

precipitation of the target product during the filtration] The toluene filtrate was concentrated under reduced pressure, then added to ethanol (150 mL) and stirred at 70 °C for 30 minutes to dissolve the target product. After cooling down to room temperature, the mixture was filtered off to remove insoluble byproducts, concentrated under reduced pressure. The mixture was added to THF (30 mL), stirred at 60 °C for 30 minutes to dissolve byproducts, then left at room temperature for overnight. White precipitate was collected by filtration, washed with small amount of cooled THF, and dried under vacuum to provide white powder. The rest of filtrate in THF was evaporated and purified again by the same purification process using ethanol (30 mL) and THF (8 mL), then combined to give the final product as a white solid (827 mg, 39%).

^1H NMR (400 MHz, CDCl_3), δ (ppm): 7.07 (t, $J_{\text{HH}} = 7.6$ Hz, *p*-**HPy** 2H) 6.72 (d, $J_{\text{HH}} = 7.6$ Hz, *m*-**HPy**, 4H), 3.97 (s, 8H), 1.32 (s, 18H, *t*Bu). $^{13}\text{C}\{^1\text{H}\}$ NMR (100 MHz, CDCl_3), δ (ppm): 159.5(*o*- C_{Py}), 135.3 (*p*- C_{Py}), 122.0 (*m*- C_{Py}), 57.8 ($-\text{CH}_2-$), 56.0 (CCH_3), 27.8 (CH_3).

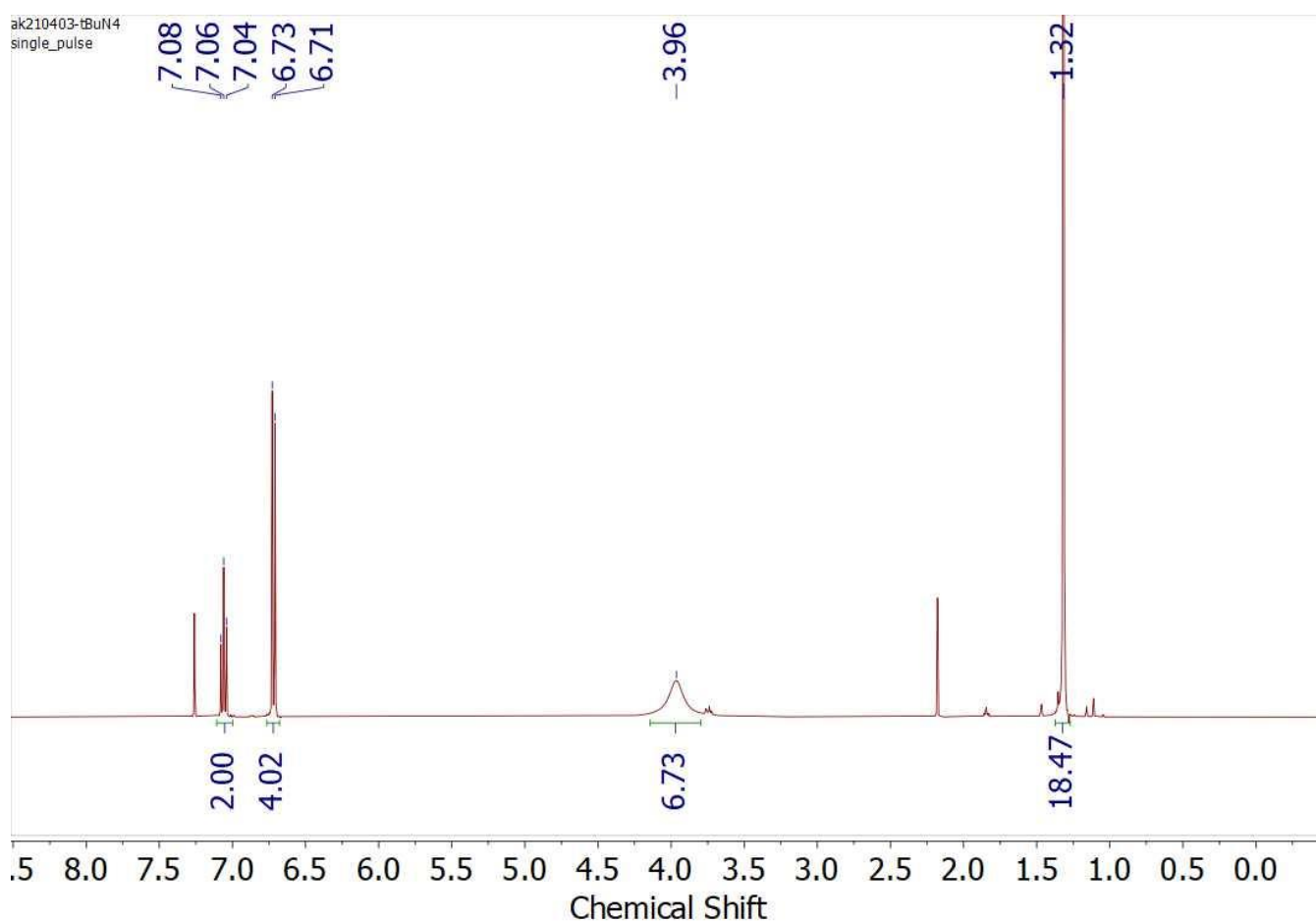


Figure S13. ^1H NMR spectrum of $t\text{BuN}_4$ in CDCl_3 at RT (400 MHz).

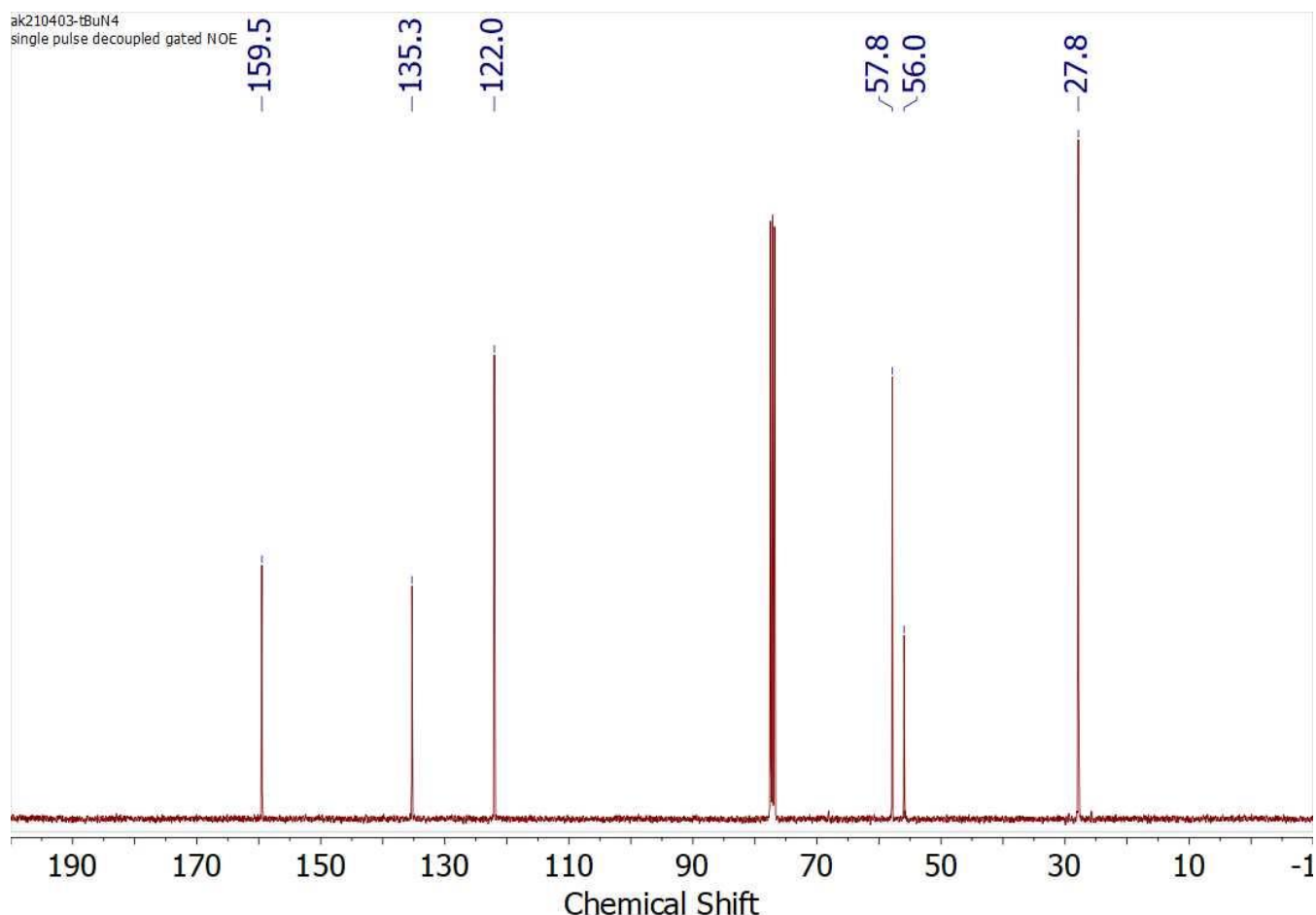
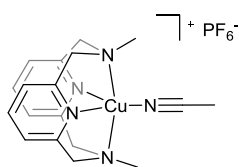


Figure S14. $^{13}\text{C}\{^1\text{H}\}$ NMR spectrum of $^t\text{BuN4}$ in CDCl_3 at RT (100 MHz).

Synthesis of 2



N,N' -dimethyl-2,11-diaza[3,3](2,6)pyridinophane (50.5 mg, 0.188 mmol,) was dissolved in 2 mL of dry acetonitrile and $[\text{Cu}(\text{MeCN})_4](\text{PF}_6)$ (77.2 mg, 0.207 mmol) was added to the solution. The mixture was stirred for 1 h, then set for crystallization by vapor diffusion with ether overnight. Red crystal was collected, washed with ether and dried under vacuum to give a product, $[(^{\text{Me}}\text{N}4)\text{Cu}(\text{MeCN})](\text{PF}_6)$ (85.9 mg, 88%).

^1H NMR (400 MHz, acetone- d_6): 7.42 (t, $^3J_{\text{HH}} = 7.8$ Hz, $p\text{-H}_{\text{Py}}$, 2H), 6.86 (d, $^3J_{\text{HH}} = 7.3$ Hz, $m\text{-H}_{\text{Py}}$, 4H), 4.16 (d, $^2J_{\text{HH}} = 15$ Hz, $\text{Py-CH}_2\text{-N}$), 3.67 (d, $^2J_{\text{HH}} = 15$ Hz, 4H, $\text{Py-CH}_2\text{-N}$), 2.43 (s, 6H, N-CH_3).

$^{13}\text{C}\{^1\text{H}\}$ NMR (100 MHz, acetone- d_6): 156.7 ($o\text{-C}_{\text{Py}}$), 137.7 ($p\text{-C}_{\text{Py}}$), 122.8 ($m\text{-C}_{\text{Py}}$), 64.7 ($\text{Py-CH}_2\text{-N}$), 49.0 ($-\text{CH}_3$), 2.0 (NCCH_3).

^{19}F NMR (376 MHz, acetone- d_6): -72.5 (d, $J_{\text{P,F}} = 708$ MHz).

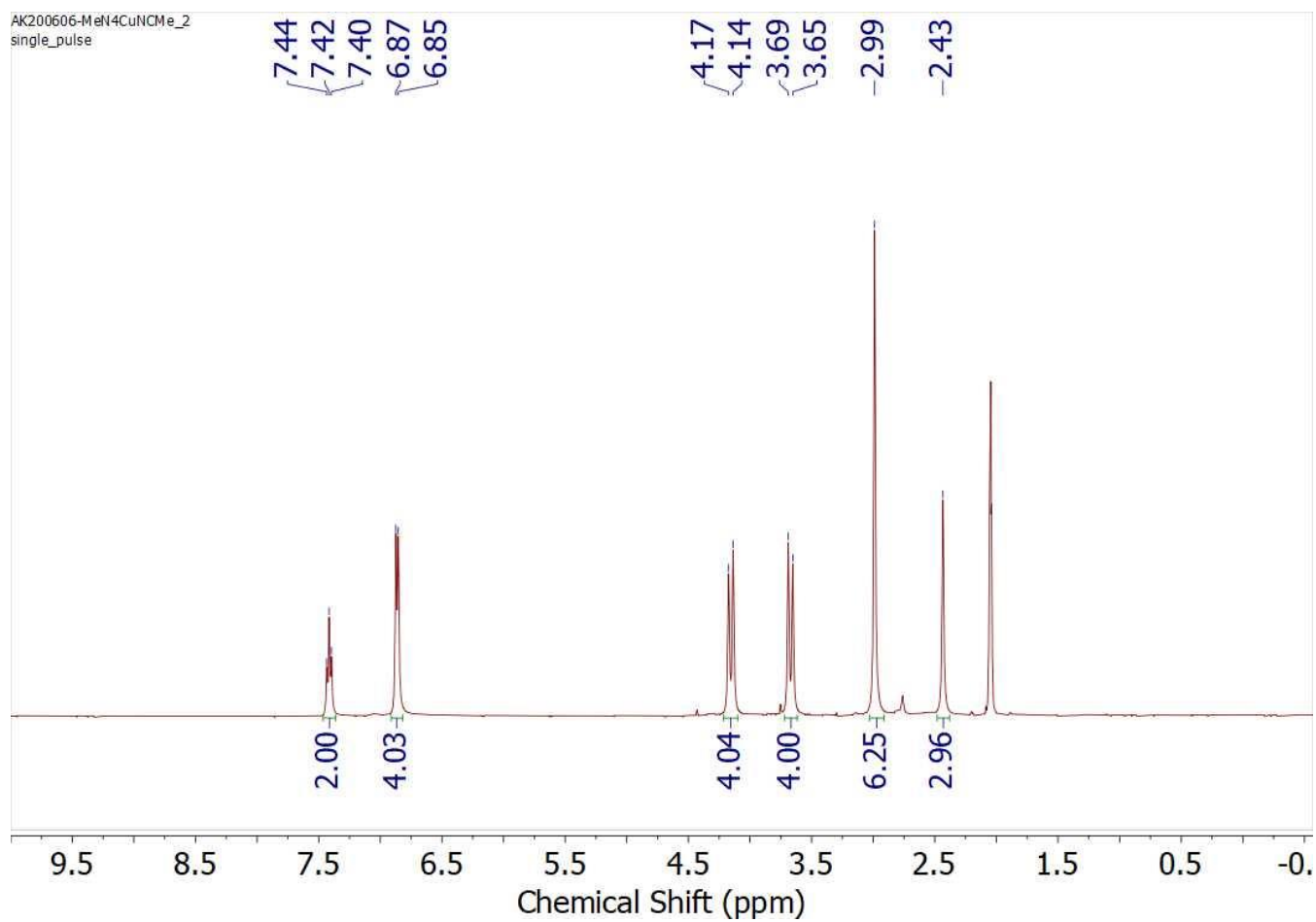


Figure S15. ¹H NMR spectrum of **2** in acetone-*d*₆ at RT (400 MHz).

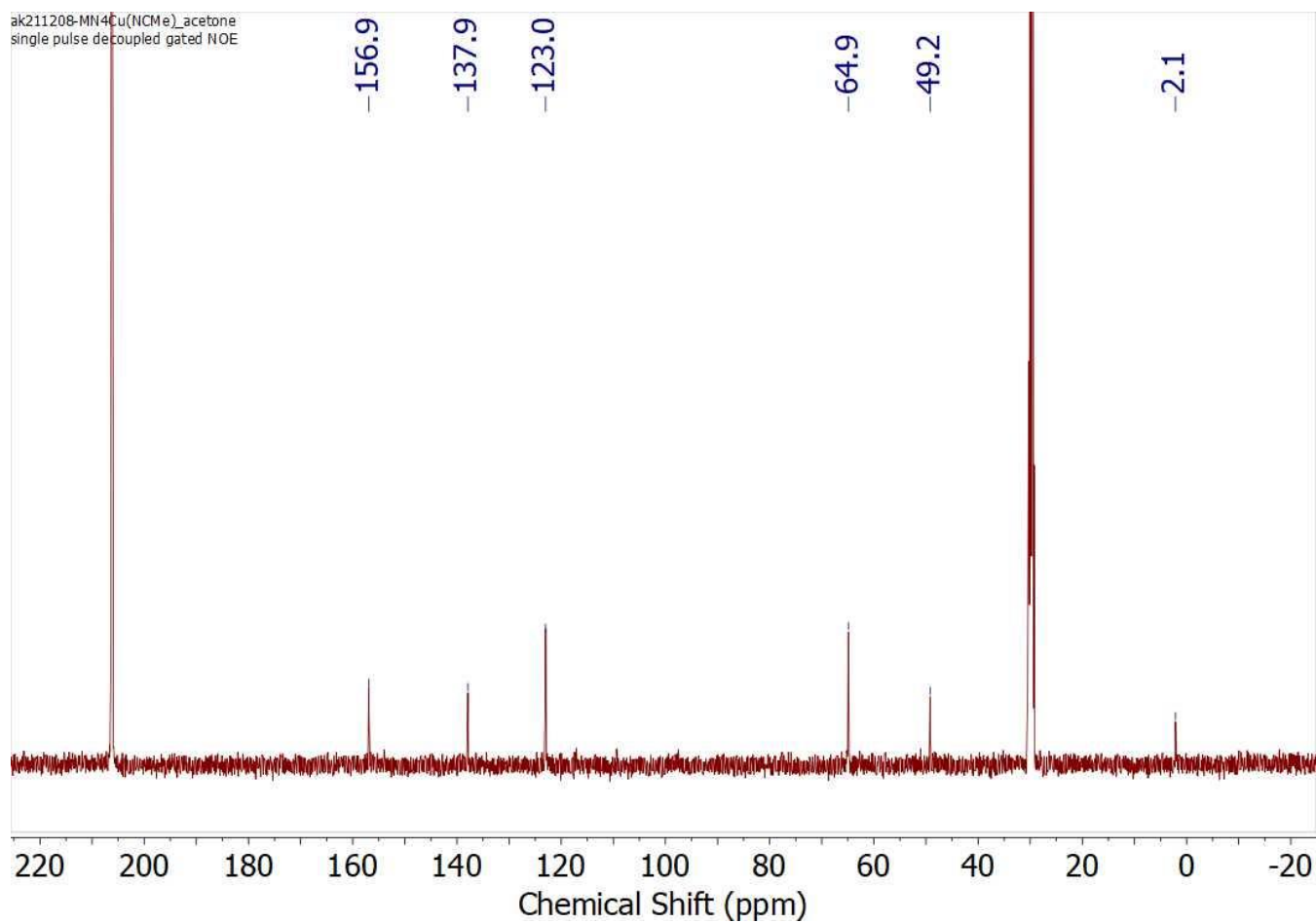


Figure S16. $^{13}\text{C}\{^1\text{H}\}$ NMR spectrum of **2** in acetone- d_6 at RT (100 MHz).

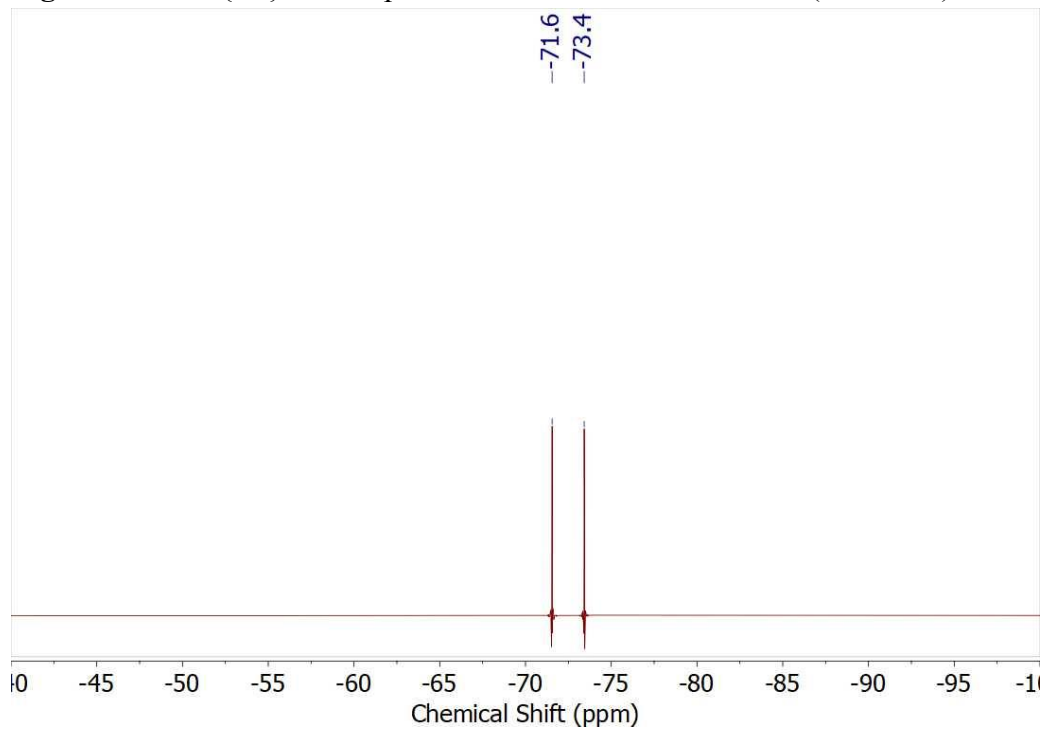


Figure S17. ^{19}F NMR spectrum of **2** in acetone- d_6 at RT (376 MHz).

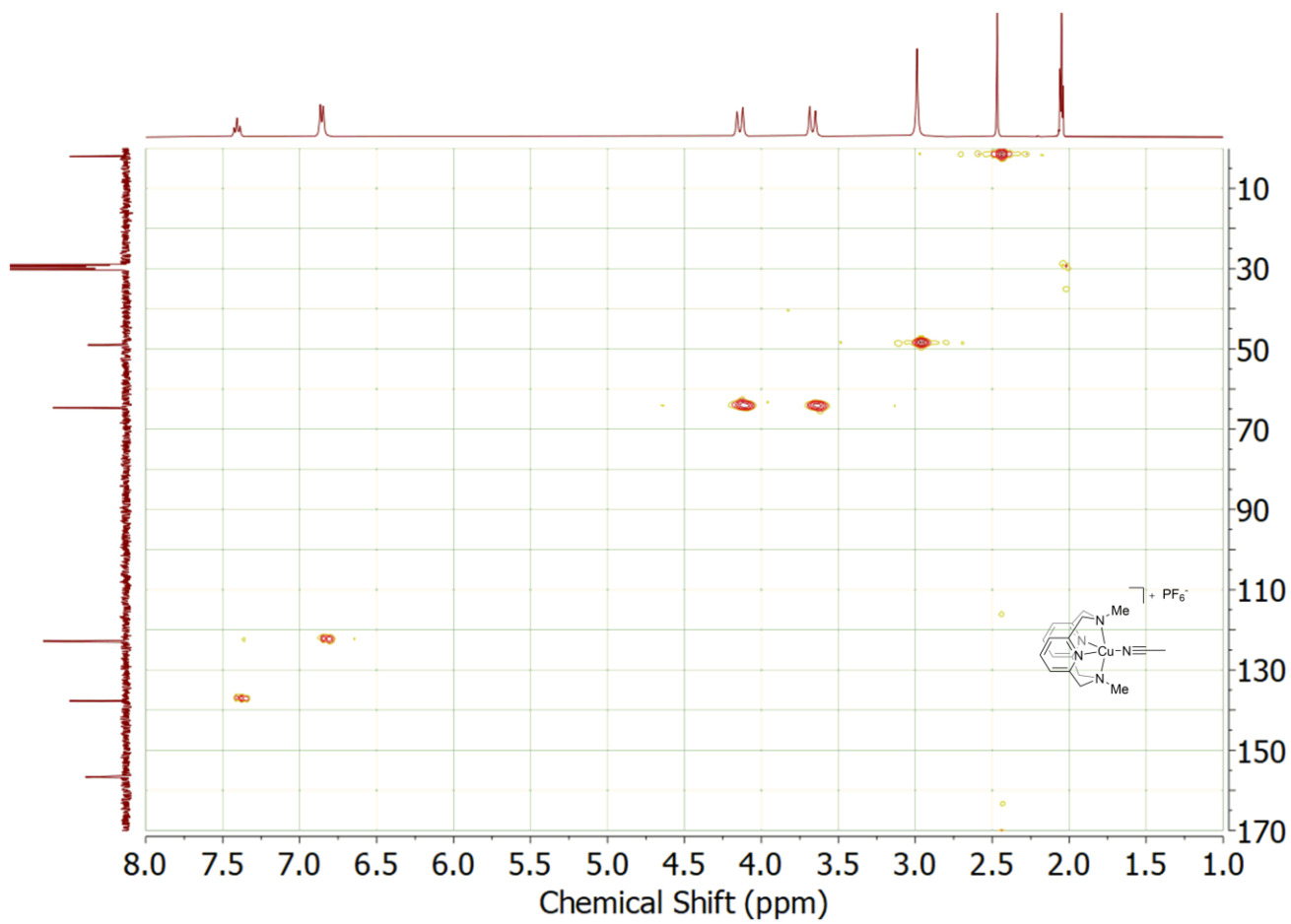


Figure S18. ^1H - ^{13}C HMQC spectrum of **2** in acetone- d_6 at RT.

Characterization of 4

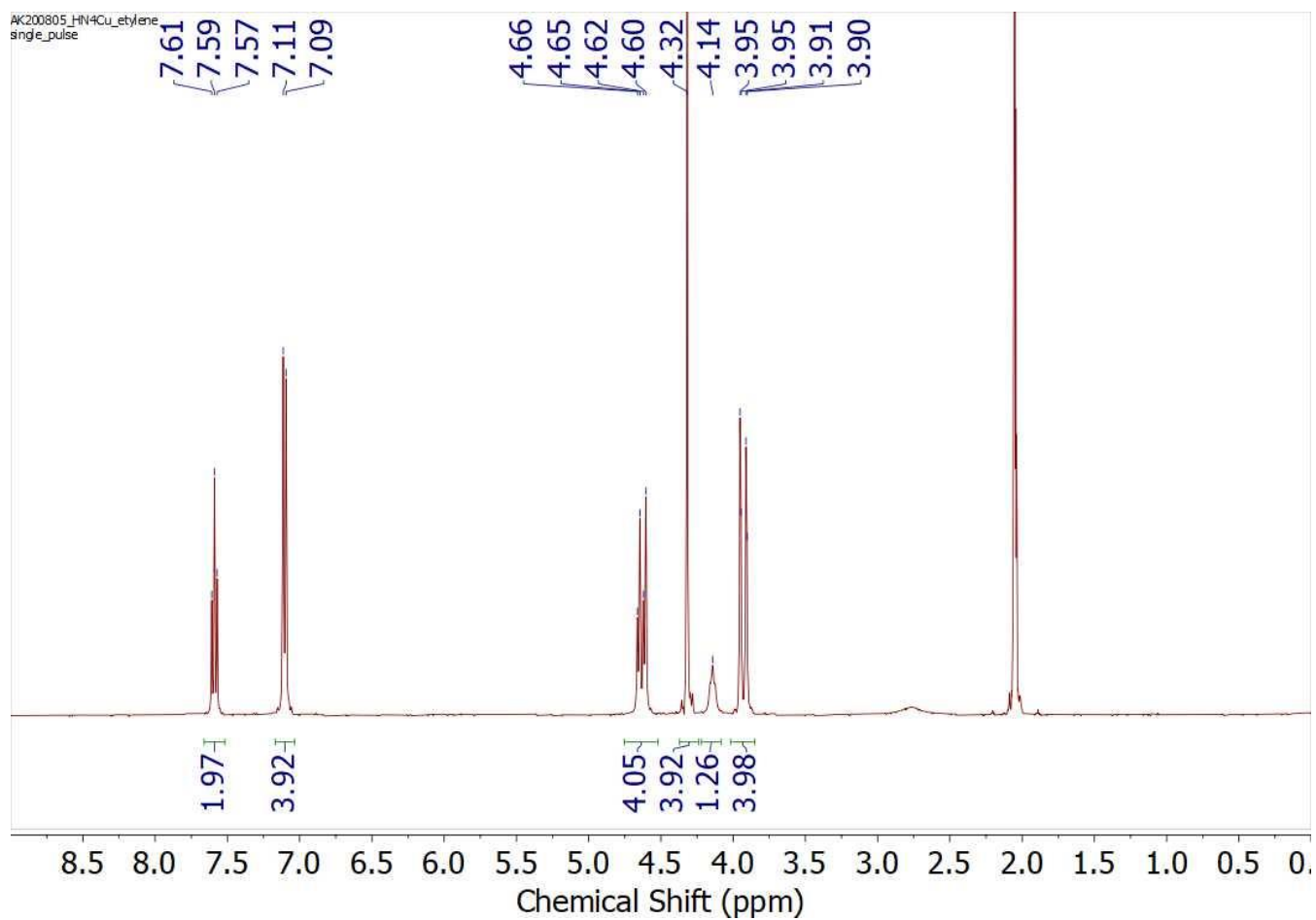


Figure S19. ^1H NMR spectrum of **4** in acetone- d_6 at RT (400 MHz).

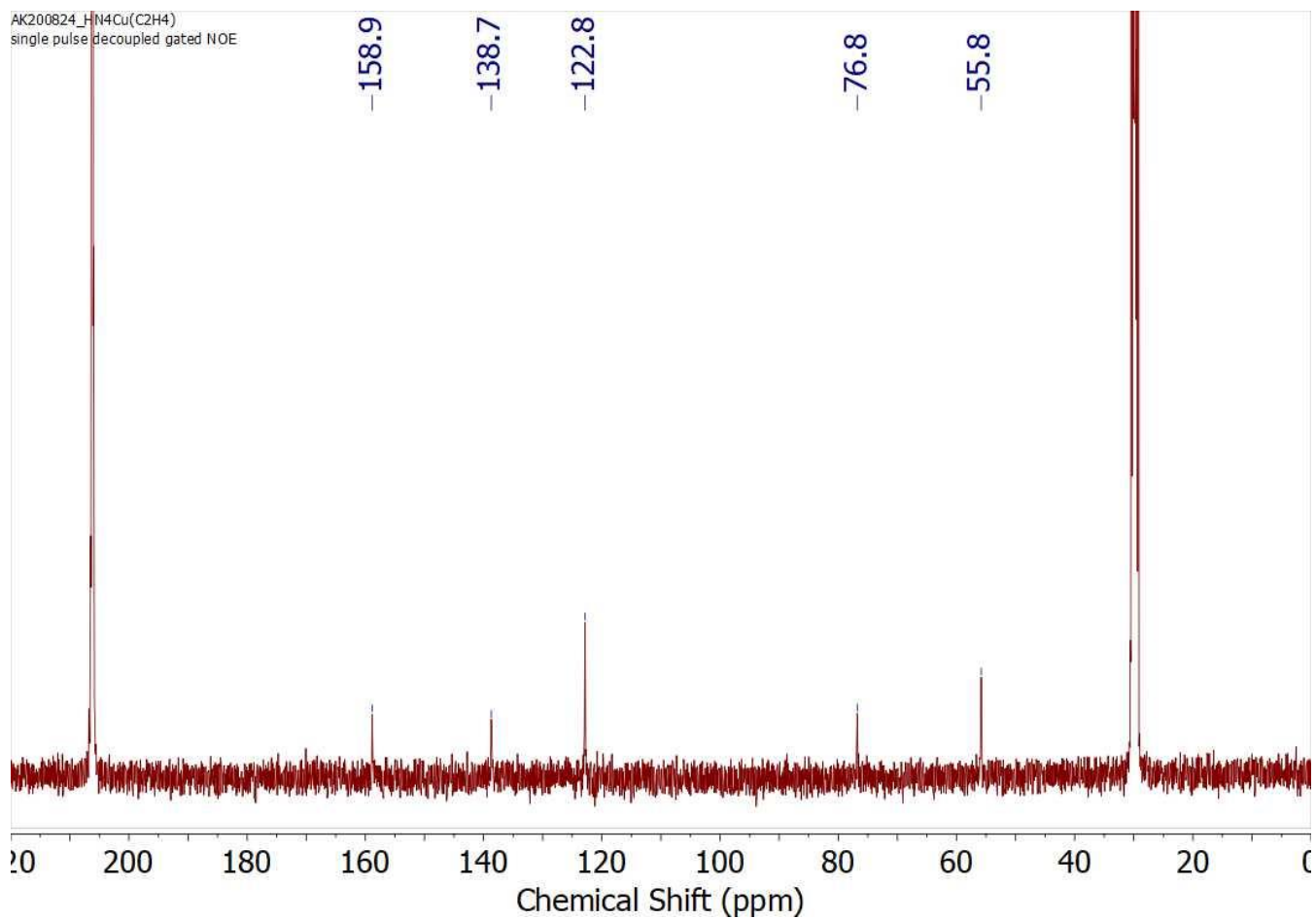


Figure S20. $^{13}\text{C}\{^1\text{H}\}$ NMR spectrum of **4** in acetone- d_6 at RT (100 MHz).

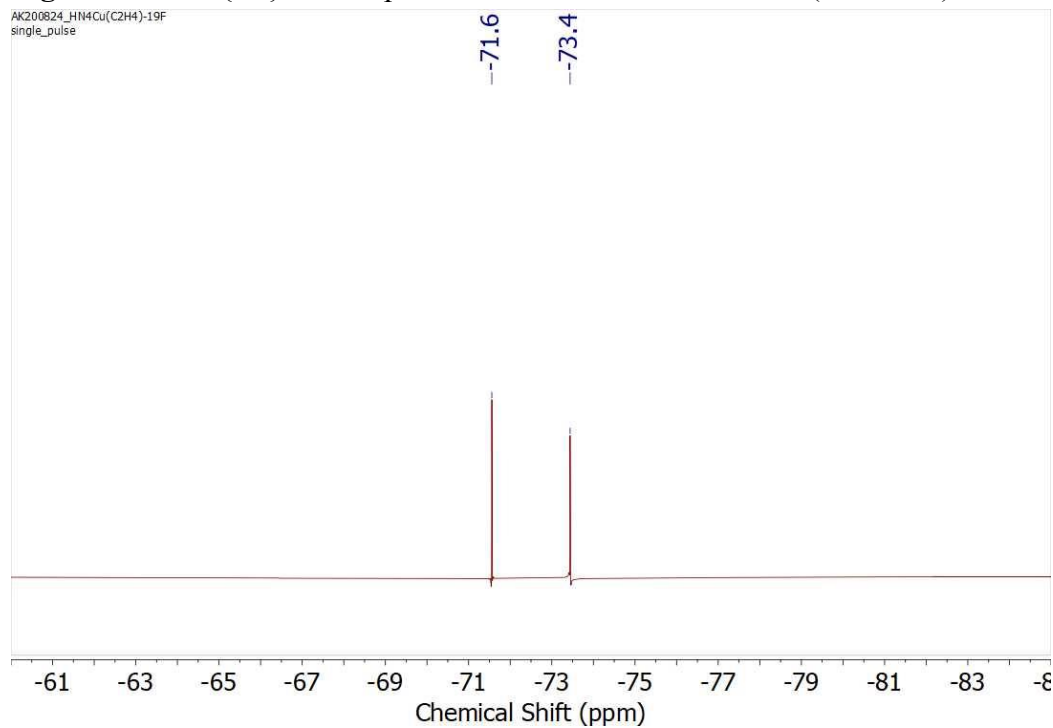


Figure S21. ^{19}F NMR spectrum of **4** in acetone- d_6 at room temperature (376 MHz)

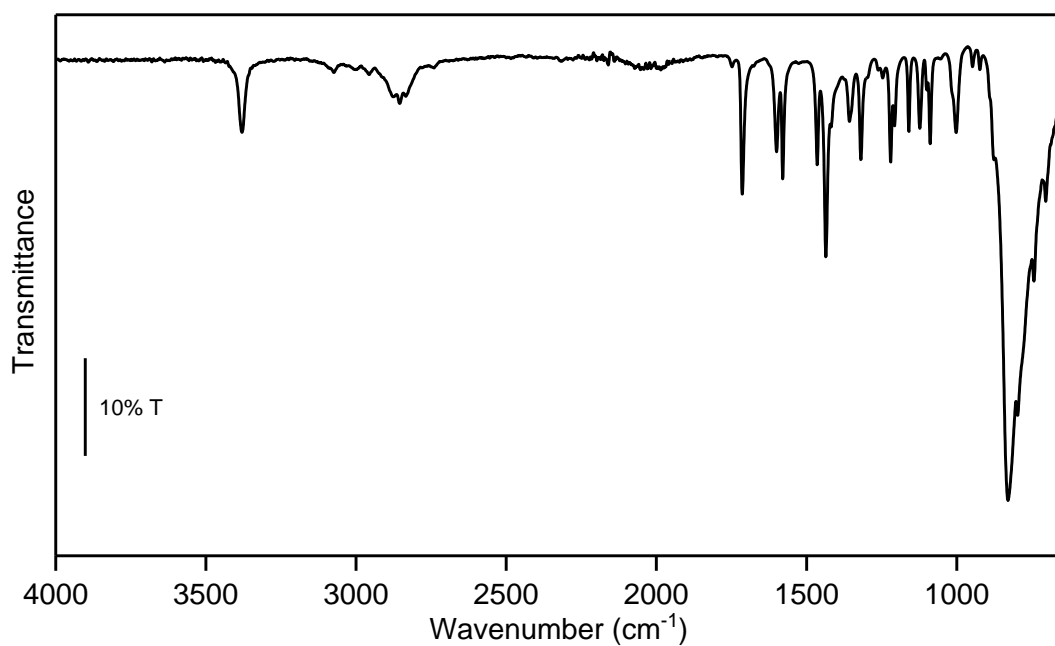


Figure S22. FT-IR spectrum of **4**.

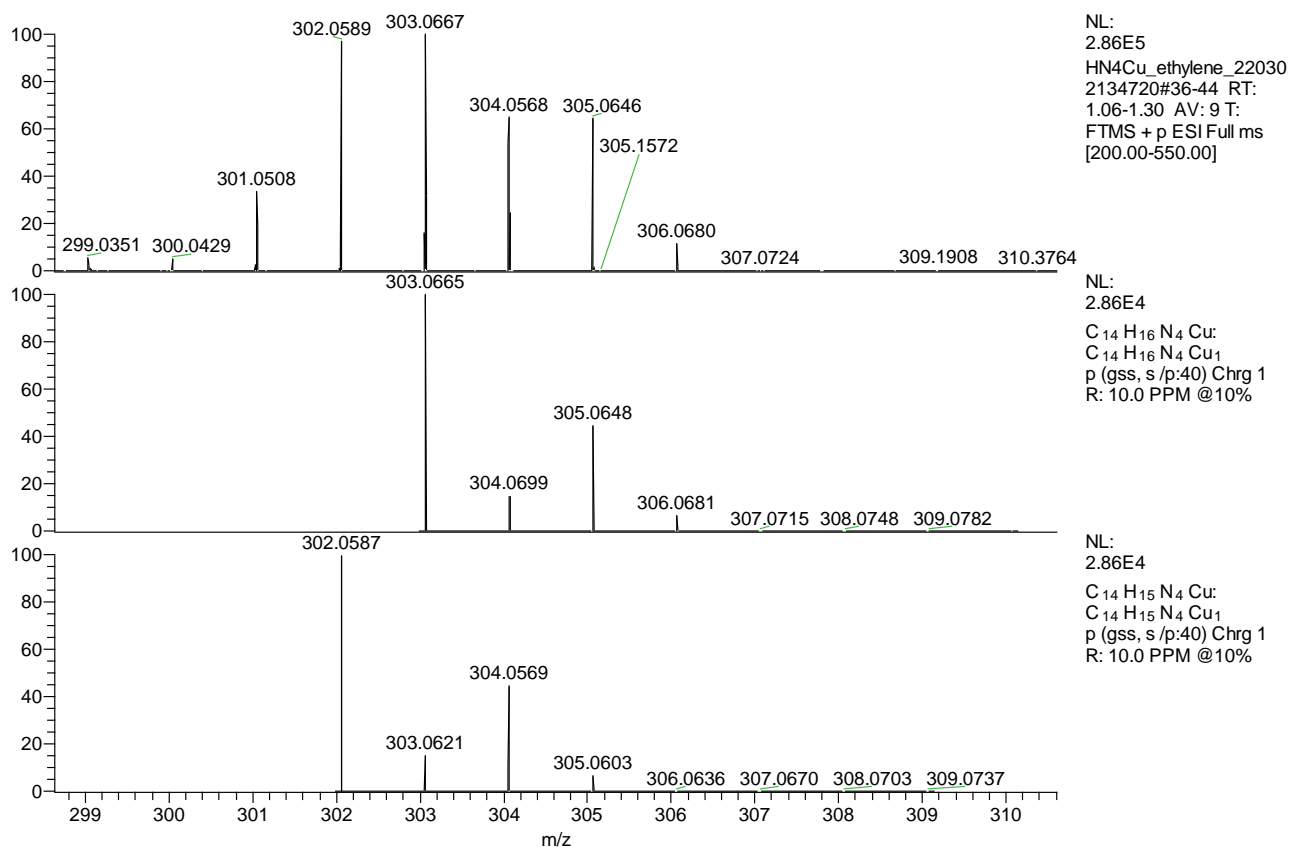


Figure S23. ESI HRMS analysis of **4**.

Characterization of 5

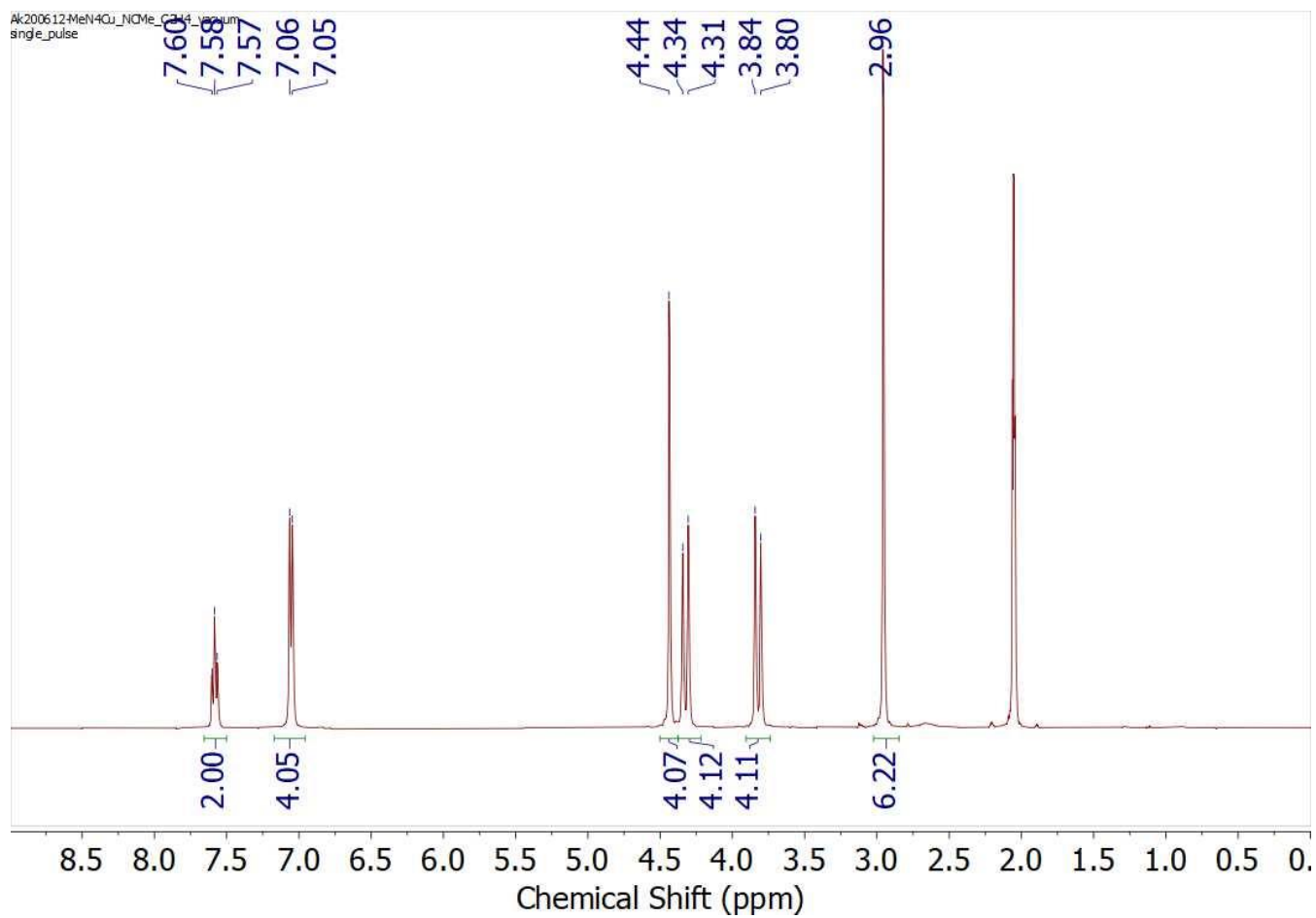


Figure S24. ^1H NMR spectrum of **5** in acetone- d_6 at RT (400 MHz).

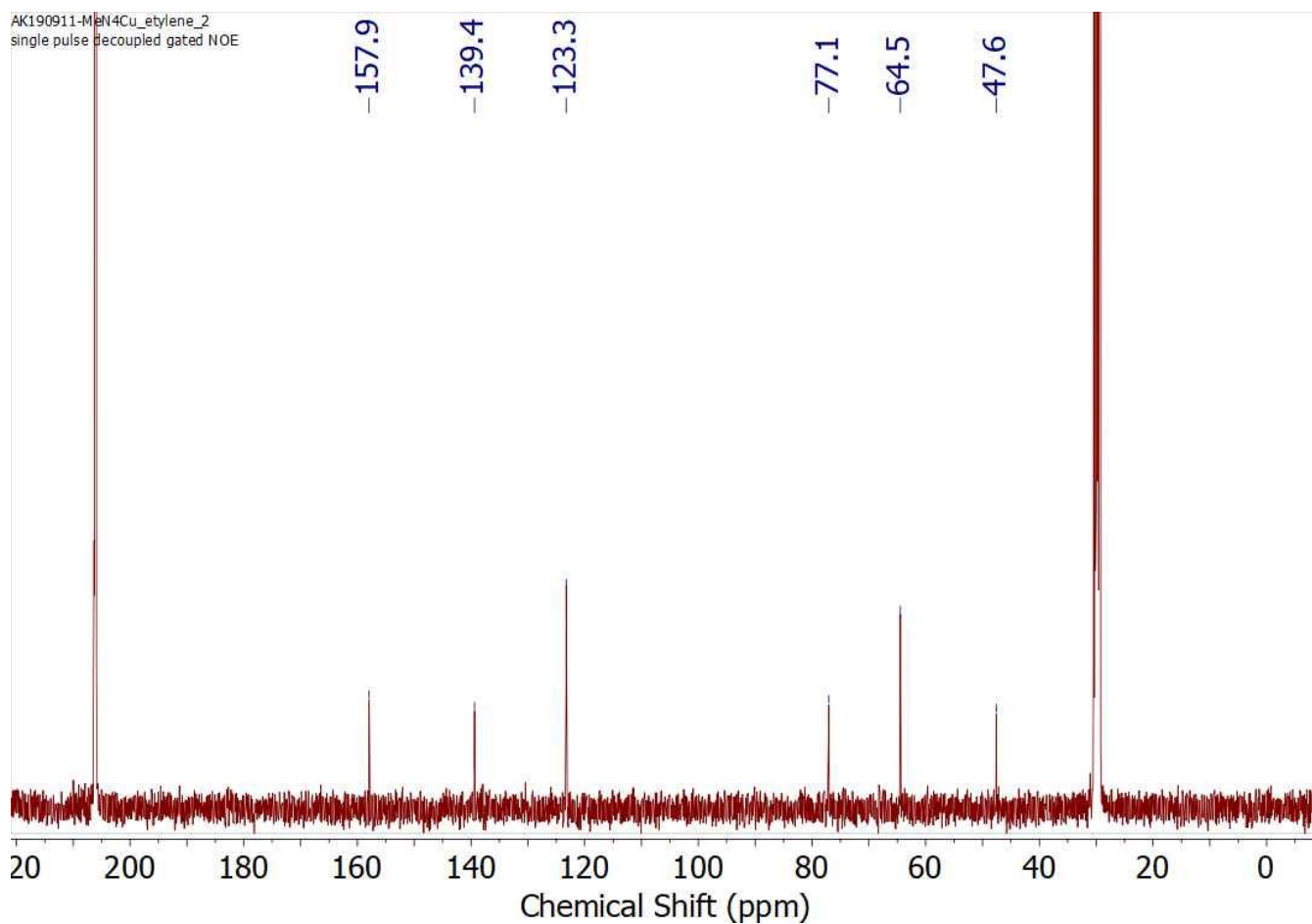


Figure S25. $^{13}\text{C}\{^1\text{H}\}$ NMR spectrum of **5** in acetone- d_6 at RT (100 MHz).

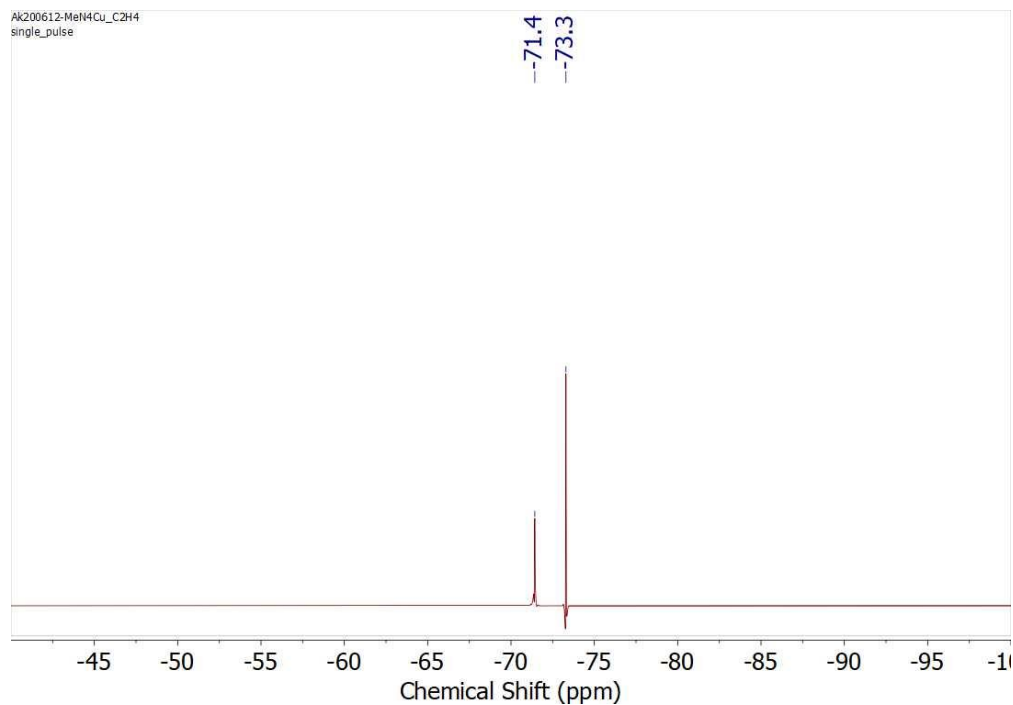


Figure S26. ^{19}F NMR spectrum of **5** in acetone- d_6 at RT (376 MHz).

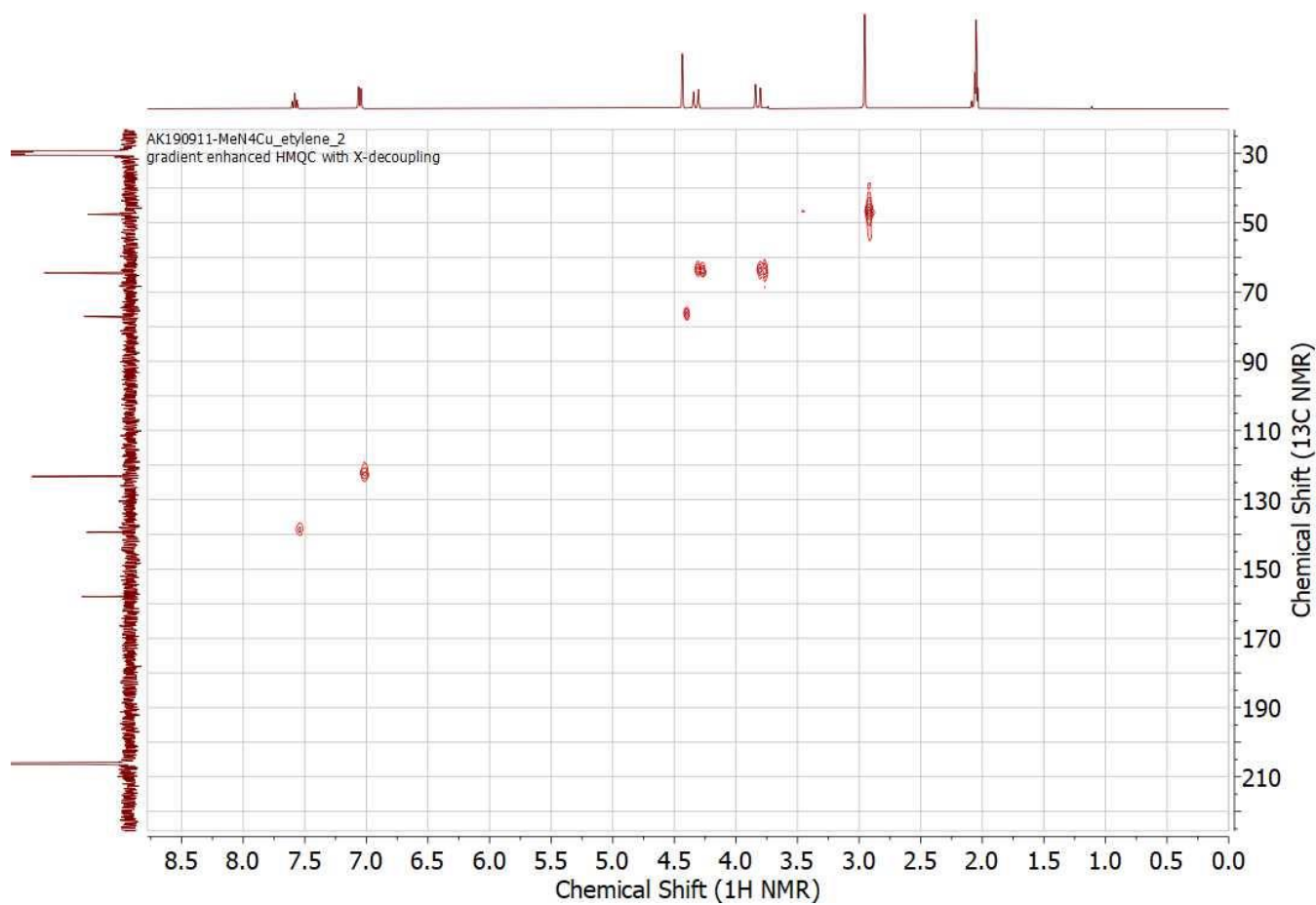


Figure S27. ^1H - ^{13}C HMQC spectrum of **5** in acetone- d_6 at RT.

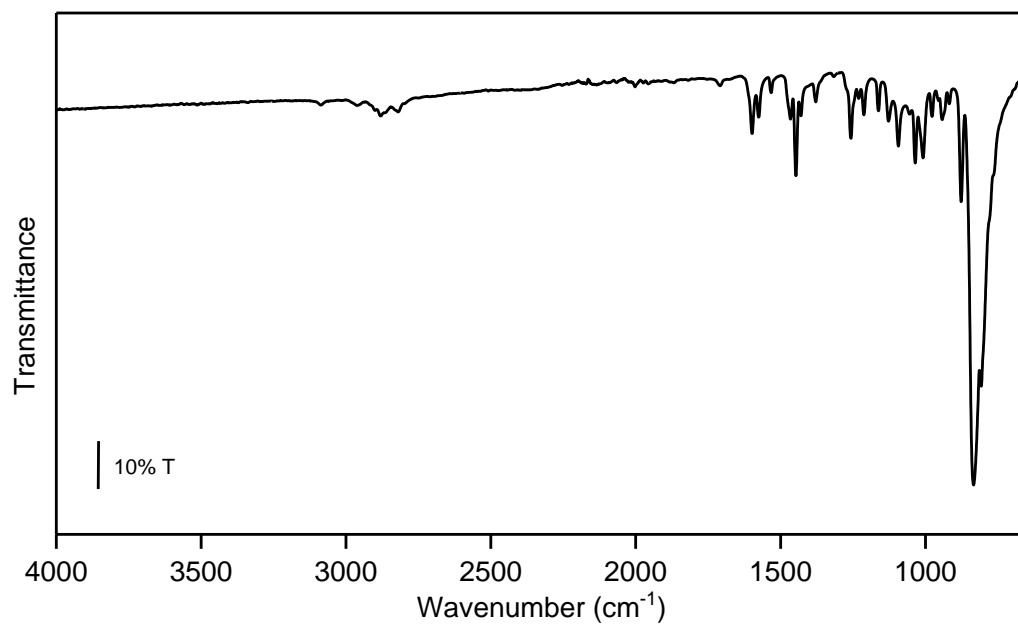


Figure S28. FT-IR spectrum of **5**.

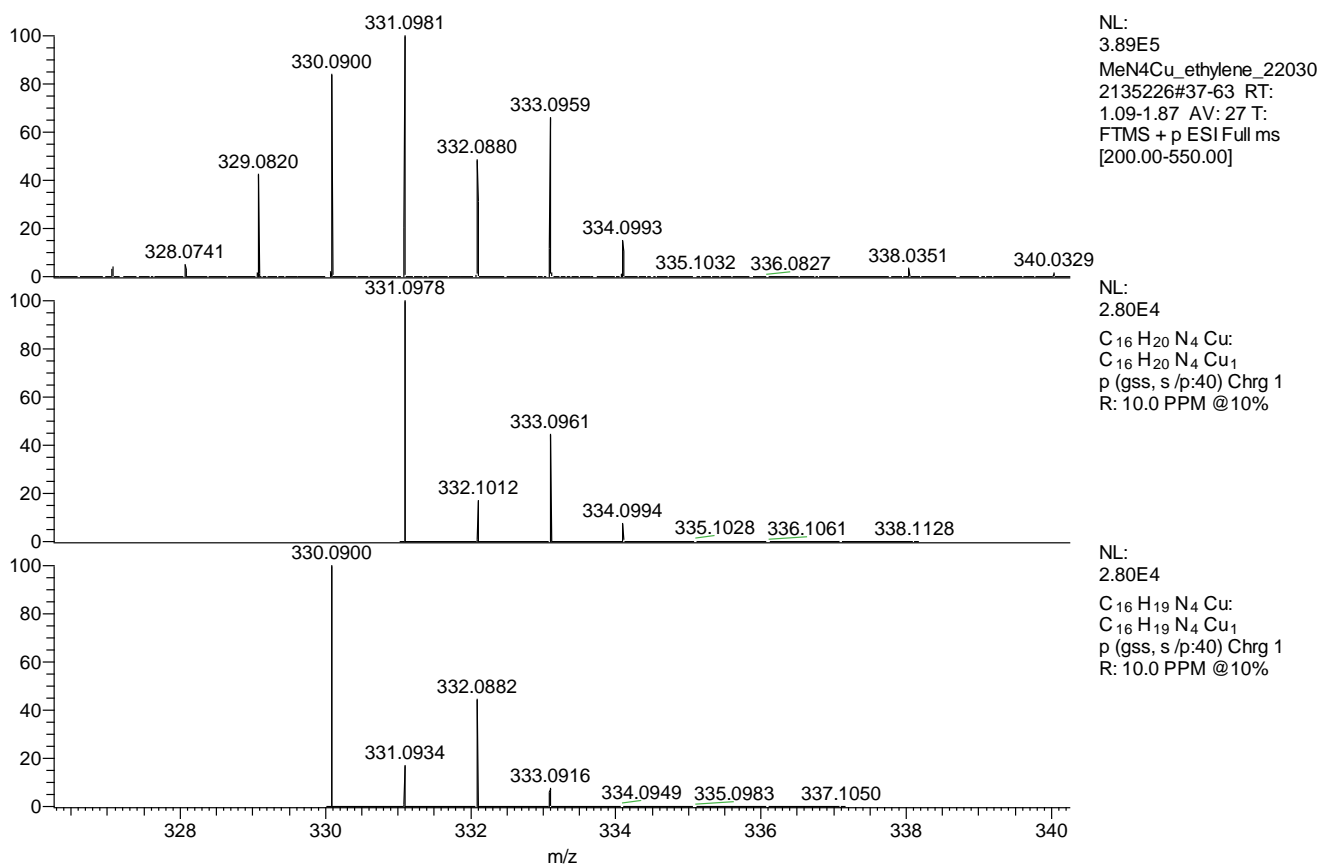


Figure S29. ESI HRMS analysis of 5.

Characterization of 6

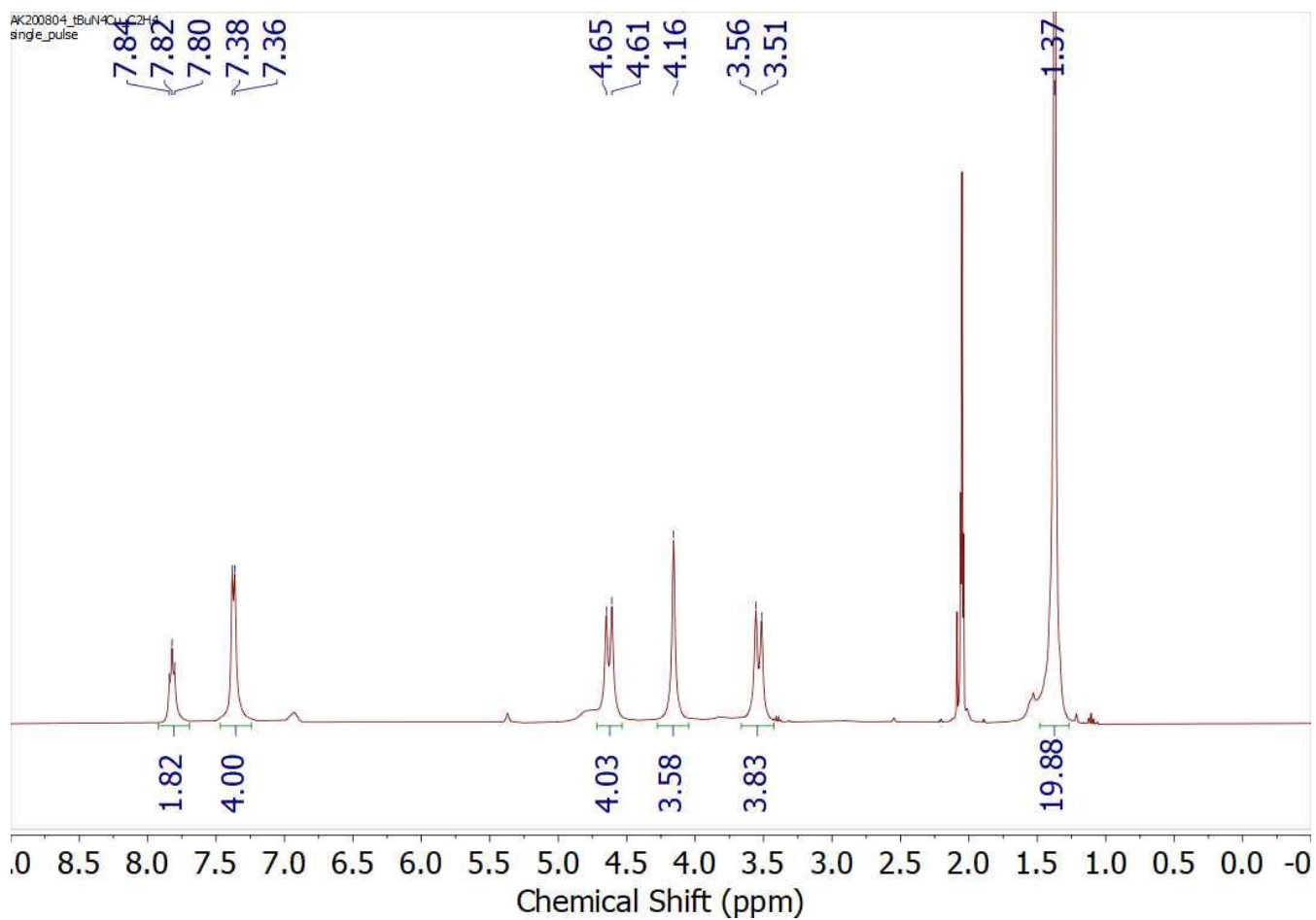


Figure S30. ^1H NMR spectrum of **6** in acetone- d_6 at RT (400 MHz).

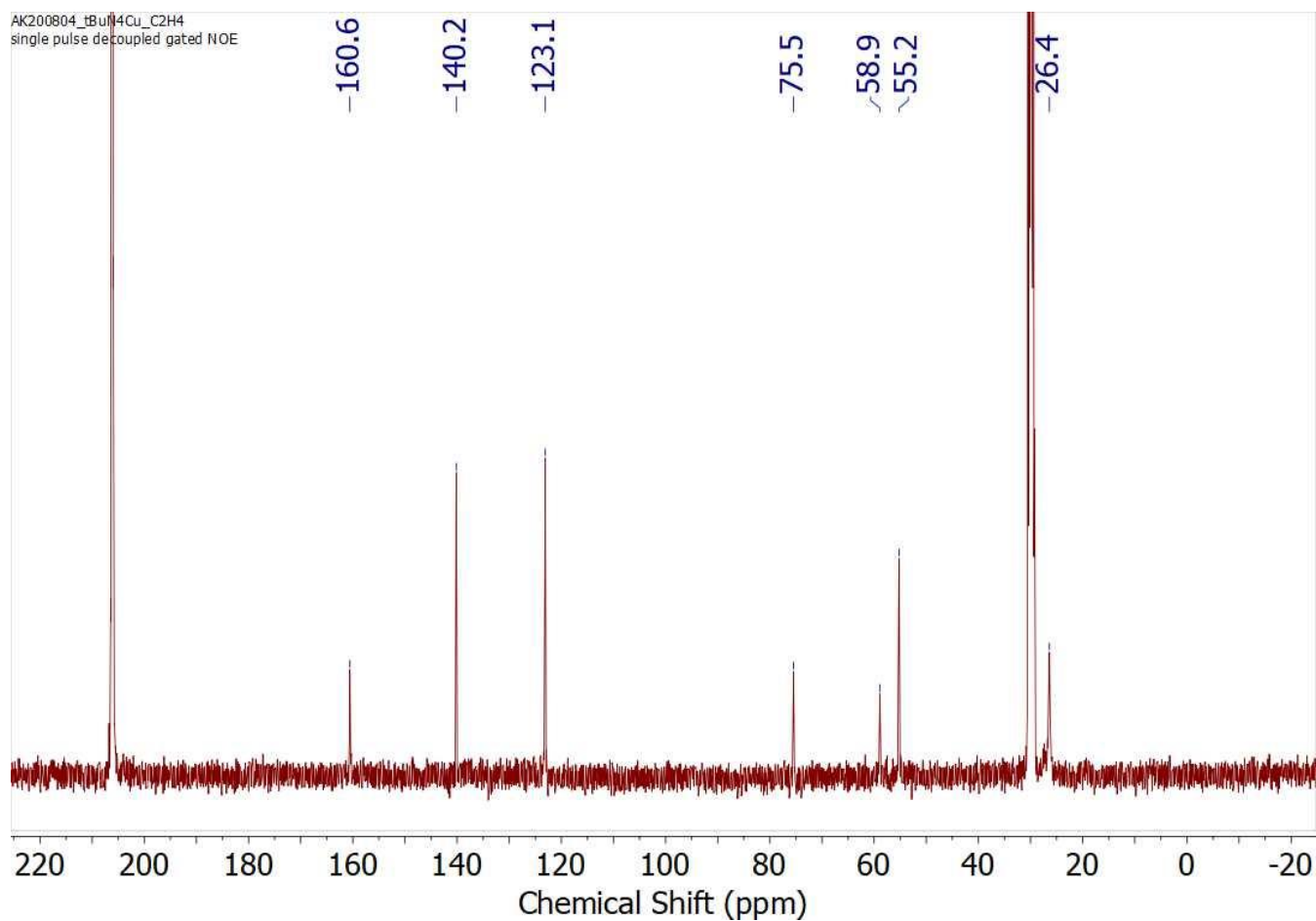


Figure S31. $^{13}\text{C}\{^1\text{H}\}$ NMR spectrum of **6** in acetone- d_6 at RT (100 MHz).

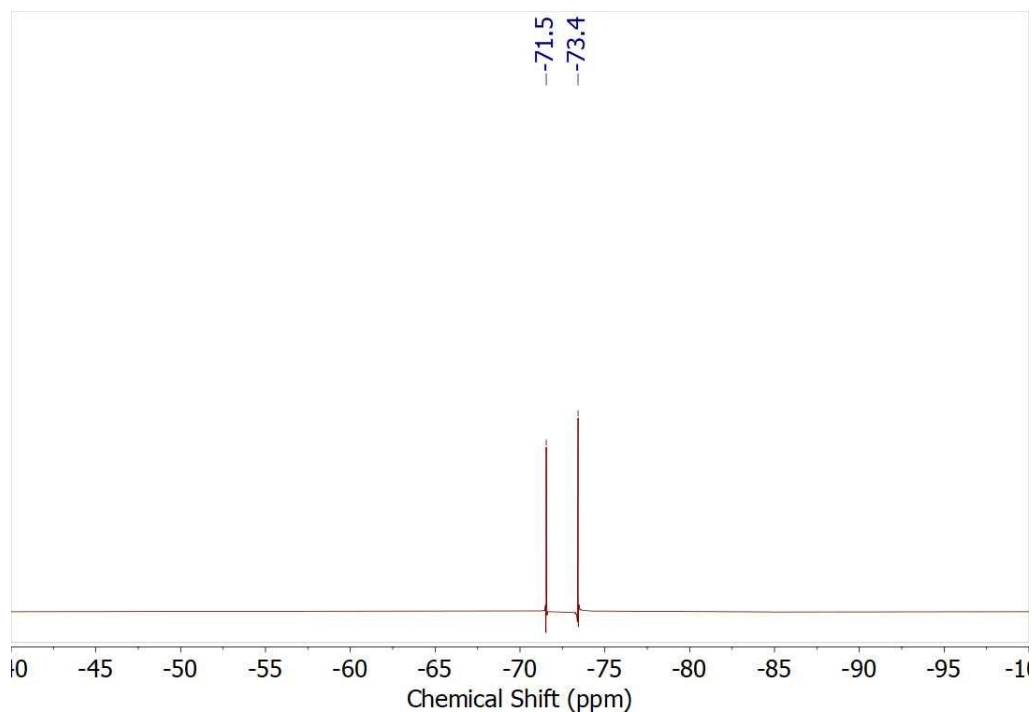


Figure S32. ^{19}F NMR spectrum of **6** in acetone- d_6 at RT (376 MHz).

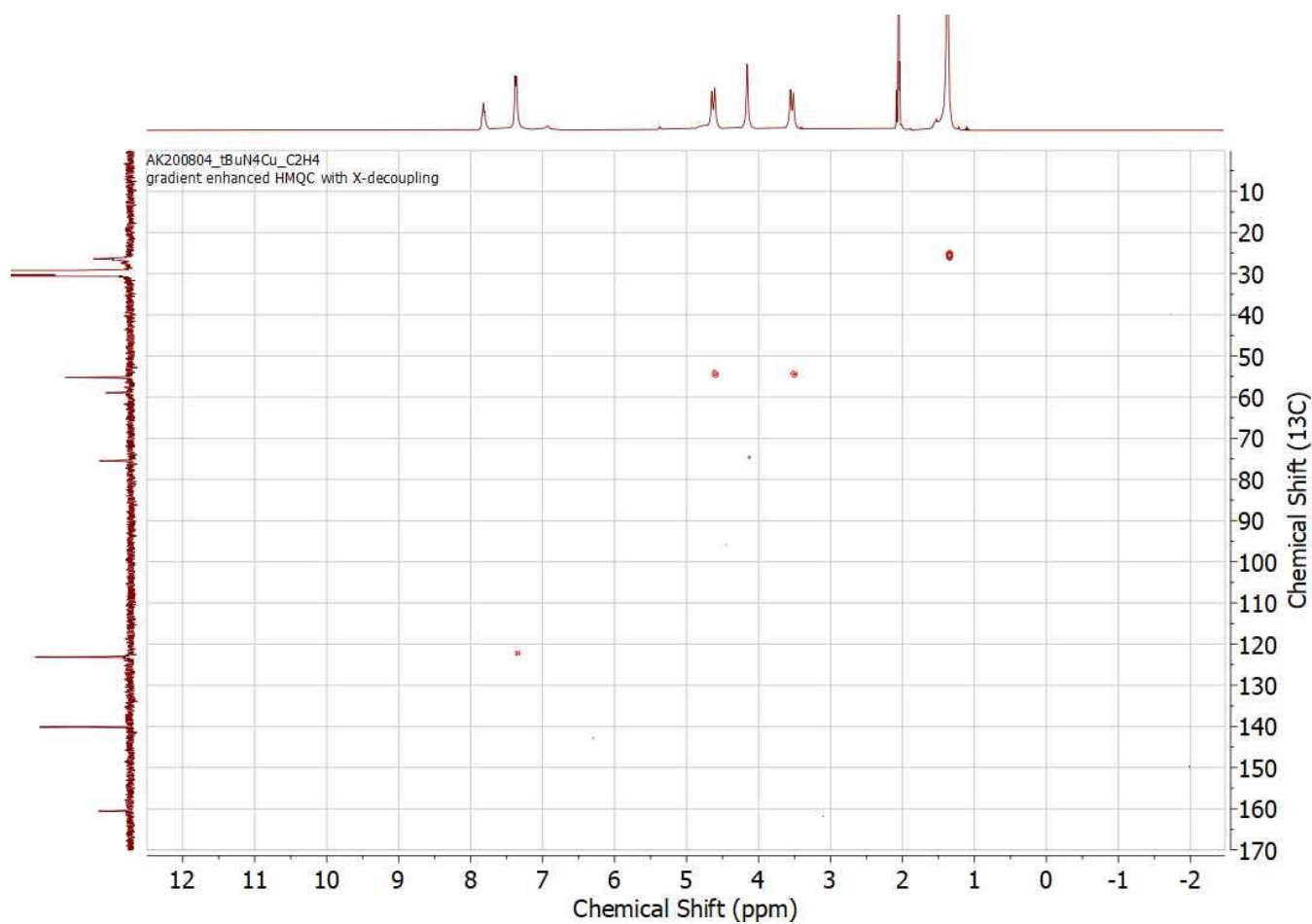


Figure S33. ^1H - ^{13}C HMQC spectrum of **6** in acetone- d_6 at RT.

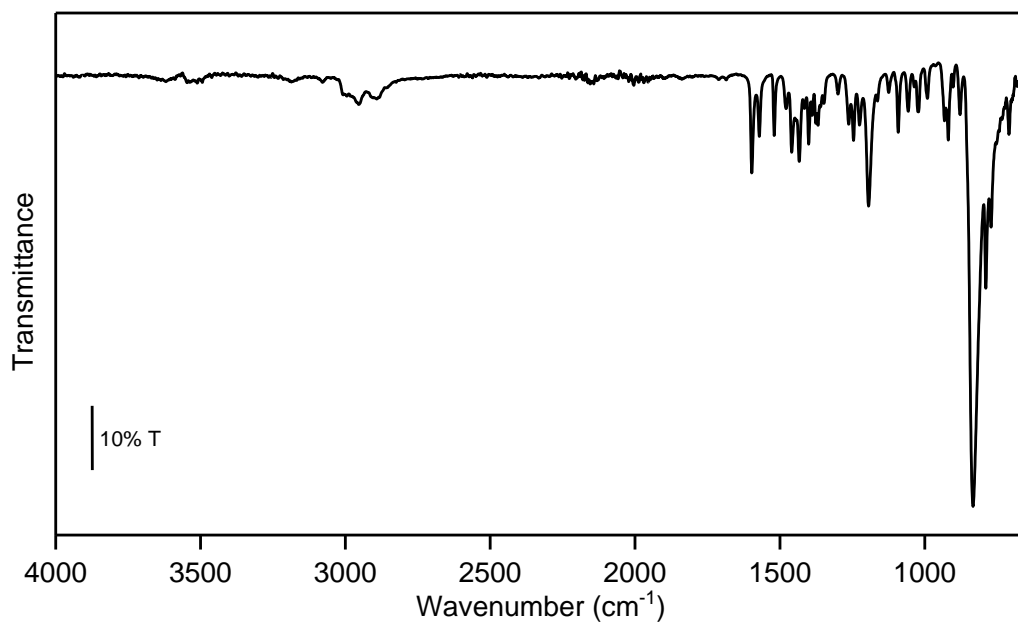


Figure S34. FT-IR spectrum of **6**.

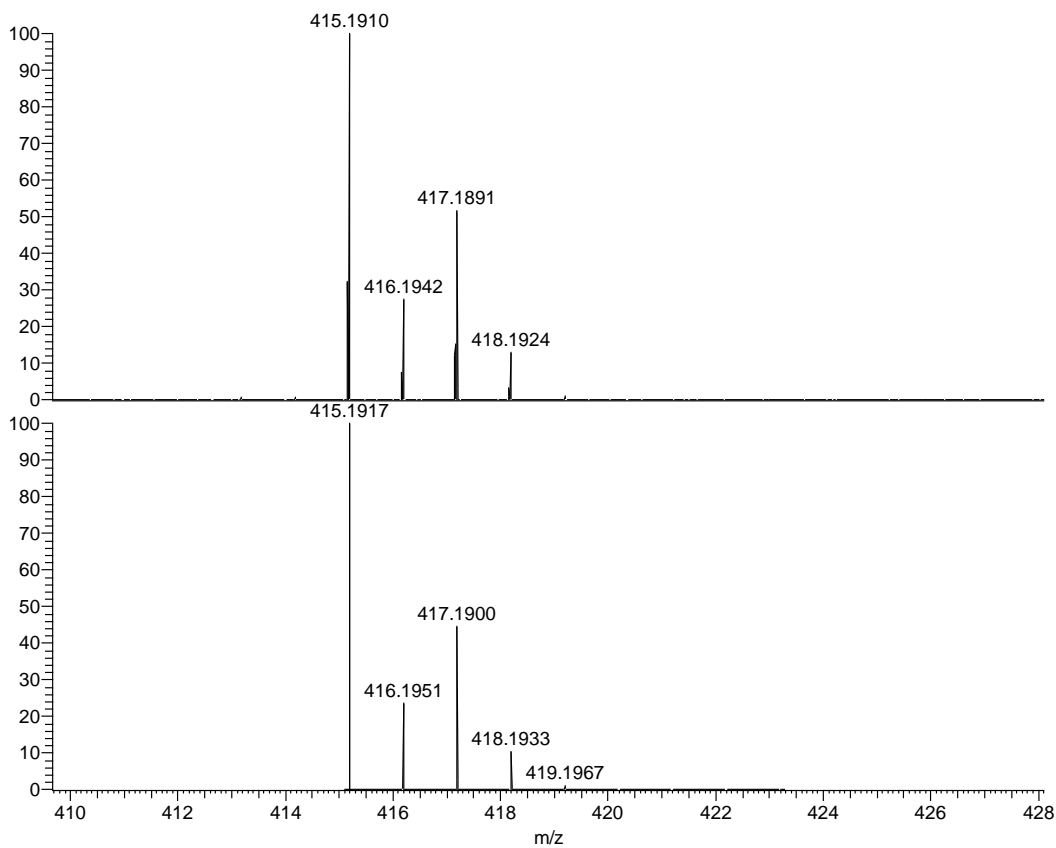


Figure S35. HRMS spectrum of **Cu6**.

Characterization of 7

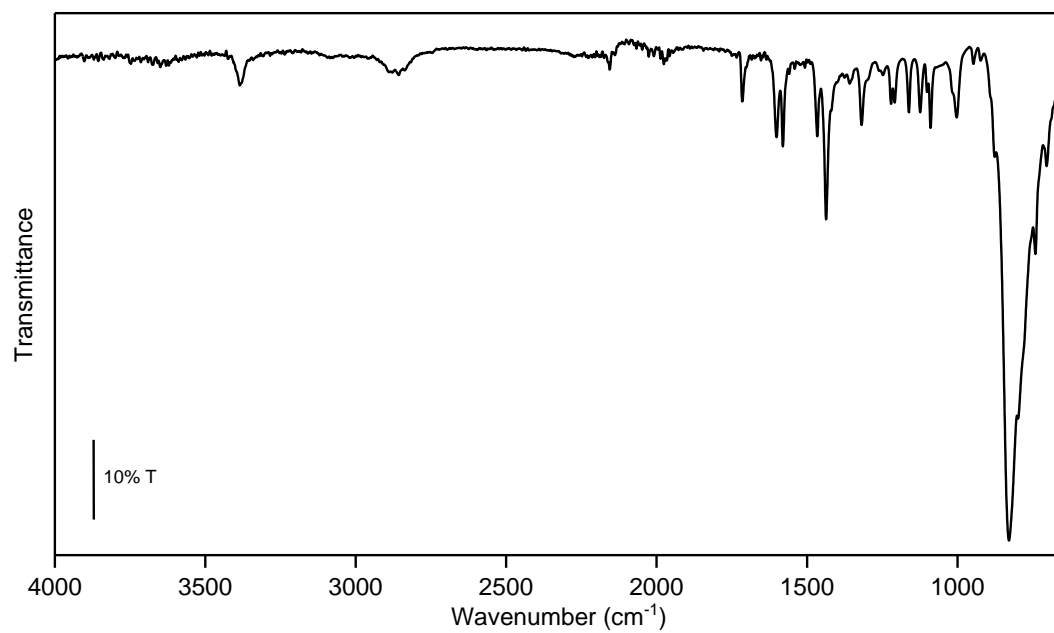


Figure S36. FT-IR spectrum of complex 7.

NMR spectra comparison before and after reaction with ethylene or MeCN

NMR spectra of 1 and 3 in acetone-*d*₆ before and after bubbling ethylene

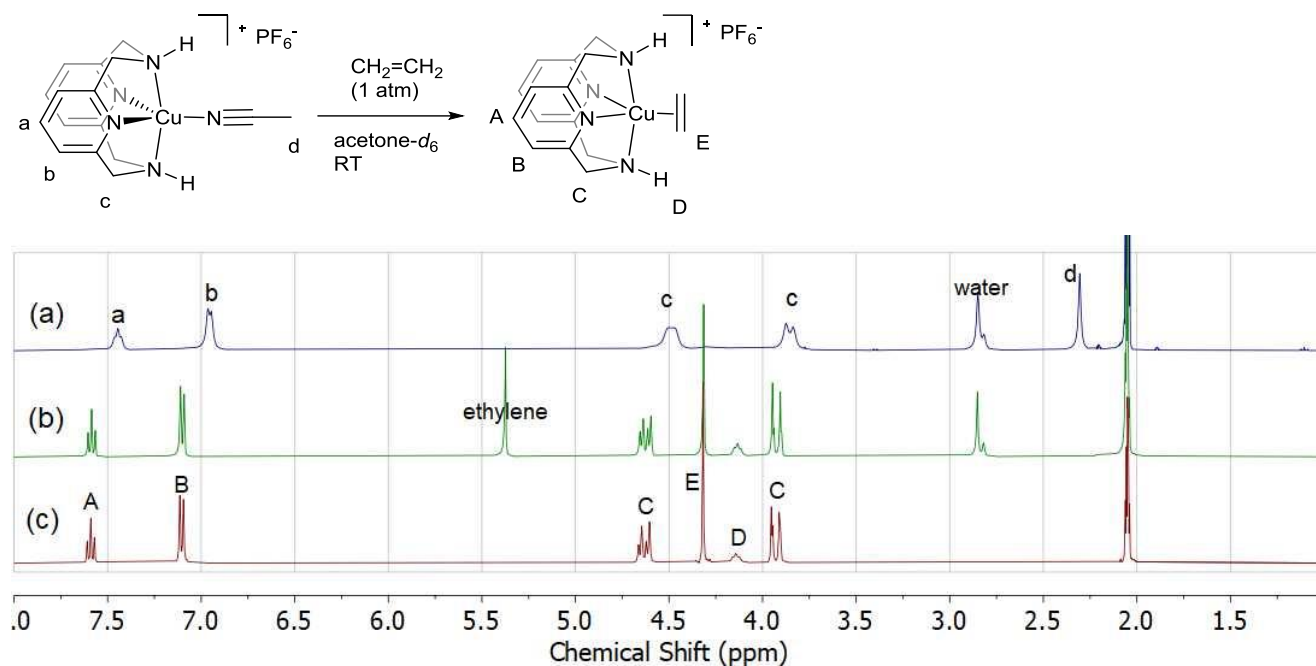


Figure S37. ^1H NMR spectrum of **1** in acetone- d_6 at 25 °C: (a) before and (b) after exposure to ethylene gas, and (c) isolated **4**.

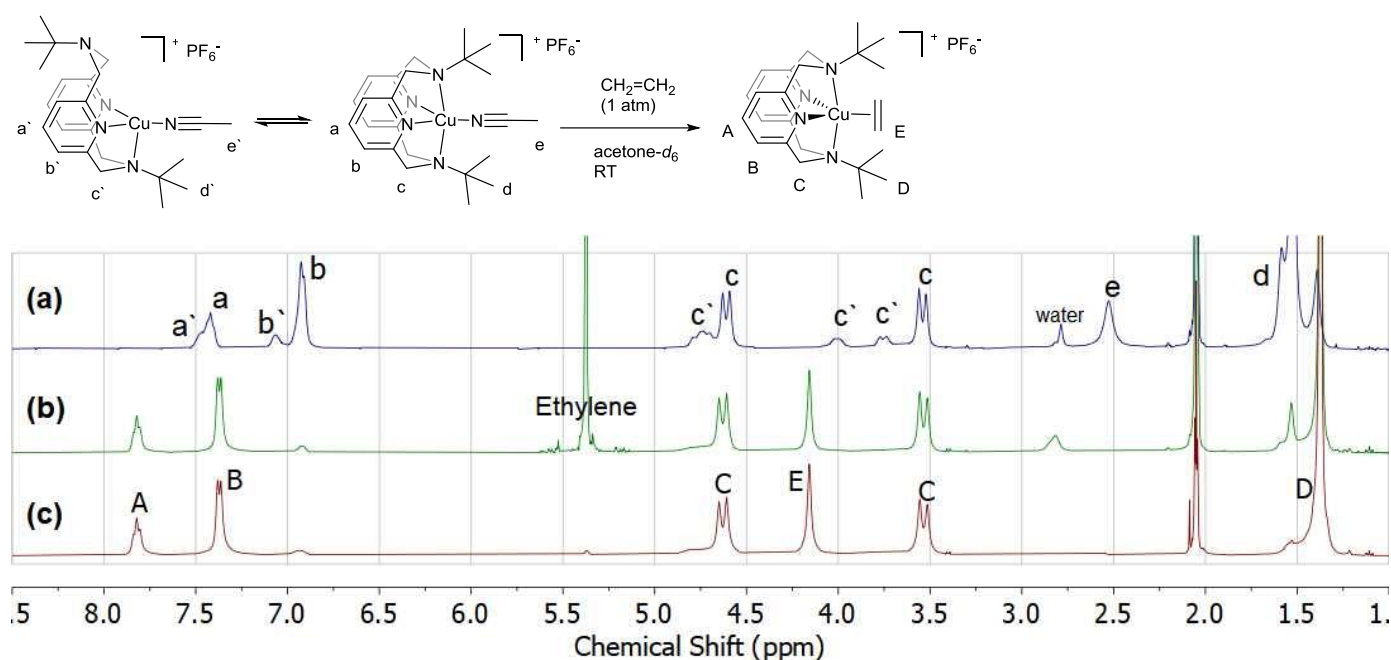


Figure S38. ^1H NMR spectrum of **3** in acetone- d_6 at 25 °C (a) before and (b) after exposure to ethylene gas, and (c) isolated **6**.

NMR spectra of 1–3 in acetonitrile-*d*₃ before and after exposure to ethylene

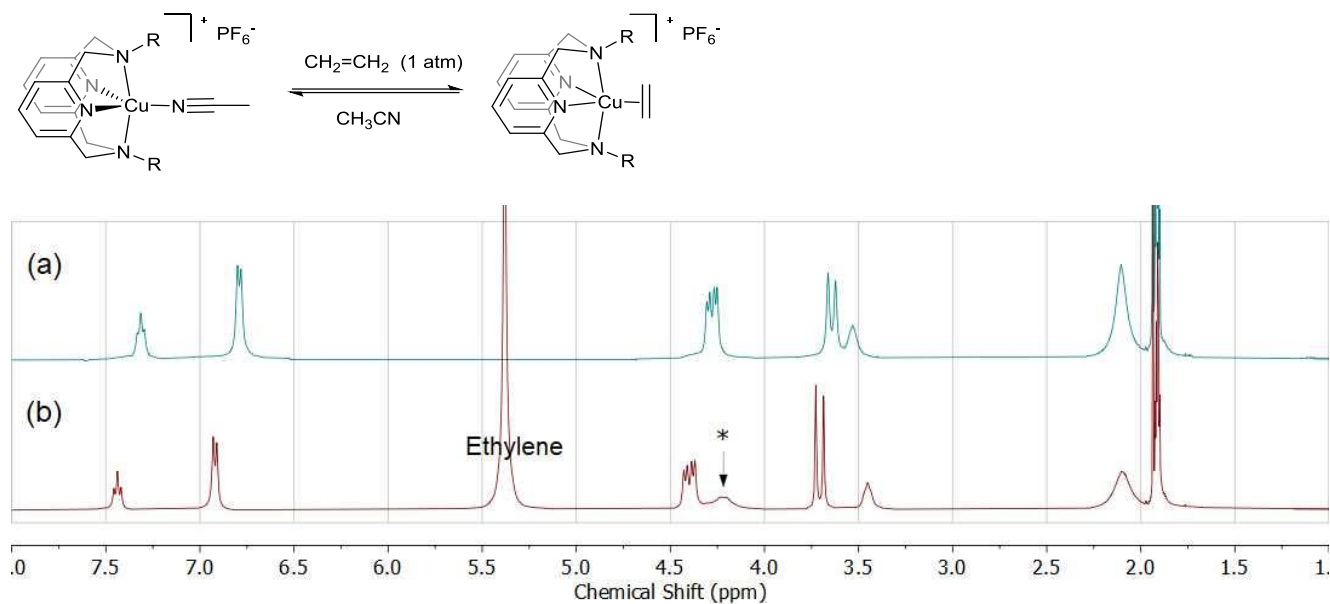


Figure S39. ¹H NMR spectra of **1** in CD₃CN under an Ar at 25 °C. (a) before and (b) after exposure to ethylene gas. The peak of coordinated ethylene is marked with as asterisk.

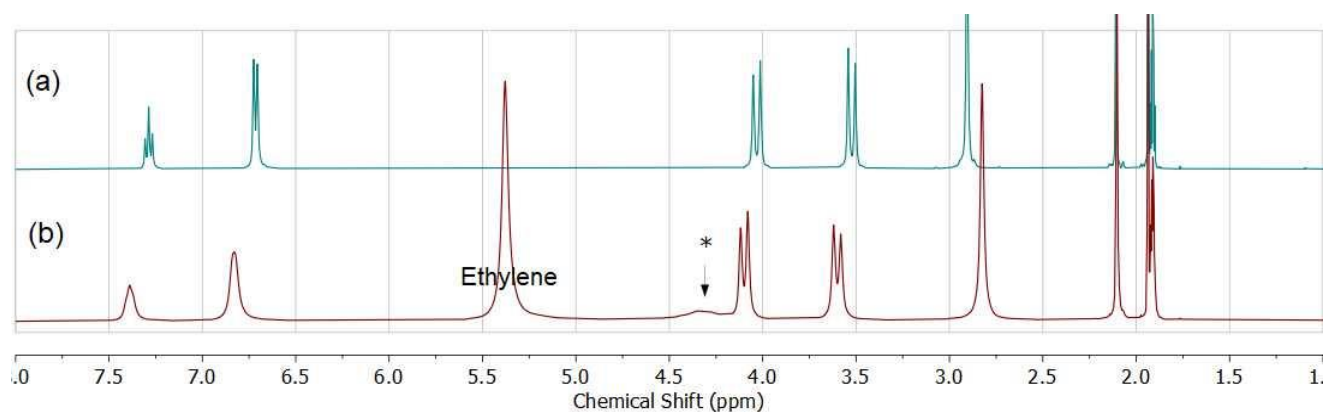


Figure S40. ¹H NMR spectra of **2** in CD₃CN under Ar. (a) before and (b) after exposure to ethylene gas. The peak of coordinated ethylene is marked with as asterisk.

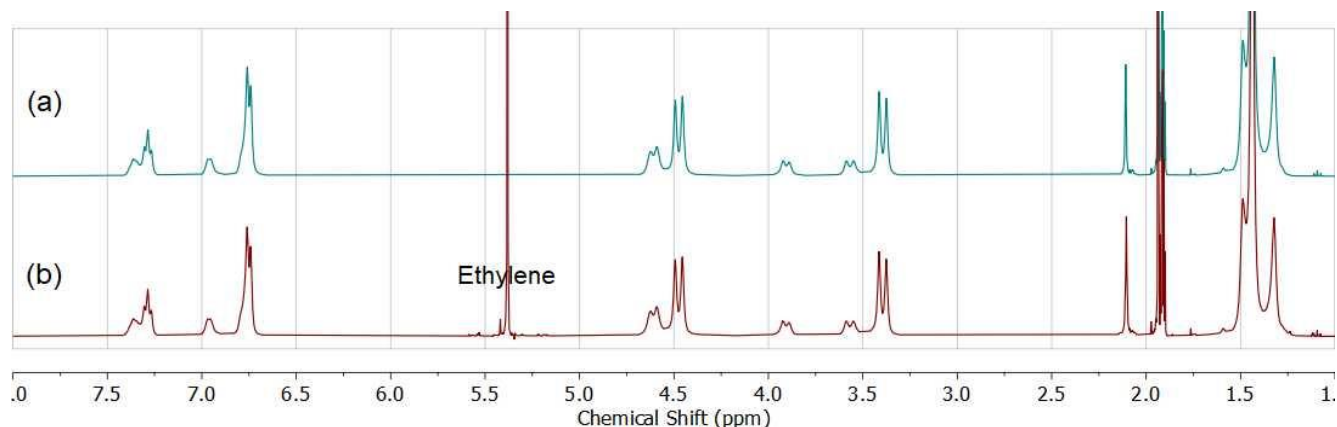


Figure S41. ¹H NMR spectra of **3** in CD₃CN under an Ar. (a) before and (b) after exposure to ethylene.

NMR spectra of 4–6 in acetonitrile- d_3

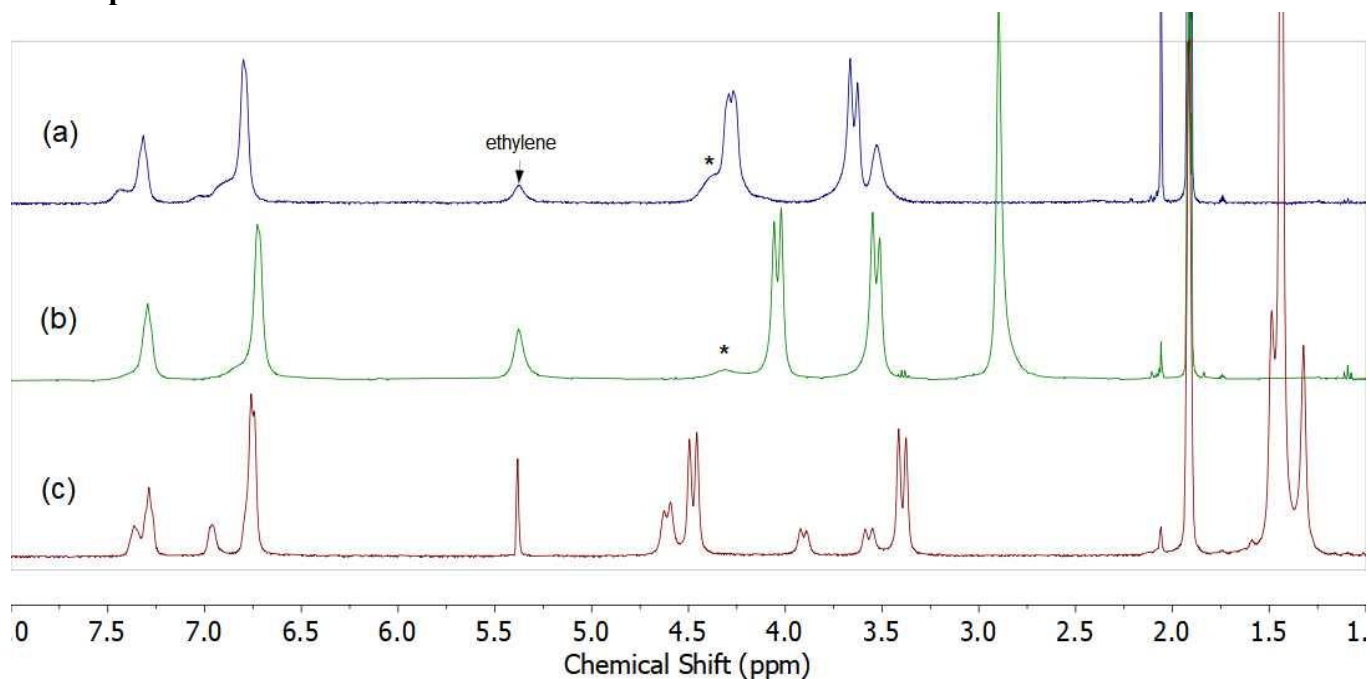


Figure S42. ^1H NMR spectra of (a) **4**, (b) **5**, and (c) **6** in acetonitrile- d_3 at 25 °C. The peak of coordinated ethylene is marked with as asterisk.

NMR spectra of free ethylene

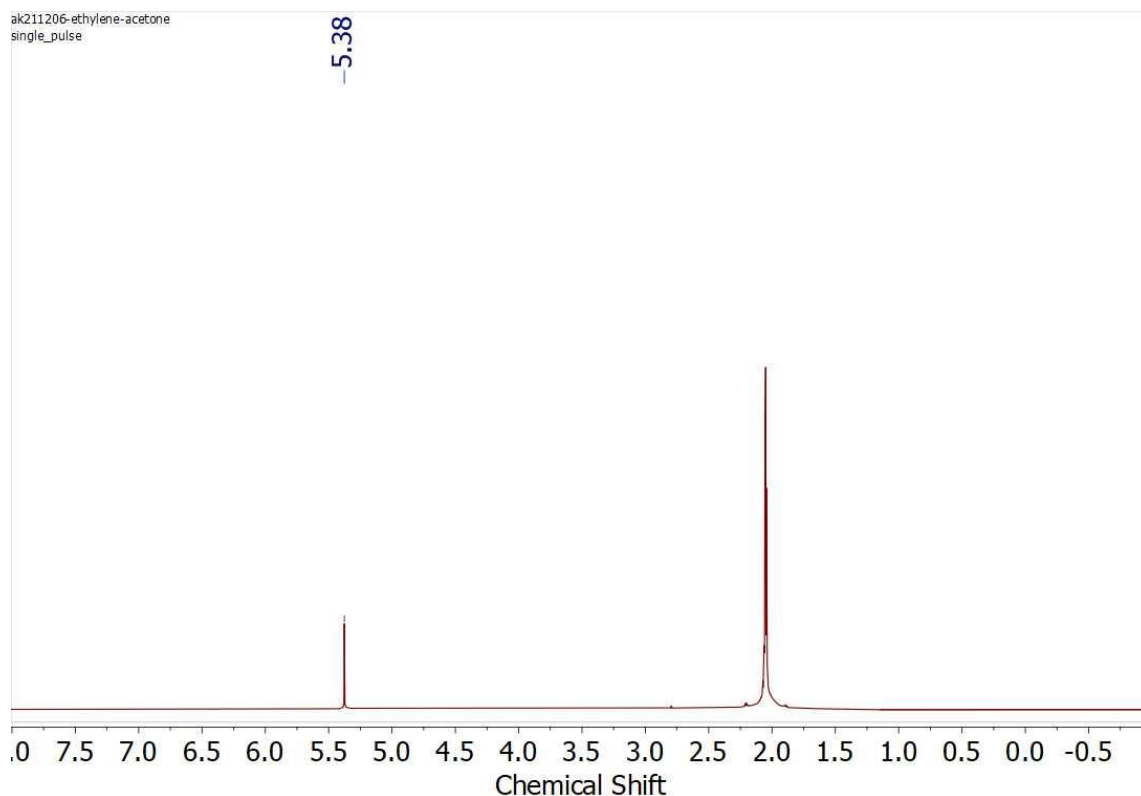


Figure S43. ^1H NMR spectrum of ethylene in acetone- d_6 at room temperature.

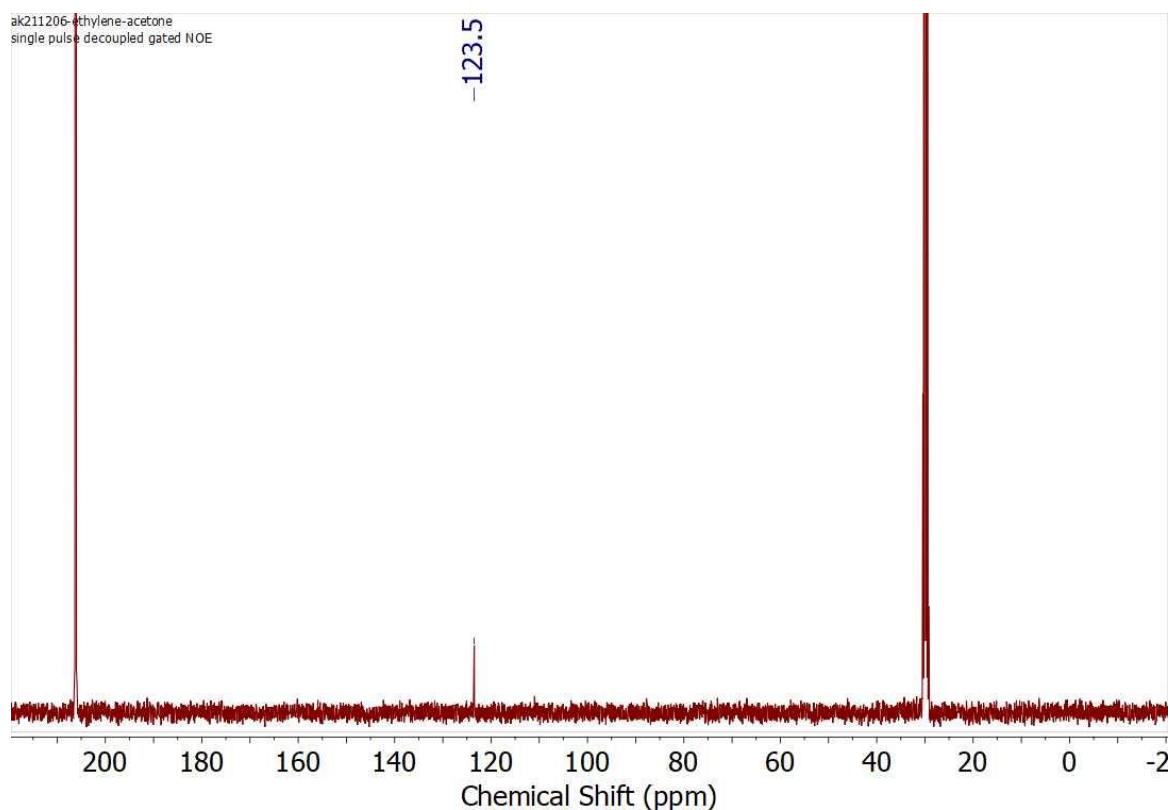


Figure S44. $^{13}\text{C}\{^1\text{H}\}$ NMR spectrum of ethylene in acetone- d_6 at room temperature (100 MHz).

NMR spectra of 4-6 in the presence of variable amounts of MeCN

In a glove box, complex **4** (1.0 mg, 2.10 μmol) was dissolved in acetone- d_6 (0.5 mL) in a J. Young NMR tube to give 4.2 mM acetone solution. The NMR tube was taken out of the glove box, then NMR spectrum of the solution was measured. And the tube was brought into the glove box, and acetonitrile (1.0 μL , 19 μmol) was added to the solution with a microsyringe. After measuring NMR, an additional portion of acetonitrile (1.0, 5.0, or 10 μL) was added in the glovebox, followed by NMR analysis. After addition of excess acetonitrile (total 40 μL , 766 μmol , 365 equiv), the NMR tube was connected to three-way stopcock that was connected to the vacuum pump and ethylene gas source, and then the atmosphere was replaced by ethylene.

The same experiments were also conducted using complex **5** (2.0 mg, 3.96 μmol) and complex **6** (2.4 mg, 4.07 μmol).

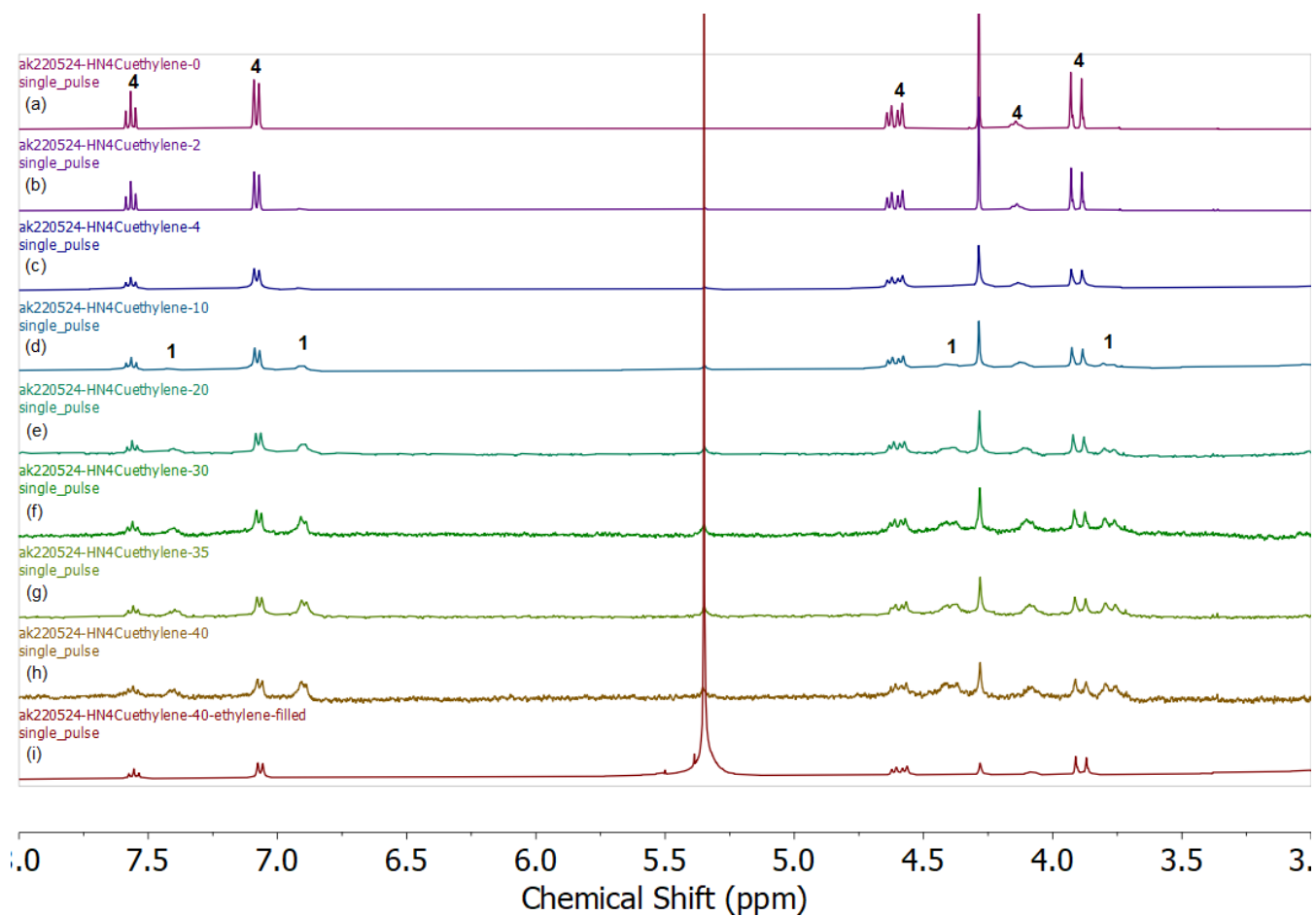


Figure S45. ^1H NMR spectra of **4** in acetone- d_6 at room temperature. (a) before addition of MeCN (b) after addition of MeCN (18 eq) (c) (37 eq) (d) (91 eq) (e) (182 eq) (f) (273 eq) (g) (319 eq) (h) (365 eq) (i) After purging ethylene gas in the presence of 365 eq. of MeCN.

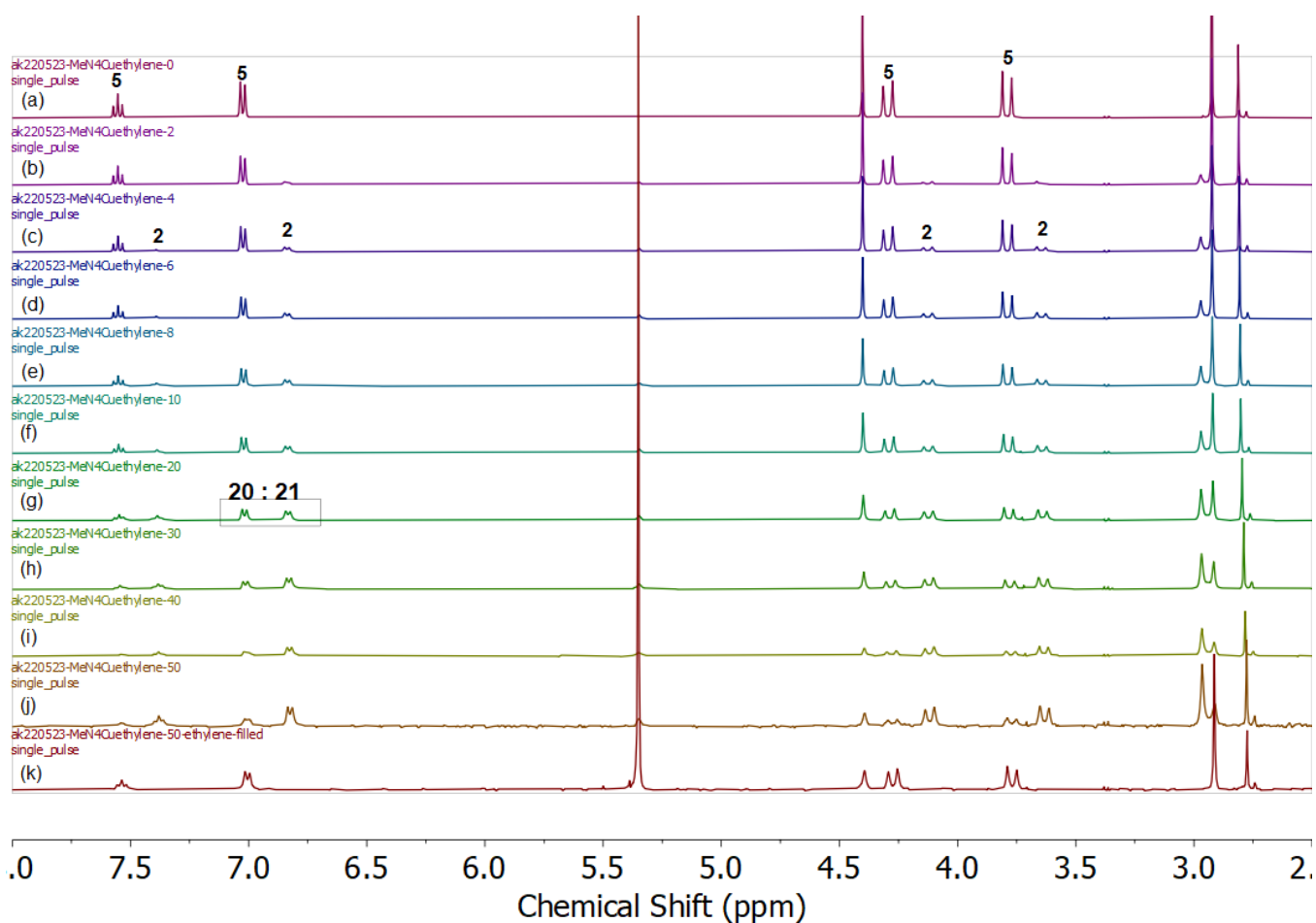


Figure S46. ¹H NMR spectra of **5** in acetone-*d*₆ at room temperature (a) before addition of MeCN (b) after addition of MeCN (9.7 eq) (c) (19 eq) (d) (29 eq) (e) (39 eq) (f) (48 eq) (g) (97 eq) (h) (145 eq) (i) (193 eq) (j) (242 eq) (k) After purging ethylene gas in the presence of 242 eq. of MeCN.

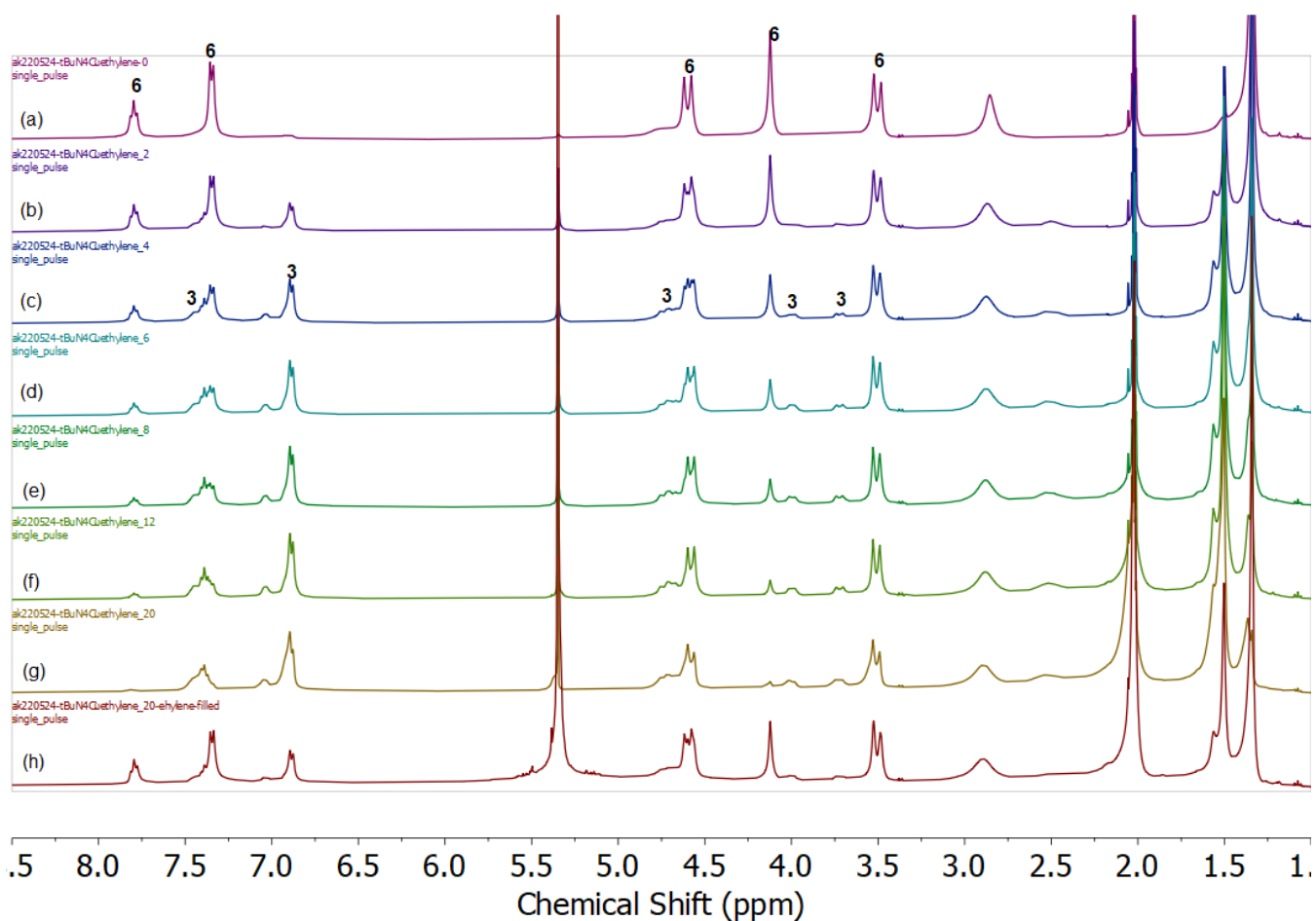


Figure S47. ^1H NMR spectra of **6** in acetone- d_6 at room temperature. (a) before addition of MeCN (b) after addition of MeCN (3.8 eq) (c) (7.6 eq) (d) (12 eq) (e) (15 eq) (f) (23 eq) (g) (38 eq) (h) After purging ethylene gas in the presence of 38 eq. of MeCN.

Cyclic voltammograms

Cyclic voltammograms of 4–6 under ethylene gas flow

Cyclic voltammograms were measured using solutions of 4–6 (1 mM) in 0.1 M solution of $n\text{Bu}_4\text{NPF}_6$ in acetone; 100 mV/s scan rate, Pt working electrode ($d = 1.6$ mm). All potentials were referenced against ferrocene ($\text{Fc}/\text{Fc}^+ = 0.18$ V). CV of 1–3 were also measured under Ar gas with the same condition. CVs were measured three times in different conditions as follows.

CVs were measured three times in different conditions as follows.

First, the solution was purged with ethylene gas for 5 min, then CV was measured. Then after purging with Ar gas for 5 min, 16 equivalents of MeCN was added, and the CV was measured again. For the final measurement, the solution was purged with ethylene gas 5 min.

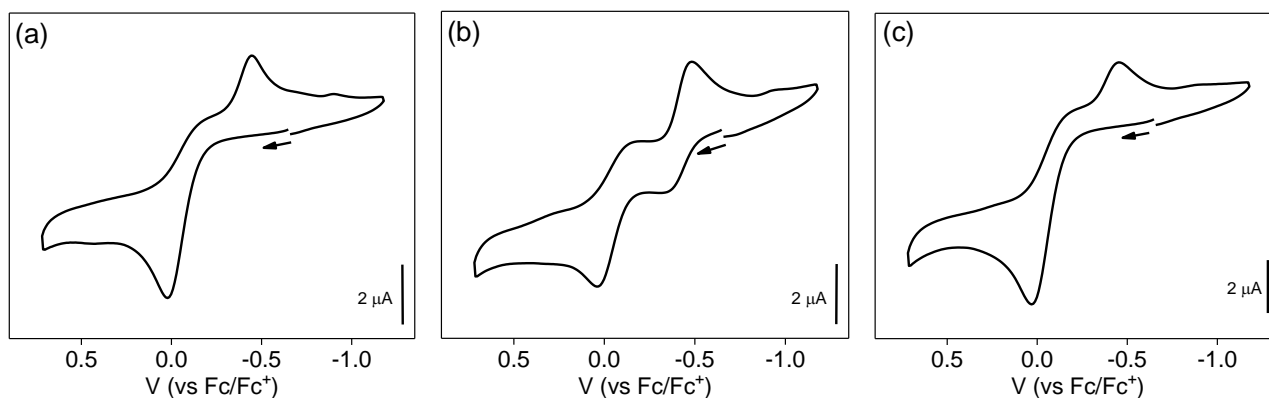


Figure S48. Cyclic voltammogram of 4 (a) under ethylene, (b) in the presence of 16 equiv of acetonitrile under Ar, and (c) in the presence of 16 equiv of acetonitrile under ethylene.

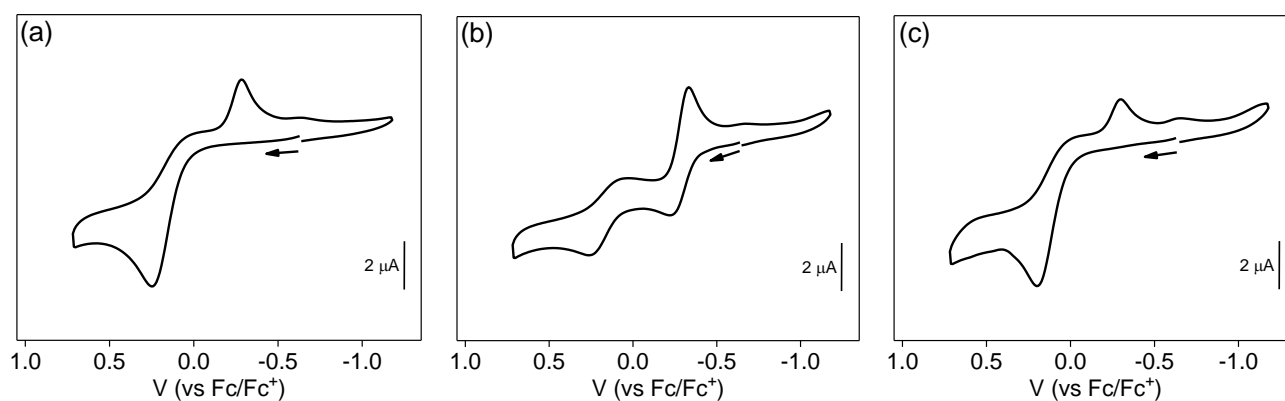


Figure S49. Cyclic voltammogram of 5 (a) under ethylene, (b) in the presence of 16 equiv of acetonitrile under Ar, and (c) in the presence of 16 equiv of acetonitrile under ethylene.

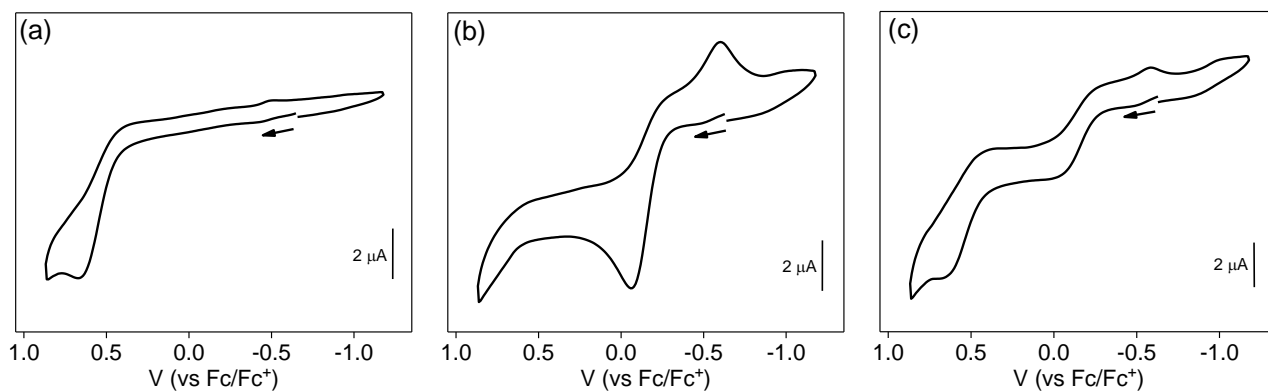


Figure S50. Cyclic voltammogram of **6** (a) under ethylene, (b) in the presence of 16 equiv of acetonitrile under Ar, and (c) in the presence of 16 equiv of acetonitrile under ethylene.

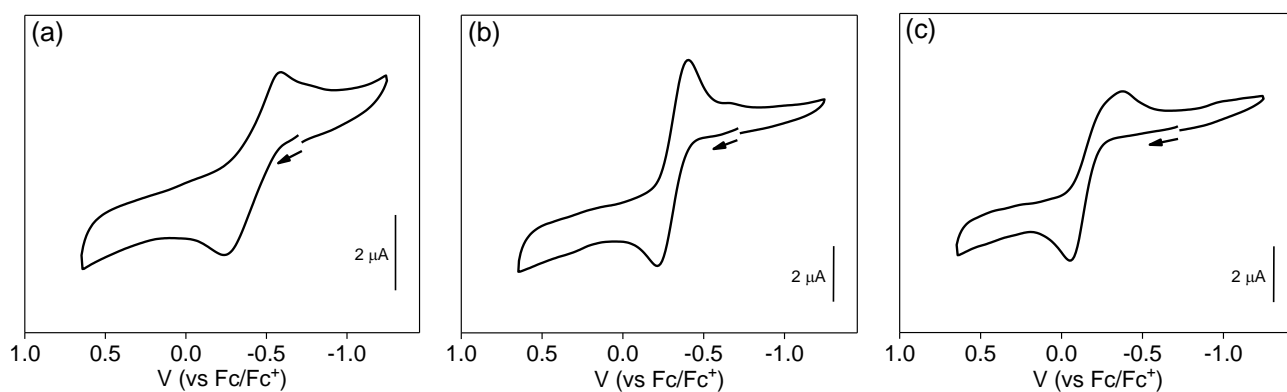


Figure S51. Cyclic voltammogram of (a) **1** (b) **2**, and (c) **3** under Ar gas atmosphere.

UV-vis spectra

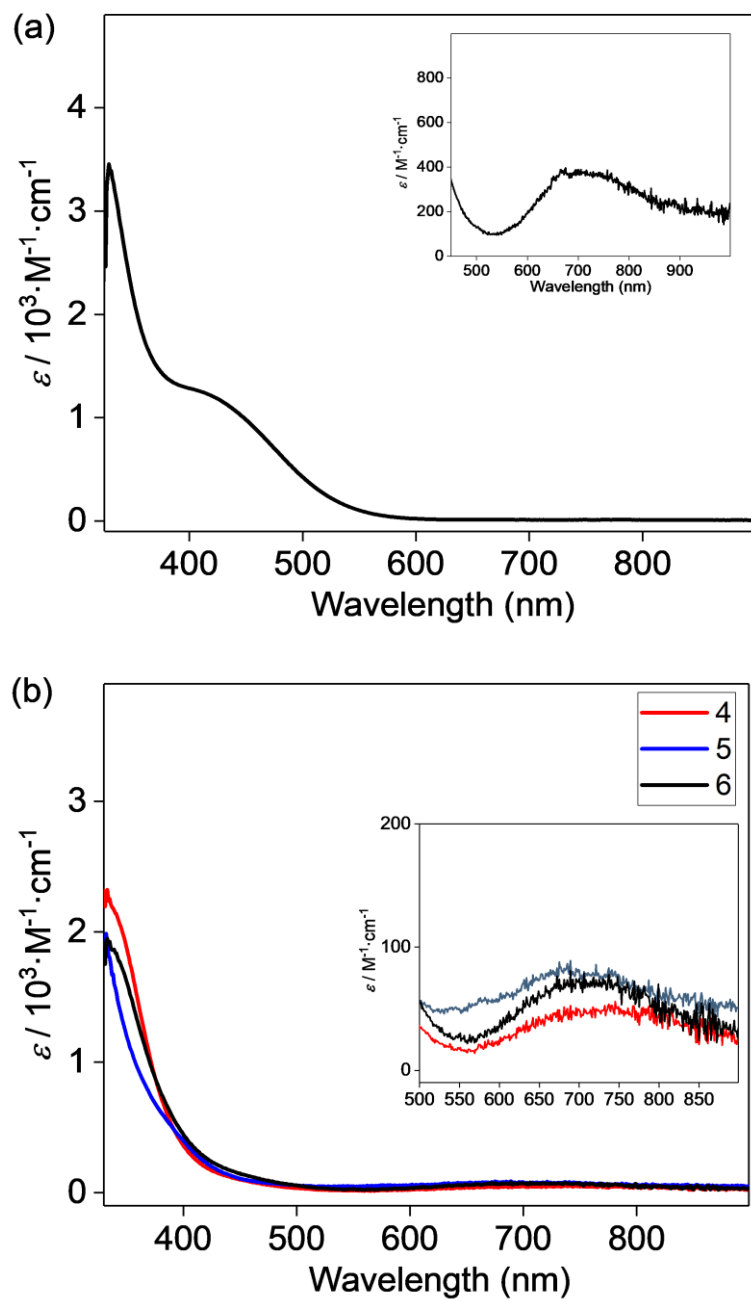


Figure S52. UV-vis absorption spectra of (a) 2 and (b) 4–6 in acetone at 25 °C.

Photoluminescent properties

Table S1. Photoluminescence properties of **2** and **4–6** in solid under N₂ gas flow.

Complex	R	In crystal		In PMMA	
		λ_{\max} (nm)	PLQY	λ_{\max} (nm)	PLQY
2	Me	702	0.01	645	0.04
4	H	n.d.	n.d.	n.d.	n.d.
5	Me	589	0.14	637	0.06
6	<i>t</i> Bu	435	<0.01	482	0.07

Poly(methylmethacrylate) (PMMA) films containing 1 wt% of **4**, **5**, or **6** were prepared as follows. In a glove box, a powder of PMMA (99 mg) was dissolved in dry THF (1.5 mL) in a 20 mL glass vial. 1.0 mg of **4**, **5**, or **6** was dissolved in dry acetone (0.5 mL), then added to the THF solution of PMMA, followed by slow evaporation under reduced pressure, and further dried under vacuum for 1 day.

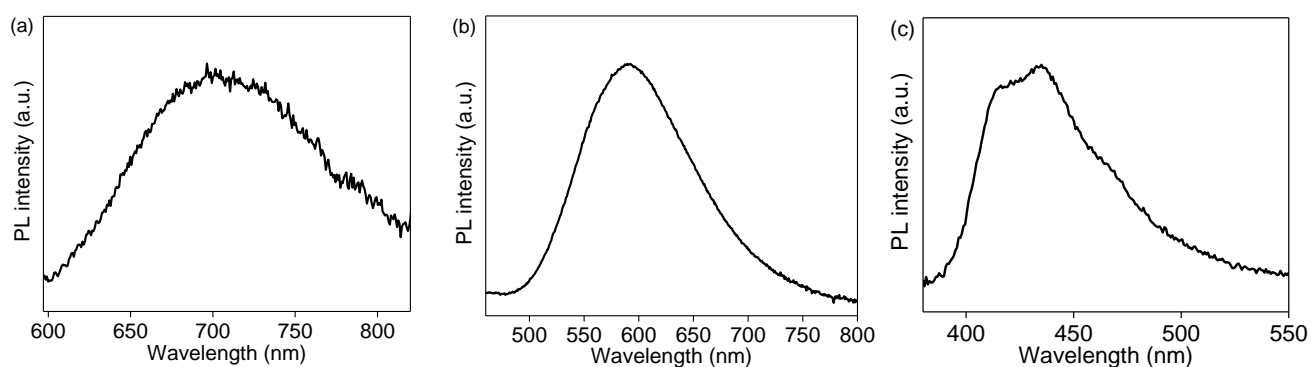


Figure S53. Photoluminescence spectra of (a) **2** and (b) **5**, and (c) **6** in crystalline solid.

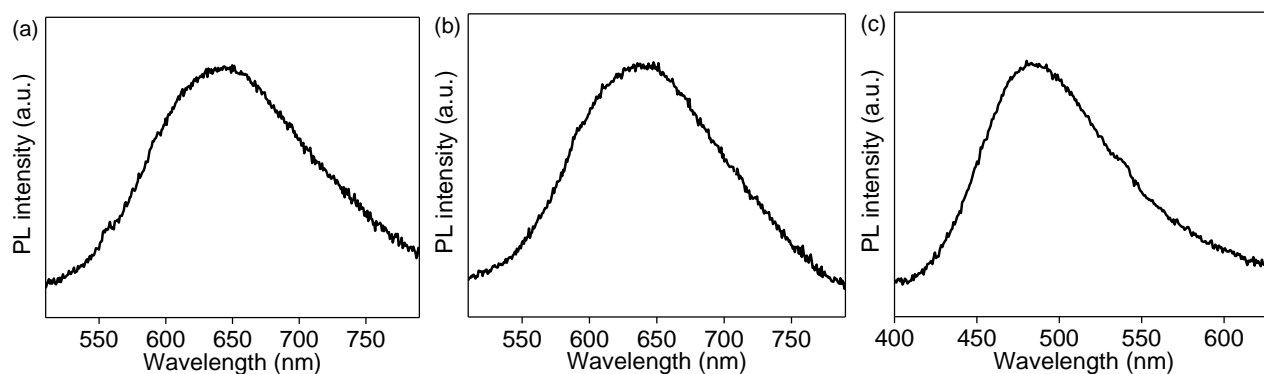


Figure S54. Photoluminescence spectra of (a) **5** and (b) **6** in PMMA.

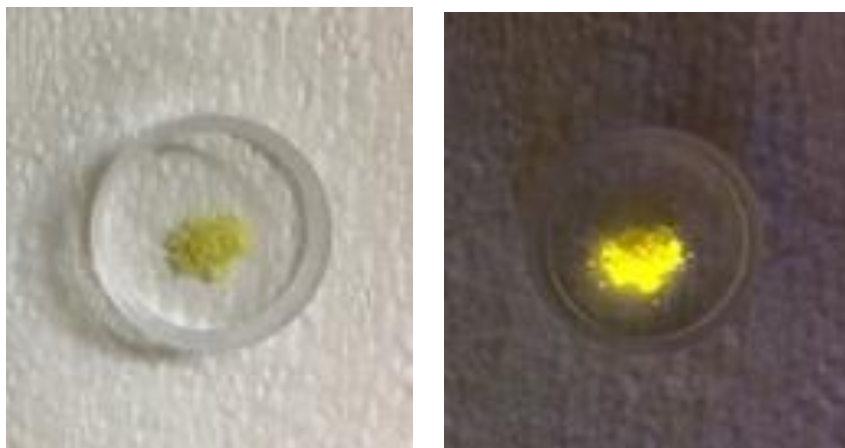


Figure S55. Photographs of crystalline powder of **5** on a quartz dish (left) under room light (right) under UV light.

Summary of representative reported mononuclear Cu^I-ethylene complexes

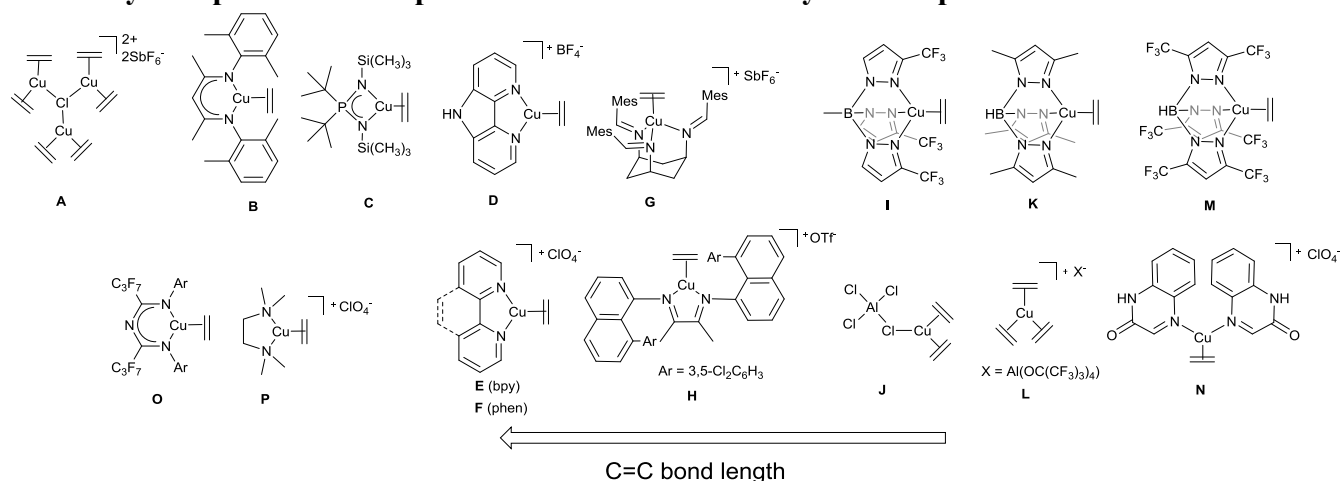


Chart S1. The representative Cu^I ethylene complexes.

Table S2. Comparison of C=C bond lengths and coordinated ethylene NMR chemical shifts in complexes shown in Chart 1.

Complex	C=C bond length (Å)	Reference	Chemical shift of C ₂ H ₄
A	1.375(8)–1.397(7)	6	
B	1.365(3)	7	δ_{H} 2.92, δ_{C} 74.74 (C ₆ D ₆)
C	1.362(6)	8	δ_{H} 3.48, δ_{C} 73.0 (C ₆ D ₆)
D	1.359(7)	9	δ_{H} 4.70, (CD ₃ COCD ₃)
E (bpy), F (phen)	1.360(13), 1.346(18) (bpy) 1.361(22) (phen)	10	δ_{H} 4.84 (bpy) δ_{H} 5.02 (phen) ¹¹
G	1.347(6), (Ar = Mes)	12	δ_{H} 3.09, δ_{C} 85.8 (CD ₂ Cl ₂)
H	1.346(8)	13	δ_{H} 4.01, δ_{C} 88.9 (X = OTf)
I	1.334(4)	14	δ_{H} 4.80, δ_{C} 85.4 (CDCl ₃)
J	1.34	15	
K	1.329(9)	16	δ_{H} 4.41 (CD ₂ Cl ₂)
L	1.30(1)–1.33(1)	6, 17	δ_{H} 5.47, δ_{C} 122 (CD ₂ Cl ₂)
M	1.325(9)	18	δ_{H} 4.98, δ_{C} 89.5 (C ₆ D ₁₂)
N	1.32 (1)	19	δ_{H} 5.22, (CD ₃ COCD ₃)
O	1.361(4) (Ar = 2-(NO ₂)C ₆ H ₄) 1.332(12) (Ar = 4-(NO ₂)C ₆ H ₄) 1.355(5) (Ar = 2-(CF ₃)C ₆ H ₄) 1.370(3) (Ar = 2-F,6-(CF ₃)C ₆ H ₃)	20	δ_{H} 3.51, δ_{C} 85.4 (Ar = 2-(NO ₂)C ₆ H ₄) δ_{H} 3.68, δ_{C} 87.6 (Ar = 4-(NO ₂)C ₆ H ₄) δ_{H} 3.48, δ_{C} 85.3 (Ar = 2-(CF ₃)C ₆ H ₄) δ_{H} 3.59, δ_{C} 85.2 (Ar = 2-F,6-(CF ₃)C ₆ H ₃) (CDCl ₃)
P	1.36(2)	21	δ_{H} 4.16 (CD ₃ COCD ₃ , -90 °C)

X-ray structure determination details

The X-ray diffraction data for the single crystals **4-7** were collected on a Rigaku XtaLab PRO instrument (κ -goniometer) with a PILATUS3 R 200K hybrid pixel array detector using Mo $K\alpha$ (0.71073 Å) [for **6** and **7**] or Cu $K\alpha$ (1.54184 Å) [for **4** and **5**] radiation monochromated by means of multilayer optics. The performance mode of MicroMaxTM-003 microfocus sealed X-ray tube was 50 kV, 0.60 mA. The diffractometer was equipped with a Rigaku GN2 system for low temperature experiments. Suitable crystals of appropriate dimensions were mounted on MiTeGen loops in random orientations. Preliminary unit cell parameters were determined with three sets of a total of 10 narrow frame scans in the case of a Mo-source and six sets of a total of 10 narrow frame scans at two different 2θ positions in the case of a Cu-source. The data were collected according to recommended strategies in an ω scan mode. Final cell constants were determined by global refinement of reflections from the complete data sets using the Lattice wizard module. Images were indexed and integrated with “smart” background evaluation using the *CrysAlisPro* data reduction package (Rigaku Oxford Diffraction). Analysis of the integrated data did not show any decay. The data were corrected for systematic errors and absorption using the *ABSPACK* module: Numerical absorption correction based on Gaussian integration over a multifaceted crystal model and empirical absorption correction based on spherical harmonics according to the point group symmetry using equivalent reflections. The *GRAL* module and the *ASSIGN SPACEGROUP* routine of the *WinGX* suite were used for analysis of systematic absences and space group determination.

The structures were solved by *intrinsic* phasing approach using *SHELXT*-2018/2²² and refined by the full-matrix least-squares on F^2 using *SHELXL*-2018/3,²³ which uses a model of atomic scattering based on spherical atoms. Calculations were mainly performed using the *WinGX*-2021.3 suite of programs.²⁴ Non-hydrogen atoms were refined anisotropically. The positions of the hydrogen atoms of ethylene ligand and [N]H were determined by the difference Fourier maps, and these atoms were refined isotropically. The positions of hydrogen atoms of methyl groups were found using rotating group refinement with idealized tetrahedral angles or determined by the Fourier maps. The other hydrogen atoms were inserted at the calculated positions and refined as riding atoms.

Crystallographic data for **4**.

C₁₆H₂₀CuF₆N₄P, pale yellow plank (0.101 × 0.050 × 0.044 mm³), formula weight 476.87 g mol⁻¹; monoclinic, $P2_1/c$ (No. 14), $a = 13.24737(5)$ Å, $b = 12.50127(5)$ Å, $c = 22.95513(12)$ Å, $\beta = 96.8516(4)^\circ$, $V = 3774.43(3)$ Å³, $Z = 8$, $Z' = 2$, $T = 95(2)$ K, $d_{\text{calc}} = 1.678$ g cm⁻³, $\mu(\text{Cu } K\alpha) = 3.069$ mm⁻¹, $F(000) = 1936$; $T_{\text{max/min}} = 1.000/0.804$; 63512 reflections were collected ($3.879^\circ \leq \theta \leq 75.735^\circ$, index ranges: $-16 \leq h \leq 16$, $-15 \leq k \leq 15$, and $-27 \leq l \leq 28$), 7838 of which were unique, $R_{\text{int}} = 0.0336$, $R_\sigma = 0.0185$; completeness to θ of 75.735° 99.7 %. The refinement of 553 parameters with 12 restraints converged to $R1 = 0.0265$ and $wR2 = 0.0713$ for 7360 reflections with $I > 2\sigma(I)$ and $R1 = 0.0282$ and $wR2 = 0.0724$ for all data with goodness-of-fit $S = 1.048$ and residual electron density $\rho_{\text{max/min}} = 0.371$ and -0.361 e Å⁻³, rms 0.051; max shift/e.s.d. in the last cycle 0.003.

Crystallographic data for **5**.

C₁₈H₂₄CuF₆N₄P, pale yellow prism (0.129 × 0.067 × 0.036 mm³), formula weight 504.92 g mol⁻¹; tetragonal, *I4cm* (No. 108), *a* = 11.00109(8) Å, *c* = 17.2226(2) Å, *V* = 2084.34(4) Å³, *Z* = 4, *Z'* = 0.25, *T* = 95(2) K, *d*_{calc} = 1.609 g cm⁻³, μ(Cu *Kα*) = 2.814 mm⁻¹, *F*(000) = 1032; T_{max/min} = 1.000/0.658; 3871 reflections were collected (5.688° ≤ θ ≤ 75.693°, index ranges: -13 ≤ *h* ≤ 11, -13 ≤ *k* ≤ 10, and -21 ≤ *l* ≤ 21), 1086 of which were unique, *R*_{int} = 0.0248, *R*_σ = 0.0242; completeness to θ of 75.693° 99.2 %. The refinement of 90 parameters with 3 restraints converged to *R*1 = 0.0260 and *wR*2 = 0.0712 for 1063 reflections with *I* > 2σ(*I*) and *R*1 = 0.0266 and *wR*2 = 0.0716 for all data with goodness-of-fit *S* = 1.081 and residual electron density ρ_{max/min} = 0.651 and -0.289 e Å⁻³, rms 0.049; max shift/e.s.d. in the last cycle 0.000.

Crystallographic data for 6.

C₂₄H₃₆CuF₆N₄P, yellow plank (0.160 × 0.092 × 0.052 mm³), formula weight 589.08 g mol⁻¹; monoclinic, *C2/c* (No. 15), *a* = 15.7889(3) Å, *b* = 8.07430(13) Å, *c* = 20.8731(3) Å, β = 97.7210(16)°, *V* = 2636.88(8) Å³, *Z* = 4, *Z'* = 0.5, *T* = 93(2) K, *d*_{calc} = 1.484 g cm⁻³, μ(Mo *Kα*) = 0.952 mm⁻¹, *F*(000) = 1224; T_{max/min} = 1.000/0.662; 49861 reflections were collected (2.604° ≤ θ ≤ 32.229°, index ranges: -23 ≤ *h* ≤ 23, -11 ≤ *k* ≤ 12, and -31 ≤ *l* ≤ 30), 4462 of which were unique, *R*_{int} = 0.0418, *R*_σ = 0.0181; completeness to θ of 32.229° 95.5 %. The refinement of 176 parameters with 1 restraint converged to *R*1 = 0.0270 and *wR*2 = 0.0770 for 4116 reflections with *I* > 2σ(*I*) and *R*1 = 0.0302 and *wR*2 = 0.0788 for all data with goodness-of-fit *S* = 1.053 and residual electron density ρ_{max/min} = 0.527 and -0.488 e Å⁻³, rms 0.064; max shift/e.s.d. in the last cycle 0.001.

Crystallographic data for 7.

C₃₃H₄₂Cu₂F₁₂N₈OP₂, yellow prism (0.088 × 0.062 × 0.042 mm³), formula weight 983.76 g mol⁻¹; orthorhombic, *Imma* (No. 74), *a* = 18.1722(3) Å, *b* = 13.8167(3) Å, *c* = 15.4821(3) Å, *V* = 3887.25(12) Å³, *Z* = 4, *Z'* = 0.25, *T* = 93(2) K, *d*_{calc} = 1.681 g cm⁻³, μ(Mo *Kα*) = 1.275 mm⁻¹, *F*(000) = 2000; T_{max/min} = 1.000/0.827; 41143 reflections were collected (1.976° ≤ θ ≤ 29.447°, index ranges: -24 ≤ *h* ≤ 25, -19 ≤ *k* ≤ 17, and -21 ≤ *l* ≤ 21), 2877 of which were unique, *R*_{int} = 0.0584, *R*_σ = 0.0206; completeness to θ of 29.447° 99.8 %. The refinement of 164 parameters with 6 restraints converged to *R*1 = 0.0491 and *wR*2 = 0.1183 for 2727 reflections with *I* > 2σ(*I*) and *R*1 = 0.0510 and *wR*2 = 0.1191 for all data with goodness-of-fit *S* = 1.095 and residual electron density ρ_{max/min} = 1.373 and -0.637 e Å⁻³, rms 0.096; max shift/e.s.d. in the last cycle 0.000.

Deposition Numbers CCDC 2176964 (4), 2176965 (5), 2176966 (6), and 2176967 (7) contain the supplementary crystallographic data for this paper. These data are provided free of charge by the joint Cambridge Crystallographic Data Centre and Fachinformationszentrum Karlsruhe Access Structures service www.ccdc.cam.ac.uk/structures.

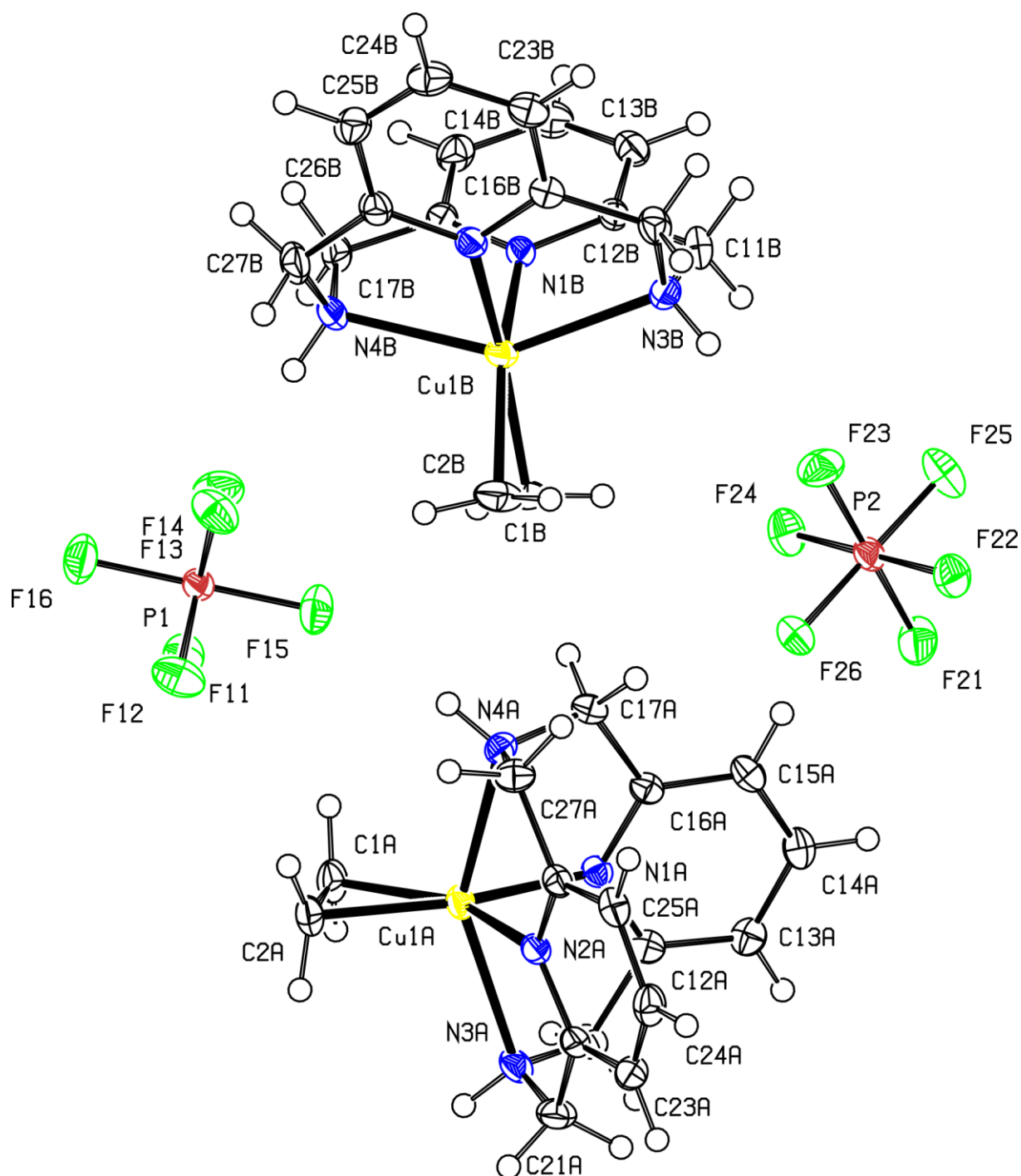


Figure S56. ORTEP at 50 % probability anisotropic displacement ellipsoids of non-hydrogen atoms for compound **4** according to SC-XRD. Selected interatomic distances [Å]: Cu1A–C1A 2.0228(16), Cu1A–C2A 2.0148(15), Cu1A–N1A 2.0334(12), Cu1A–N2A 2.0159(12), Cu1A–N3A 2.3858(13), Cu1A–N4A 2.3454(12), C1A–C2A 1.371(2), Cu1B–C1B 2.0039(15), Cu1B–C2B 2.0251(17), Cu1B–N1B 2.0238(12), Cu1B–N2B 2.0057(12), Cu1B–N3B 2.3572(13), Cu1B–N4B 2.3794(13), C1B–C2B 1.369(3).

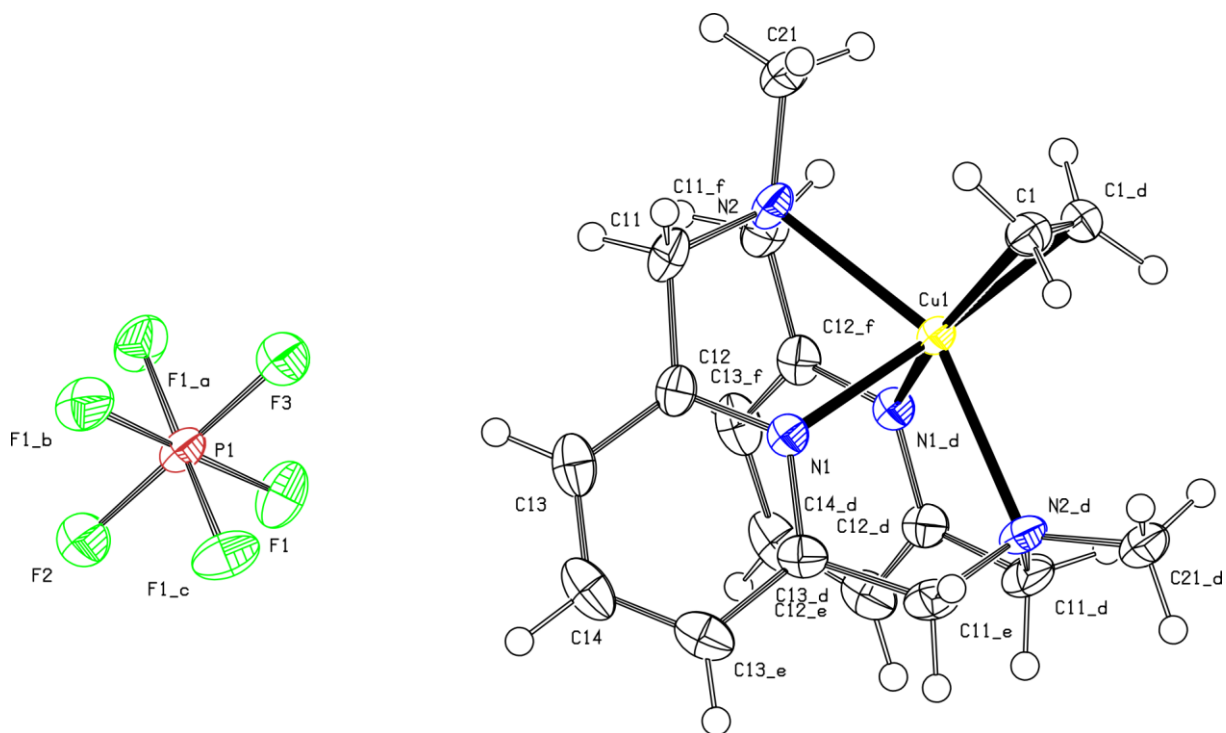


Figure S57. ORTEP at 50 % probability anisotropic displacement ellipsoids of non-hydrogen atoms for compound **5** according to SC-XRD data. Selected interatomic distances [Å]: Cu1–C1 2.033(4), Cu1–N1 2.047(3), Cu1–N2 2.389(3), C1–C1_d 1.359(7).

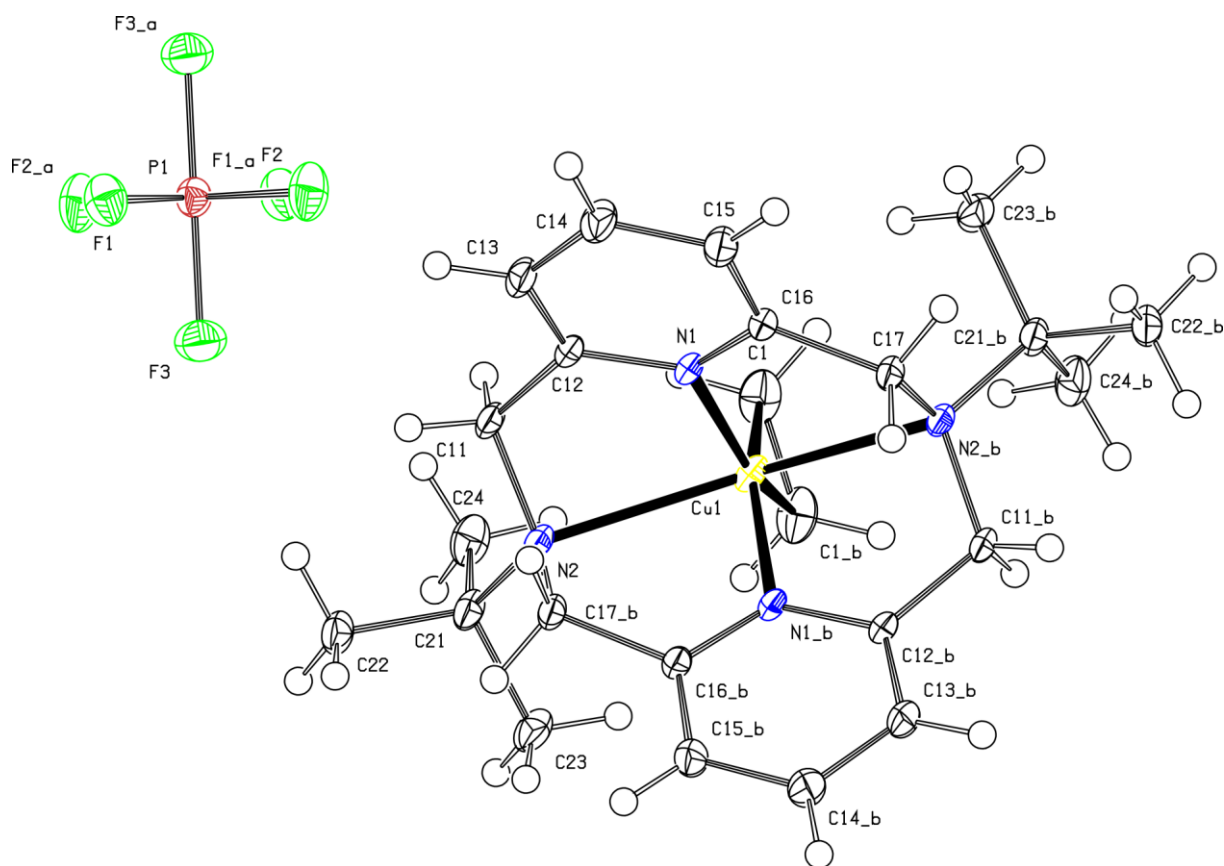


Figure S58. ORTEP at 50 % probability anisotropic displacement ellipsoids of non-hydrogen atoms for compound **6** according to SC-XRD data. Selected interatomic distances [\AA]: Cu1–C1 2.0197(11), Cu1–N1 2.0035(8), Cu1–N2 2.5119(8), C1–C1_b 1.382(3).

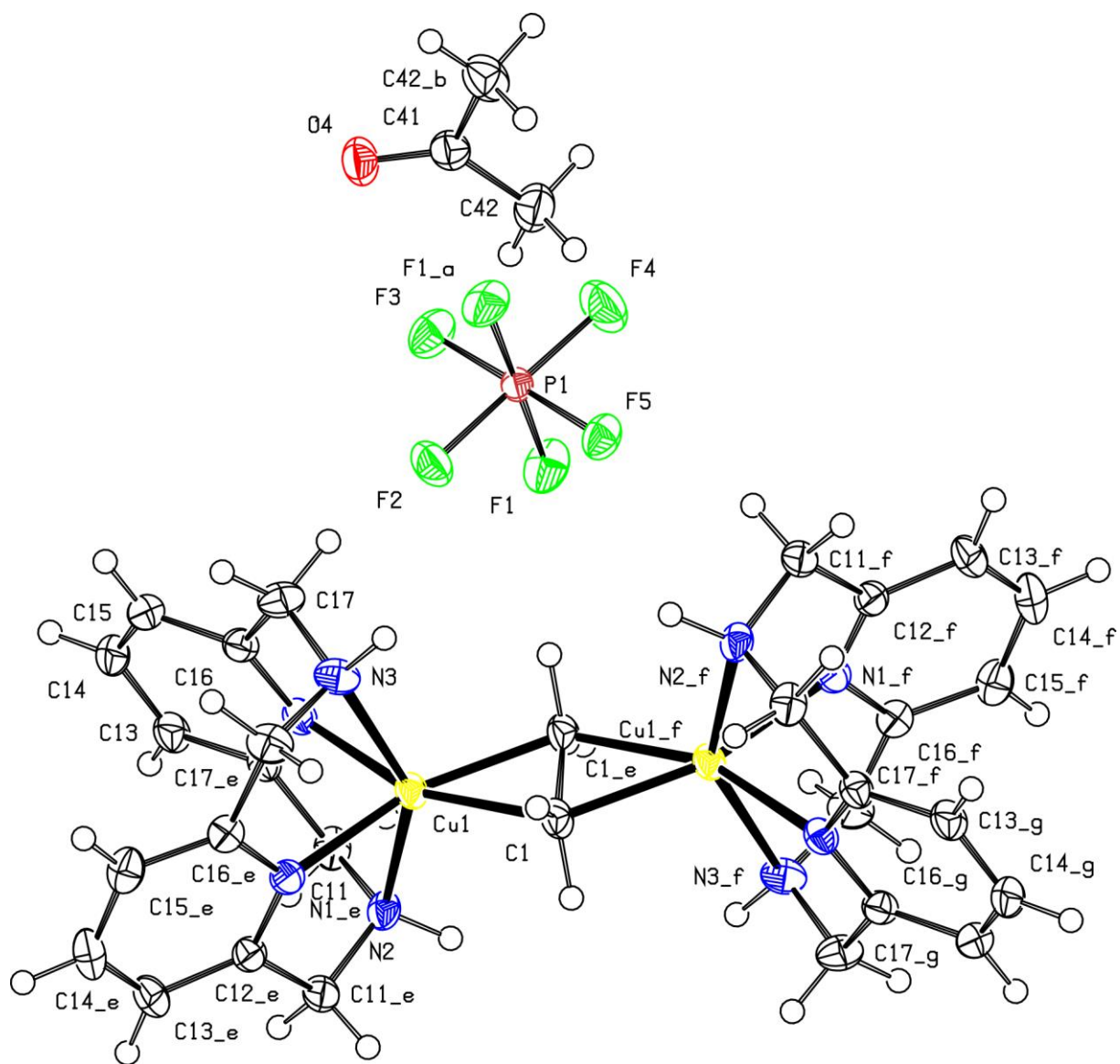


Figure S59. ORTEP at 50 % probability anisotropic displacement ellipsoids of non-hydrogen atoms for compound **7** according to SC-XRD data. Selected interatomic distances [Å]: Cu1–C1 2.0907(15), Cu1–N1 2.063(2), Cu1–N2 2.377(3), Cu1–N3 2.361(4), C1–C1_e 1.444(8).

Computational details

All calculations were performed using density functional theory (DFT) as implemented in the Gaussian 16 suite of programs.²⁵ Geometry optimizations and frequency analyses were carried out in the gas-phase without symmetry restrictions. The initial atomic coordinates were taken from the crystal structures determined by SC XRD. Geometry optimizations of ethylene and the cationic parts of complexes **4**, **5**, **6**, and **7** were carried out in the gas phase without symmetry restrictions using an initially selected set of functionals (M06L,²⁶ ω B97xd,²⁷ B3LYP) and basis sets (SDD²⁸ for Cu/6-31++g(d,p)²⁹⁻³² for other elements; lanl2dz for Cu³³⁻³⁶/6-31++g(d,p) for other elements, and def2tzvp^{33, 37}), among which best fit to the experimental data and trends in bond lengths was obtained using M06L functional, SDD basis set for Cu and 6-31++g(d,p) basis set for other elements. The following describes the computational methods corresponding to (1) **QTAIM analysis**, and (2) **NBO analysis**.

(1) QTAIM Analysis

The quantum-topological analysis of the calculated electron density of the “gas-phase” structures (provided as a multi-XYZ file named ‘QTAIM_Structures.xyz’) was performed within the quantum topological theory of atoms in molecules by means of the *AIMAll* package (v 19.10.12).³⁸

According to Quantum Theory of Atoms in Molecules (QTAIM),³⁹ the bonding between two atoms is indicated by the presence of a bond critical point, bcp (in other words, a (3,-1) critical point of $\rho(\mathbf{r})$) along a bond path connecting two neighboring atoms. The character of the bonding can be characterized by local indicators at the bcp and by the electron delocalization indices (*DIs*, an average number of electrons shared between pair of atoms) related to the degree of covalence and bond multiplicity.⁴⁰ Negative and positive values of the Laplacian at the bcp, $\nabla^2\rho_b$, are characteristics of “shared” and “closed-shell” interactions, respectively.⁴⁰⁻⁴¹ The value of ρ at bcp, ρ_b , is characteristic of a bond strength.⁴² Metal-ligand interactions are typically characterized by positive values of $\nabla^2\rho_b$ and low ρ_b .^{40, 43-45}

(2) NBO Analysis

Second order perturbation theory analysis data is summarized below using NBO 7.0.⁴⁶ The structures for all complexes were optimized as described above. The NBO orbitals were visualized using ChemCraft.⁴⁷ Notations for orbital contributions are as follows: BD – bonding orbital; BD* - antibonding orbital; LP – lone pair; LV – lone vacant orbital.

QTAIM analysis

Ethylene

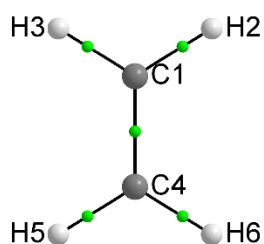


Figure S60. Molecular graph for “gas-phase” DFT-optimized ethylene. Bond critical points (3, -1) with a threshold of electron density above 0.025 a.u. and corresponding bond paths are shown with green dots and black lines, respectively.

Table S3. Quantum-topological parameters [in a.u.] at the bond critical points involving metal atoms for “gas-phase” DFT-optimized ethylene.

Bonding atoms	ρ_b^a	$\nabla^2\rho_b^b$	ϵ^c	λ_1^d	λ_2^d	λ_3^d	V_b^e	G_b^f	H_b^g	DI^h
C1 - C4	0.341973	-0.979035	0.355652	-0.704817	-0.51991	0.245692	-0.525176	0.140209	-0.384967	1.896141
C1 - H2	0.278763	-0.951969	0.005452	-0.70996	-0.70611	0.464101	-0.330419	0.046213	-0.284205	0.971044
C1 - H3	0.278764	-0.951979	0.005452	-0.709965	-0.706115	0.464101	-0.330422	0.046214	-0.284208	0.971057
C4 - H5	0.278763	-0.951969	0.005452	-0.70996	-0.70611	0.464101	-0.330419	0.046213	-0.284205	0.971069
C4 - H6	0.278764	-0.951979	0.005452	-0.709965	-0.706115	0.464101	-0.330422	0.046214	-0.284208	0.971054

^aElectron density; ^bLaplacian of electron density; ^cBond ellipticity; ^dEigenvalues of the Hessian matrix of $\rho(\mathbf{r})$ at the bcp; ^ePotential energy density; ^fKinetic energy density; ^gTotal energy density; ^hDelocalization index. All values are given for the corresponding bcps.

Complex 4:

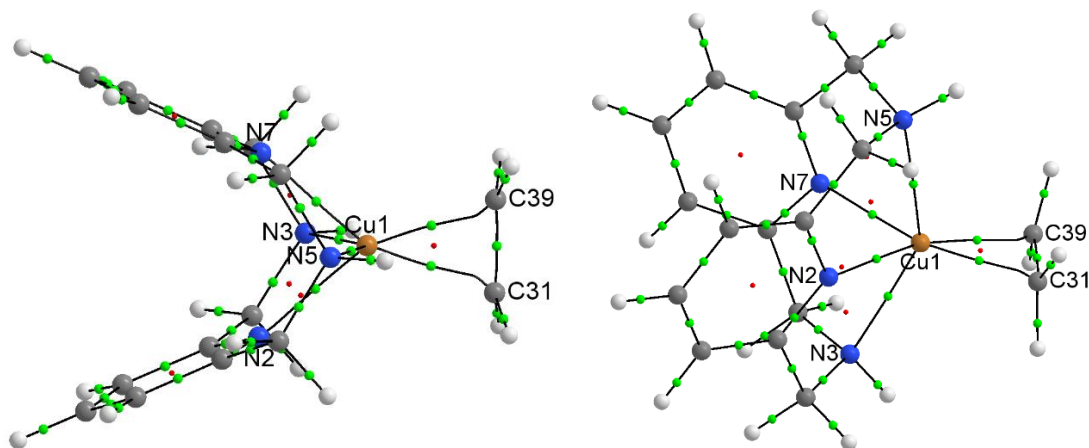


Figure S61. Molecular graph for “gas-phase” DFT-optimized **4** (top and side views with respect to Cu-ethylene coordination). Bond critical points (3, -1) with a threshold of electron density above 0.025 a.u. and corresponding bond paths are shown with green dots and black lines, respectively. Ring critical points are shown as red dots.

Table S4. Quantum-topological parameters [in a.u.] at the bond critical points involving metal atoms and ethylene CC bond for “gas-phase” DFT-optimized **4**.

Bonding atoms	ρ_b^a	$\nabla^2\rho_b^b$	ϵ^c	λ_1^d	λ_2^d	λ_3^d	V_b^e	G_b^f	H_b^g	DI^h
C31 - C39	0.308346	-0.79288	0.282047	-0.61264	-0.47786	0.29761	-0.42653	0.114155	-0.312375	1.443194
Cu1 - C31	0.087811	0.311957	1.463748	-0.10884	-0.04418	0.46498	-0.10835	0.093167	-0.015178	0.572229
Cu1 - C39	0.087811	0.311957	1.463736	-0.10884	-0.04418	0.46498	-0.10835	0.093167	-0.015178	0.572236
Cu1 - N2	0.065086	0.358829	0.10034	-0.07973	-0.07246	0.511016	-0.08724	0.088475	0.00123	0.376249
Cu1 - N3	0.036771	0.13287	0.06829	-0.03307	-0.03096	0.196895	-0.03663	0.034924	-0.001707	0.220951
Cu1 - N5	0.036772	0.132875	0.068291	-0.03307	-0.03096	0.196903	-0.03663	0.034925	-0.001707	0.221301
Cu1 - N7	0.065085	0.358823	0.10034	-0.07973	-0.07246	0.511008	-0.08724	0.088473	0.00123	0.375918

^aElectron density; ^bLaplacian of electron density; ^cBond ellipticity; ^dEigenvalues of the Hessian matrix of $\rho(r)$ at the bcp; ^ePotential energy density; ^fKinetic energy density; ^gTotal energy density; ^hDelocalization index. All values are given for the corresponding bcps.

Complex 5:

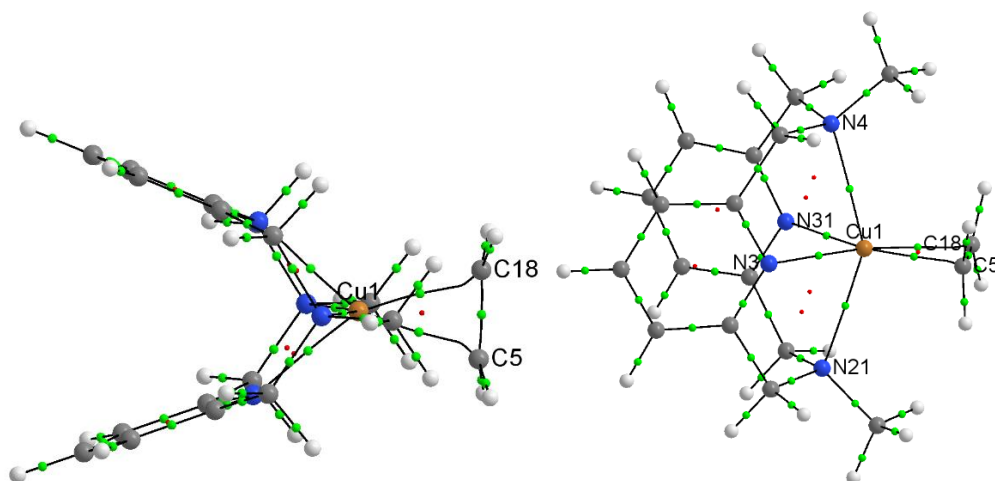


Figure S62. Molecular graph for “gas-phase” DFT-optimized **5** (top and side views with respect to Cu-ethylene coordination). Bond critical points (3, -1) with a threshold of electron density above 0.025 a.u. and corresponding bond paths are shown with green dots and black lines, respectively. Ring critical points are shown as red dots.

Table S5. Quantum-topological parameters [in a.u.] at the bond critical points involving metal atoms and ethylene CC bond for “gas-phase” DFT-optimized **5**.

Bonding atoms	ρ_b^a	$\nabla^2\rho_b^b$	ϵ^c	λ_1^d	λ_2^d	λ_3^d	V_b^e	G_b^f	H_b^g	DI^h
C5 - C18	0.308322	-0.79247	0.281142	-0.61229	-0.47793	0.297756	-0.4265	0.11419	-0.312306	1.442074
Cu1 - C18	0.088202	0.313045	1.488385	-0.10954	-0.04402	0.4666	-0.10901	0.093633	-0.015372	0.572324
Cu1 - C5	0.088202	0.313049	1.488573	-0.10954	-0.04402	0.466599	-0.10901	0.093633	-0.015371	0.572372
Cu1 - N21	0.035762	0.121597	0.057662	-0.0316	-0.02988	0.183071	-0.03492	0.032657	-0.002258	0.211517
Cu1 - N3	0.065368	0.358208	0.097635	-0.08031	-0.07317	0.51169	-0.08736	0.088456	0.0011	0.378127
Cu1 - N31	0.065367	0.358206	0.097637	-0.08031	-0.07317	0.511686	-0.08736	0.088456	0.0011	0.378183
Cu1 - N4	0.035799	0.121855	0.057683	-0.03165	-0.02992	0.183426	-0.03496	0.032713	-0.002249	0.211651

^aElectron density; ^bLaplacian of electron density; ^cBond ellipticity; ^dEigenvalues of the Hessian matrix of $\rho(\mathbf{r})$ at the bcp; ^ePotential energy density; ^fKinetic energy density; ^gTotal energy density; ^hDelocalization index. All values are given for the corresponding bcps.

Complex 6:

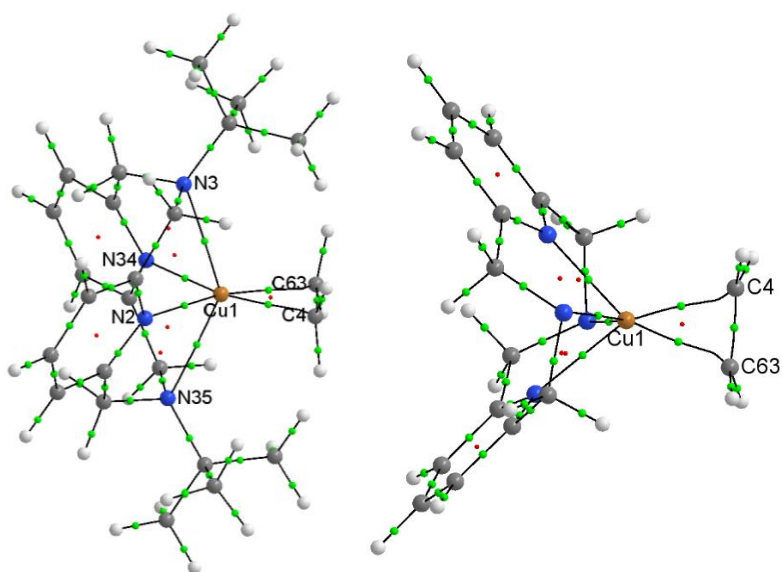


Figure S63. Molecular graph for “gas-phase” DFT-optimized **6** (left: side view; right: top view, with tBu groups not shown for clarity). Bond critical points (3, -1) with a threshold of electron density above 0.025 a.u. and corresponding bond paths are shown with green dots and black lines, respectively. Ring critical points are shown as red dots.

Table S6. Quantum-topological parameters [in a.u.] at the bond critical points involving metal atoms and ethylene CC bond for “gas-phase” DFT-optimized **X**.

Bonding atoms	ρ_b^a	$\nabla^2\rho_b^b$	ε^c	λ_1^d	λ_2^d	λ_3^d	V_b^e	G_b^f	H_b^g	DI^h
C4 - C63	0.304607	-0.77149	0.272332	-0.6007	-0.47212	0.301333	-0.41678	0.111954	-0.304826	1.410416
Cu1 - C4	0.091656	0.3104	1.294452	-0.11581	-0.05047	0.476678	-0.11292	0.09526	-0.01766	0.595371
Cu1 - C63	0.091656	0.310399	1.294404	-0.11581	-0.05047	0.476679	-0.11292	0.095259	-0.01766	0.595571
Cu1 - N2	0.072467	0.414501	0.09483	-0.09277	-0.08473	0.592004	-0.10451	0.104068	-0.000443	0.400392
Cu1 - N3	0.029877	0.084516	0.070126	-0.02383	-0.02227	0.130608	-0.02781	0.024468	-0.003339	0.173199
Cu1 - N34	0.072467	0.414499	0.094831	-0.09277	-0.08473	0.592002	-0.10451	0.104068	-0.000443	0.400403
Cu1 - N35	0.029878	0.08452	0.070124	-0.02383	-0.02227	0.130613	-0.02781	0.024469	-0.003339	0.172847

^aElectron density; ^bLaplacian of electron density; ^cBond ellipticity; ^dEigenvalues of the Hessian matrix of $\rho(\mathbf{r})$ at the bcp; ^ePotential energy density; ^fKinetic energy density; ^gTotal energy density; ^hDelocalization index. All values are given for the corresponding bcps.

Complex 7:

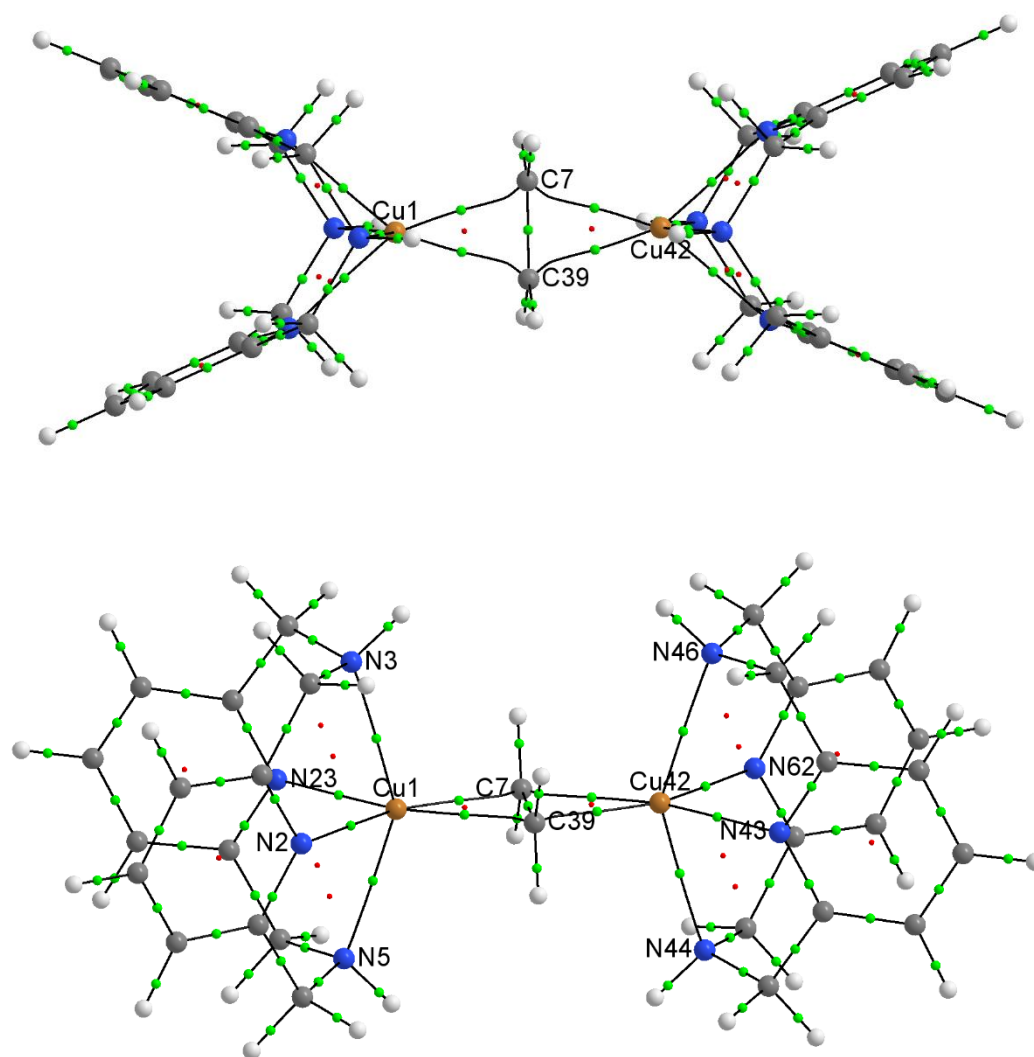


Figure S64. Molecular graph for “gas-phase” DFT-optimized **X** (top and side views with respect to Cu-ethylene coordination). Bond critical points (3, -1) with a threshold of electron density above 0.025 a.u. and corresponding bond paths are shown with green dots and black lines, respectively. Ring critical points are shown as red dots.

Table S7. Quantum-topological parameters [in a.u.] at the bond critical points involving metal atoms and ethylene CC bond for “gas-phase” DFT-optimized **X**.

Bonding atoms	ρ_b^a	$\nabla^2 \rho_b^b$	ϵ^c	λ_1^d	λ_2^d	λ_3^d	V_b^e	G_b^f	H_b^g	DI^h
C7 - C39	0.272931	-0.5918	0.353825	-0.51942	-0.38367	0.311293	-0.34912	0.100586	-0.248535	1.207341
Cu1 - C39	0.075613	0.290586	1.368593	-0.08907	-0.03761	0.417262	-0.09178	0.082213	-0.009567	0.464246
Cu1 - C7	0.075613	0.290586	1.368592	-0.08907	-0.03761	0.417262	-0.09178	0.082213	-0.009567	0.464188
Cu1 - N2	0.065563	0.357363	0.100499	-0.08043	-0.07309	0.510882	-0.0874	0.088368	0.00097	0.380413
Cu1 - N23	0.065563	0.357364	0.100499	-0.08043	-0.07309	0.510884	-0.0874	0.088368	0.00097	0.380752
Cu1 - N3	0.037005	0.133711	0.054781	-0.03306	-0.03135	0.198118	-0.03689	0.03516	-0.001732	0.227041
Cu1 - N5	0.037003	0.133697	0.054778	-0.03306	-0.03134	0.198098	-0.03689	0.035156	-0.001732	0.227308
C7 - Cu42	0.075612	0.290586	1.368599	-0.08907	-0.03761	0.417261	-0.09178	0.082213	-0.009567	0.464283
C39-Cu42	0.075612	0.290585	1.368599	-0.08907	-0.03761	0.417261	-0.09178	0.082213	-0.009567	0.464201
Cu42-N43	0.065563	0.357363	0.100499	-0.08043	-0.07309	0.510882	-0.0874	0.088368	0.00097	0.380703
Cu42-N44	0.037006	0.133712	0.054781	-0.03306	-0.03135	0.198119	-0.03689	0.03516	-0.001732	0.227206
Cu42-N46	0.037003	0.133696	0.054777	-0.03306	-0.03134	0.198097	-0.03689	0.035156	-0.001732	0.226954
Cu42-N62	0.065563	0.357364	0.100499	-0.08043	-0.07309	0.510884	-0.0874	0.088368	0.00097	0.380453

^aElectron density; ^bLaplacian of electron density; ^cBond ellipticity; ^dEigenvalues of the Hessian matrix of $\rho(\mathbf{r})$ at the bcp; ^ePotential energy density;

^fKinetic energy density; ^gTotal energy density; ^hDelocalization index. All values are given for the corresponding bcps.

NBO analysis

Ethylene

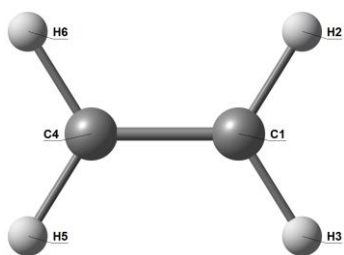


Figure S65. Atom numbering scheme used in NBO analysis.

Table S8. Natural bond indices (NBI) in ethylene.

	C1	C4
C1	-	1.4299
C4	1.4299	-

Table S9. Wiberg bond indices (WBI) in ethylene.

	C1	C4
C1	-	2.0446
C4	2.0446	-

Complex 4:

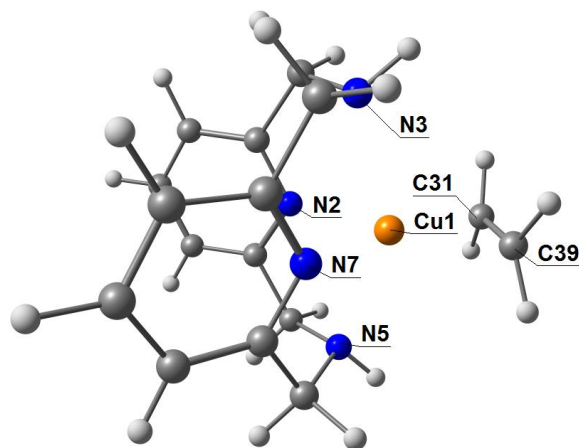


Figure S66. Atom numbering scheme in complex 4 used in NBO analysis.

Interactions between Cu and ethylene: As expected, the main contribution to binding between Cu and ethylene come from ligand-to-metal σ -donation from ethylene $\pi(\text{C}=\text{C})$ orbital to an empty Cu-based s-type orbital ($E^{(2)} = 67.18$ kcal/mol) and π -back-donation from a filled Cu-based dx^2-y^2 orbital to the $\pi^*(\text{C}=\text{C})$ orbital ($E^{(2)} = 27.82$ kcal/mol). Very weak ligand-to-metal π -donation is also observed from $\sigma(\text{C}=\text{C})$ orbital to a Cu-based s-type orbital ($E^{(2)} = 1.06$ kcal/mol). The back-donation from Cu-based dx^2-y^2 -type orbital to $\sigma^*(\text{C}=\text{C})$ is essentially almost negligible ($E^{(2)} 0.16$ kcal/mol).

Table S10. Key interactions in complex 4.

Donor			Acceptor			$E^{(2)}$, kcal/mol
#	Orbital	NAO (%contribution)	#	Orbital	NAO (%contribution)	
76	BD(2)C31-C39	C31(50.00%) s(4.02%) p(95.83%) d(0.15%) C39(50.00%) s(4.02%) p(95.83%) d(0.15%)	82	LV(1)Cu1	Cu1 s(98.73%) p(0.03%) d(1.24%)	67.18
29	LP(5)Cu1	Cu1 s(0.00%) p(0.04%) d(99.96%)	125	BD*(2)C31-C39	C31(50.00%) s(4.02%) p(95.83%) d(0.15%) C39(50.00%) s(4.02%) p(95.83%) d(0.15%)	27.82
75	BD(1)C31-C39	C31(50.00%) s(34.63%) p(65.29%) d(0.07%) C39(50.00%) s(34.63%) p(65.29%) d(0.07%)	82	LV(1)Cu1	Cu1 s(98.73%) p(0.03%) d(1.24%)	1.06
29	LP(5)Cu1	Cu1 s(0.00%) p(0.04%) d(99.96%)	124	BD*(1)C31-C39	C31(50.00%) s(34.63%) p(65.29%) d(0.07%) C39(50.00%) s(34.63%) p(65.29%) d(0.07%)	0.16

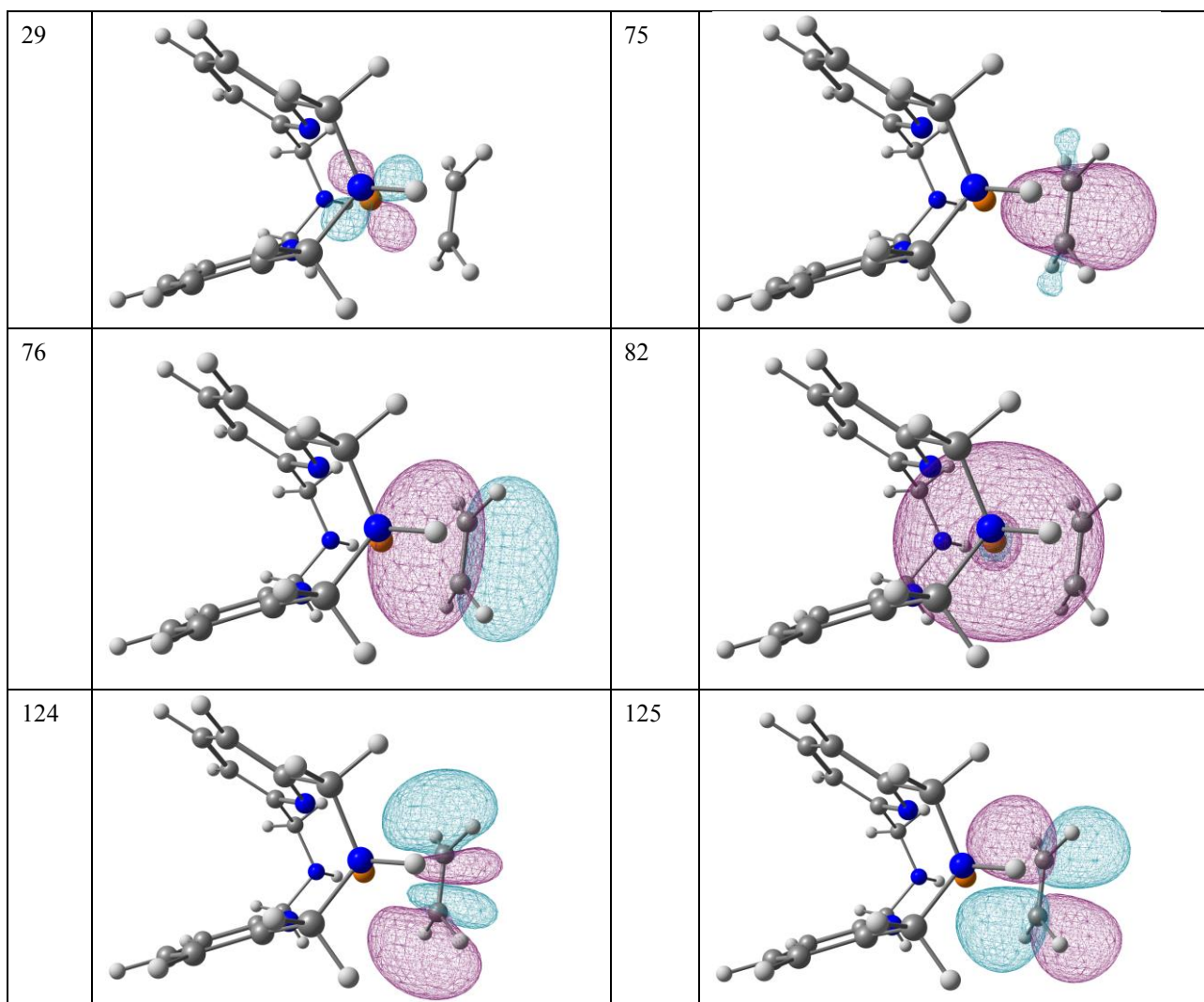


Figure S67. Orbital plots for complex 4.

Table S11. Natural bond indices (NBI) corresponding to Cu(ethylene) motif in complex 4.

	Cu1	C31	C39
Cu1	-	0.5822	0.5822
C31	0.5822	-	1.2812
C39	0.5822	1.2812	-

Table S12. Wiberg bond indices (WBI) corresponding to Cu(ethylene) motif in complex 4.

	Cu1	C31	C39
Cu1	-	0.3390	0.3390
C31	0.3390	-	1.6414
C39	0.3390	1.6414	-

Complex 5:

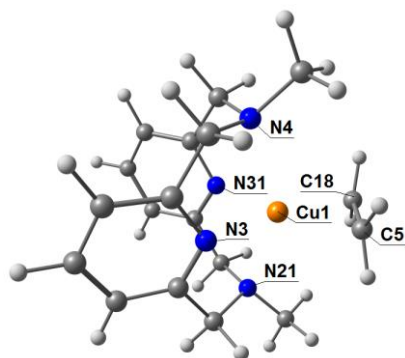


Figure S68. Atom numbering scheme in complex **5** used in NBO analysis.

Interactions between Cu and ethylene: Main contribution to binding between Cu and ethylene come from ligand-to-metal σ -donation from ethylene $\pi(\text{C}=\text{C})$ orbital to an empty Cu-based s -type orbital ($E^{(2)} = 67.40$ kcal/mol) and π -back-donation from a filled Cu-based dx^2-y^2 orbital to the $\pi^*(\text{C}=\text{C})$ orbital ($E^{(2)} = 27.74$ kcal/mol), similar to $^{\text{H}}\text{N4}$ -ligated complex described above. Similarly, very weak ligand-to-metal π -donation is also observed from $\sigma(\text{C}=\text{C})$ orbital to a Cu-based s -type orbital ($E^{(2)} = 1.17$ kcal/mol), as well as negligible back-donation from Cu-based dx^2-y^2 -type orbital to $\sigma^*(\text{C}=\text{C})$ ($E^{(2)} 0.16$ kcal/mol).

Table S13. Key interactions in complex **5**.

Donor			Acceptor			$E^{(2)}$,
#	Orbital	NAO (%contribution)	#	Orbital	NAO (%contribution)	kcal/mol
44	BD(2)C5-C18	C5(50.00%) s(4.07%) p(95.79%) d(0.15%) C18(50.00%) s(4.07%) p(95.79%) d(0.15%)	90	LV(1)Cu1	Cu1 s(98.62%) p(0.02%) d(1.36%)	67.40
31	LP(5)Cu1	s(0.00%) p(0.04%) d(99.96%)	99	BD*(2)C5-C18	C5(50.00%) s(4.07%) p(95.79%) d(0.15%) C18(50.00%) s(4.07%) p(95.79%) d(0.15%)	27.74
43	BD(1)C5-C18	C5(50.00%) s(34.52%) p(65.41%) d(0.07%) C18(50.00%) s(34.52%) p(65.41%) d(0.07%)	90	LV(1)Cu1	Cu1 s(98.62%) p(0.02%) d(1.36%)	1.17
31	LP(5)Cu1	s(0.00%) p(0.04%) d(99.96%)	98	BD*(1)C5-C18	C5(50.00%) s(34.52%) p(65.41%) d(0.07%) C18(50.00%) s(34.52%) p(65.41%) d(0.07%)	0.16

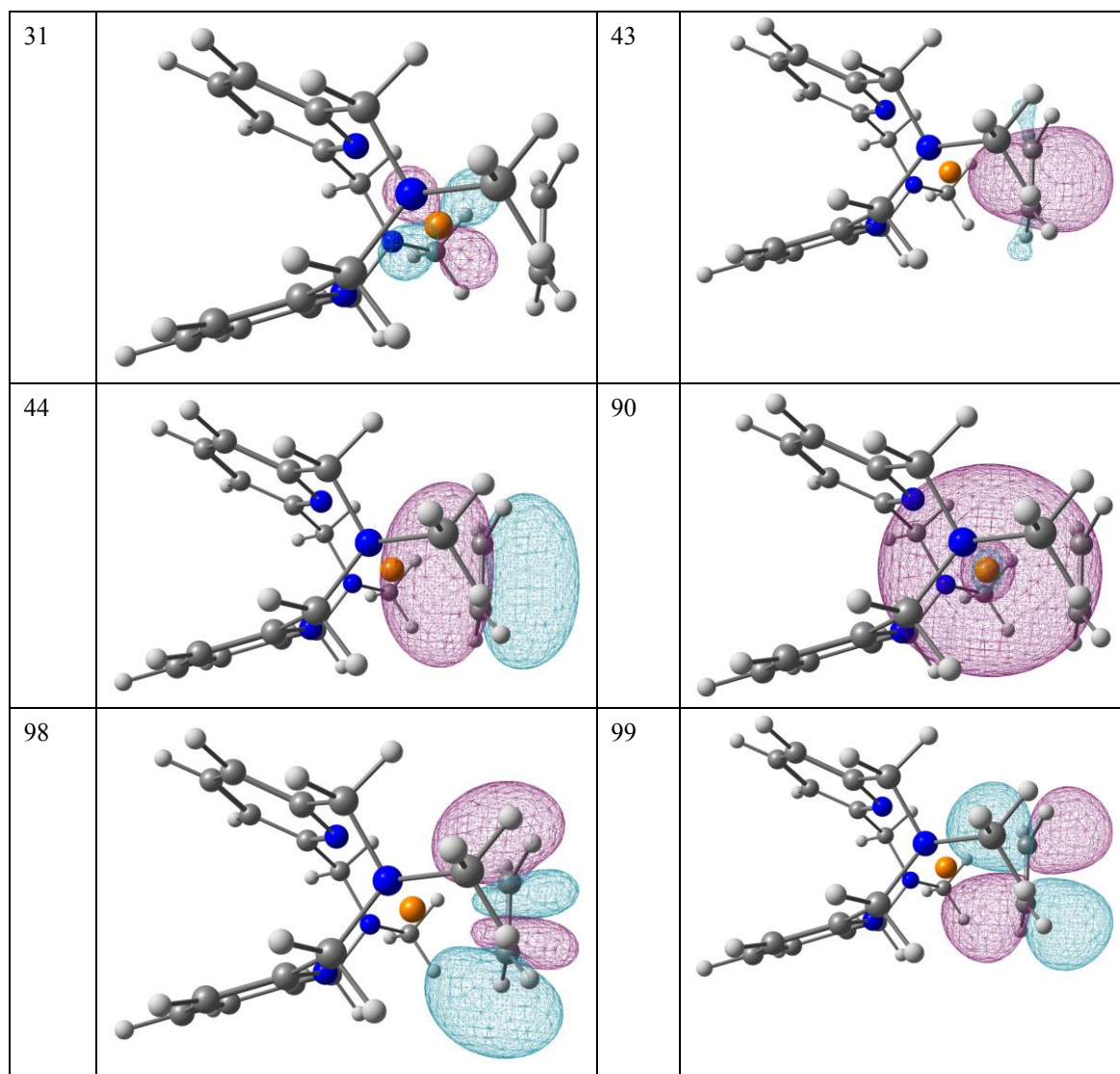


Figure S69. Orbital plots for complex 5.

Table S14. Natural bond indices (NBI) corresponding to Cu(ethylene) motif in complex 5.

	Cu1	C5	C18
Cu1	-	0.5800	0.5800
C5	0.5800	-	1.2824
C18	0.5800	1.2824	-

Table S15. Wiberg bond indices (WBI) corresponding to Cu(ethylene) motif in complex 5.

	Cu1	C5	C18
Cu1	-	0.3364	0.3364
C5	0.3364	-	1.6445
C18	0.3364	1.6445	-

Complex 6:

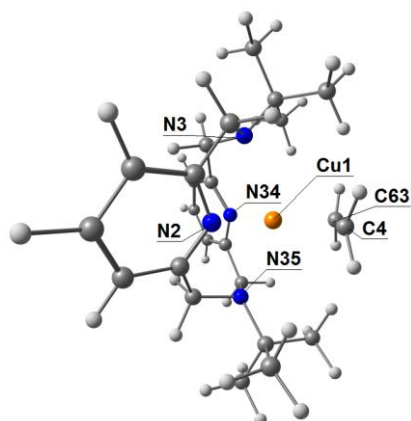


Figure S70. Atom numbering scheme in complex **6** used in NBO analysis.

Interactions between Cu and ethylene: Main contribution to binding between Cu and ethylene come from ligand-to-metal σ -donation from ethylene $\pi(\text{C}=\text{C})$ orbital to an empty Cu-based s-type orbital ($E^{(2)} = 71.92.40$ kcal/mol) and π -back-donation from a filled Cu-based dx^2-y^2 orbital to the $\pi^*(\text{C}=\text{C})$ orbital ($E^{(2)} = 29.90$ kcal/mol), slightly more prominent compared to $^{\text{H}}\text{N}4$ - or $^{\text{Me}}\text{N}4$ -ligated complexes described above. At the same time, ligand-to-metal π -donation from $\sigma(\text{C}=\text{C})$ orbital to a Cu-based s-type orbital ($E^{(2)} = 0.85$ kcal/mol) and back-donation from Cu-based dx^2-y^2 -type orbital to $\sigma^*(\text{C}=\text{C})$ ($E^{(2)} 0.16$ kcal/mol) are essentially negligible.

Table S16. Key interactions in complex **6**.

Donor			Acceptor			$E^{(2)}$, kcal/mol
#	Orbital	NAO (%contribution)	#	Orbital	NAO (%contribution)	
51	BD(2)C4-C63	C4(50.00%) s(4.59%) p(95.26%) d(0.15%) C63(50.00%) s(4.59%) p(95.26%) d(0.15%)	114	LV(1)Cu1		71.92
37	LP(5)Cu1	Cu1 s(0.00%) p(0.03%) d(99.97%)	124	BD*(2)C4-C63	C4(50.00%) s(4.59%) p(95.26%) d(0.15%) C63(50.00%) s(4.59%) p(95.26%) d(0.15%)	29.90
50	BD(1)C4-C63	C4(50.00%) s(33.65%) p(66.27%) d(0.07%) C63(50.00%) s(33.65%) p(66.27%) d(0.07%)	114	LV(1)Cu1	Cu1 s(98.37%) p(0.03%) d(1.60%)	0.85
37	LP(5)Cu1	Cu1 s(0.00%) p(0.03%) d(99.97%)	123	BD*(1)C4-C63	C4(50.00%) s(33.65%) p(66.27%) d(0.07%) C63(50.00%) s(33.65%) p(66.27%) d(0.07%)	0.16

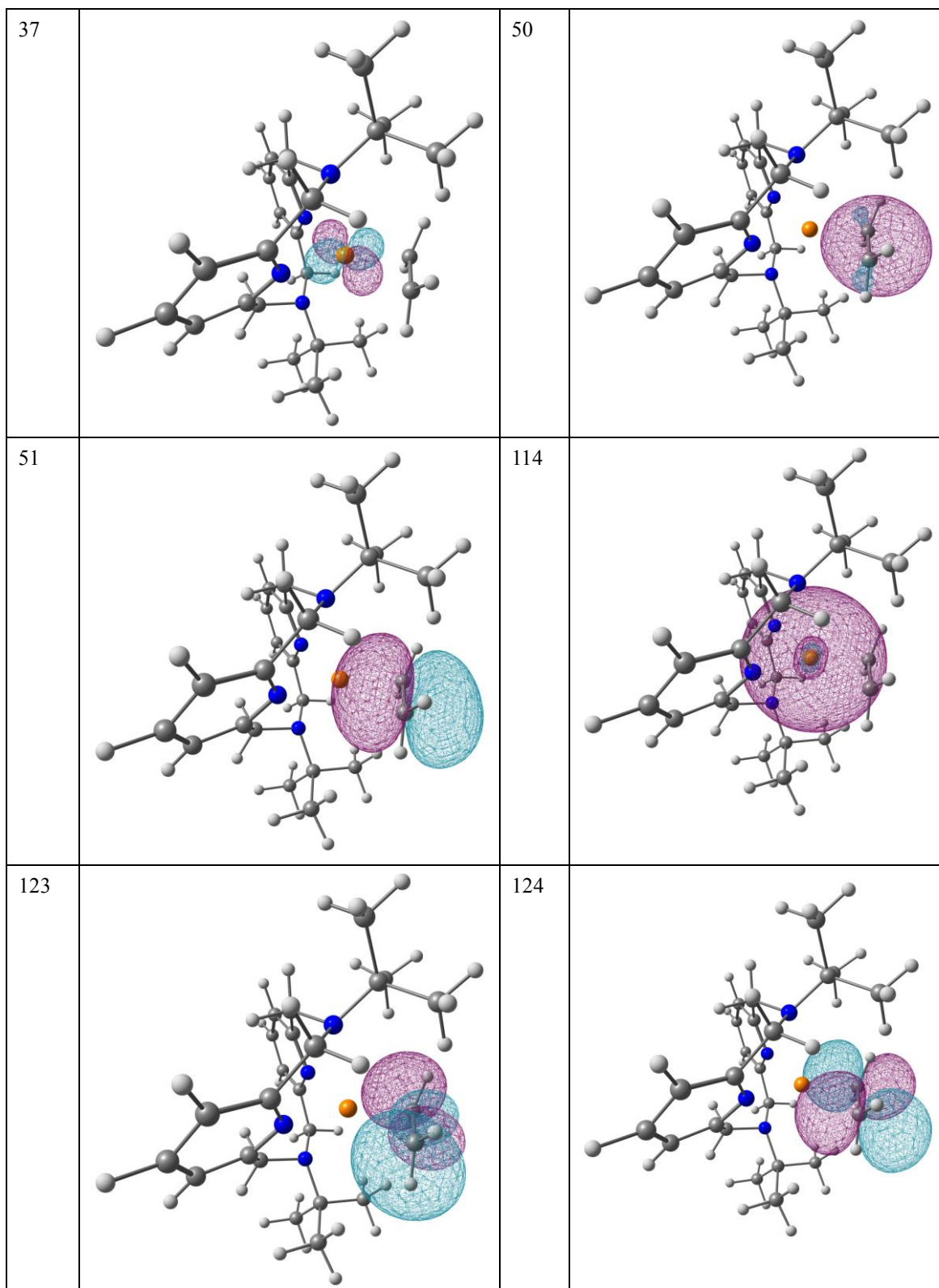


Figure S71. Orbital plots for complex 6.

Table S17. Natural bond indices (NBI) corresponding to Cu(ethylene) motif in complex **6**.

	Cu1	C4	C63
Cu1	-	0.5856	0.5856
C4	0.5856	-	1.2722
C63	0.5856	1.2722	-

Table S18. Wiberg bond indices (WBI) corresponding to Cu(ethylene) motif in complex **6**.

	Cu1	C4	C63
Cu1	-	0.3429	0.3429
C4	0.3429	-	1.6185
C63	0.3429	1.6185	-

Complex 7:

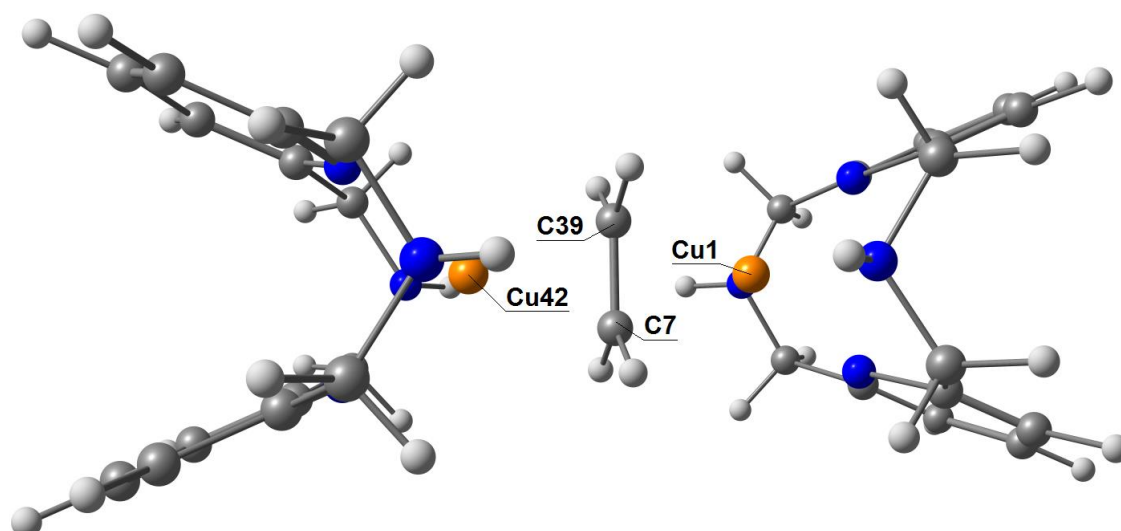


Figure S72. Atom numbering scheme in complex 7 used in NBO analysis.

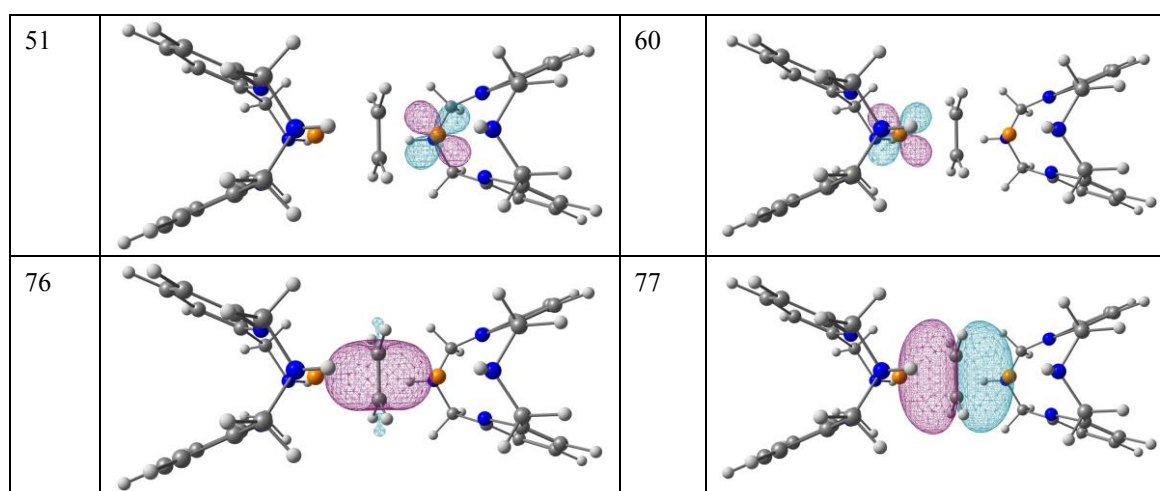
Interactions between Cu and ethylene:

Compared to monocopper complex, σ -donation from ethylene $\pi(\text{C}=\text{C})$ orbital to each Cu-based s -type orbital is weaker ($E^{(2)} = 28.34$ kcal/mol), while π -back-donation from each Cu-based dx^2-y^2 orbital to the $\pi^*(\text{C}=\text{C})$ orbital ($E^{(2)} = 28.53$ and 28.52 kcal/mol) remains similar to $^{\text{H}}\text{N}4$ -ligated monocopper complex described above. Interestingly, ligand-to-metal π -donation from $\sigma(\text{C}=\text{C})$ orbital to each Cu-based s -type orbital becomes slightly more prominent, albeit still comparatively weak ($E^{(2)} = 4.87$ kcal/mol). Very weak back-donation from each Cu-based dx^2-y^2 -type orbital to $\sigma^*(\text{C}=\text{C})$ ($E^{(2)} 0.93$ kcal/mol) is also present, although its contribution remains almost negligible.

Table S19. Key interactions in complex 7.

Donor			Acceptor			$E^{(2)}$, kcal/mol
#	Orbital	NAO (%contribution)	#	Orbital	NAO (%contribution)	
51	LP(5)Cu1	Cu1 s(0.00%) p(0.03%) d(99.97%)	169	BD*(2)C 7-C39	C7(50.00%) s(0.00%) p(99.87%) d(0.13%) C39(50.00%) s(0.00%) p(99.87%) d(0.13%)	28.53
60	LP(5)Cu4 2	Cu42 s(0.00%) p(0.03%) d(99.97%)	169	BD*(2) C7-C39	C7(50.00%) s(0.00%) p(99.87%) d(0.13%) C39(50.00%) s(0.00%) p(99.87%) d(0.13%)	28.52
77	BD(2)C7- C39	C7(50.00%) s(0.00%) p(99.87%) d(0.13%) C39(50.00%) s(0.00%)	155	LV(1)Cu 1	Cu1 s(98.85%) p(0.02%) d(1.13%)	28.34

		p(99.87%) d(0.13%)				
77	BD(2)C7-C39	C7(50.00%) s(0.00%) p(99.87%) d(0.13%) C39(50.00%) s(0.00%) p(99.87%) d(0.13%)	156	LV(1)Cu 42	Cu42 s(98.85%) p(0.02%) d(1.13%)	28.34
76	BD(1)C7-C39	C7(50.00%) s(36.92%) p(63.01%) d(0.07%) C39(50.00%) s(36.92%) p(63.01%) d(0.07%)	155	LV(1)Cu 1	Cu1 s(98.85%) p(0.02%) d(1.13%)	4.87
76	BD(1)C7-C39	C7(50.00%) s(36.92%) p(63.01%) d(0.07%) C39(50.00%) s(36.92%) p(63.01%) d(0.07%)	156	LV(1)Cu 42	Cu42 s(98.85%) p(0.02%) d(1.13%)	4.87
51	LP(5)Cu1	Cu1 s(0.00%) p(0.03%) d(99.97%)	168	BD*(1)C 7-C39	C7(50.00%) s(36.92%) p(63.01%) d(0.07%) C39(50.00%) s(36.92%) p(63.01%) d(0.07%)	0.93
60	LP(5)Cu4 2	Cu42 s(0.00%) p(0.03%) d(99.97%)	168	BD*(1) C7-C39	C7(50.00%) s(36.92%) p(63.01%) d(0.07%) C39(50.00%) s(36.92%) p(63.01%) d(0.07%)	0.93



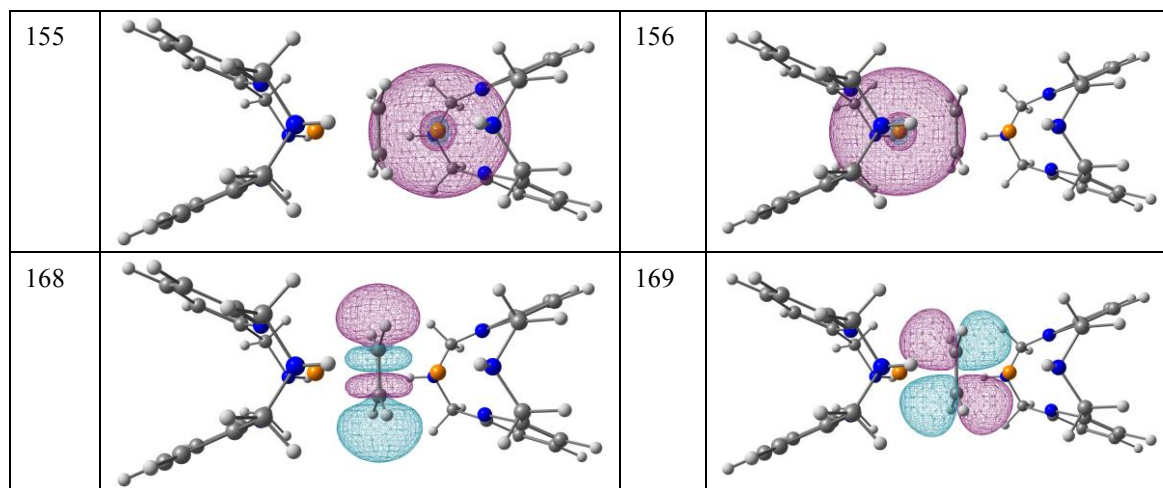


Figure S73. Orbital plots for complex 7.

Table S20. Natural bond indices (NBI) corresponding to Cu(ethylene)Cu motif in complex 7.

	Cu1	C7	C39	Cu42
Cu1	-	0.4955	0.4955	0.2415
C7	0.4955	-	1.1928	0.4955
C39	0.4955	1.1928	-	0.4955
Cu42	0.2415	0.4955	0.4955	-

Table S21. Wiberg bond indices (WBI) corresponding to Cu(ethylene)Cu motif in complex 7.

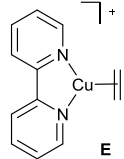
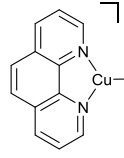
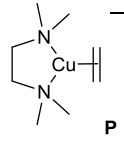
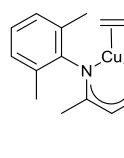
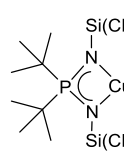
	Cu1	C7	C39	Cu42
Cu1	-	0.2455	0.2455	0.0583
C7	0.2455	-	1.4228	0.2455
C39	0.2455	1.4228	-	0.2455
Cu42	0.0583	0.2455	0.2455	-

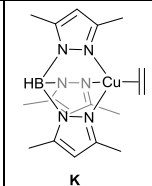
NBO analysis of Cu-ethylene binding in selected complexes with N-donor ligands reported in the literature

The cationic parts of complexes **E**, **F**, and **P**, and neutral complexes **B**, **C**, **K** were optimized M06L functional, SDD basis set for Cu and 6-31++g(d,p) basis set for other elements as described in computational section above; the initial atomic coordinates were taken from the crystal structures determined by SC XRD as reported in CSD.

The comparison of key interactions between Cu and ethylene in literature-reported complexes with N-donor ligands and complexes **4-6** shows that in all cases, the main components of Cu-ethylene binding correspond to the σ -donation from the π -bonding C=C orbital to a Cu-based s -type orbital and back-donation from the Cu-based dx^2-y^2 -type orbital to the π -antibonding C=C orbital of ethylene. When comparing the complexes with bidentate and tridentate ligands, greater σ -donation is observed in complexes **E**, **F**, **P**, **B**, **C** with bidentate ligands, while the strength of donation in complex **K** with a tridentate ligand is weaker, similar to that in R^N4 -pyridinophane complexes **4-6**. In all cases, the contribution from the donation of the σ -C=C orbital to Cu(s) is very weak.

Table S22. Summary of key interactions between ethylene and Cu (see Tables 4 and 5 for comparison).

Donor (orbital #)	Acceptor (orbital #)	E ⁽²⁾ , kcal mol ⁻¹	WBI (C=C)	Chemical structure
[(bpy)Cu ^I (ethylene)] ⁺ (complex E in Chart S1)			1.6053	
π (C=C)	Cu(s)	91.37		
Cu(dx^2-y^2)	π^* (C=C)	28.84		
σ (C=C)	Cu(s)	2.29		
[(phen)Cu ^I (ethylene)] ⁺ (complex F in Chart S1)			1.6102	
π (C=C)	Cu(s)	89.50		
Cu(dx^2-y^2)	π^* (C=C)	28.67		
σ (C=C)	Cu(s)	2.30		
[(tmen)Cu ^I (ethylene)] ⁺ (complex P in Chart S1)			1.5959	
π (C=C)	Cu(s)	88.47		
Cu(dx^2-y^2)	π^* (C=C)	29.34		
σ (C=C)	Cu(s)	2.99		
(nacnac)Cu(ethylene) (complex B in Chart S1)			1.5745	
π (C=C)	Cu(s)	82.47		
Cu(dx^2-y^2)	π^* (C=C)	31.50		
σ (C=C)	Cu(s)	1.60		
(NPN)Cu(ethylene) (complex C in Chart S1)			1.5512	
π (C=C)	Cu(s)	78.85		
Cu(dx^2-y^2)	π^* (C=C)	32.87		
σ (C=C)	Cu(s)	1.63		
(Tp ^{Me2})Cu(ethylene) (complex K in Chart S1)			1.6081	

$\pi(\text{C}=\text{C})$	$\text{Cu}(s)$	64.94	
$\text{Cu}(dx^2-y^2)$	$\pi^*(\text{C}=\text{C})$	30.59	
$\sigma(\text{C}=\text{C})$	$\text{Cu}(s)$	1.28	

tmen = tetramethylethylenediamine; bpy = 2,2'-bipyridine; phen = 1,10-phenanthroline; WBI (C=C) = Wiberg Bond Index of C=C bond of coordinated ethylene.

(See Chart S1 for comparison of NMR chemical shifts and C=C bond lengths)

Complex [(bpy)Cu(ethylene)]⁺ (complex **E** in Chart S1):

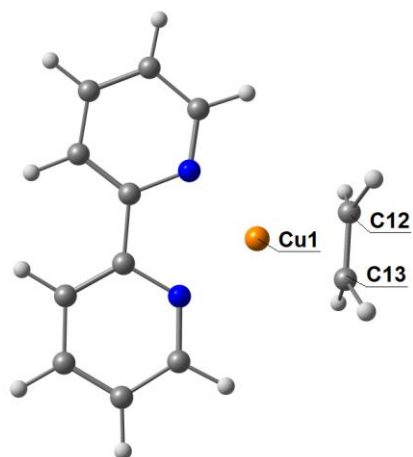


Figure S74. Atom numbering scheme in complex **E** used in NBO analysis.

Table S23. Key interactions in complex **E**.

Donor			Acceptor			E ⁽²⁾ , kcal/mol
#	Orbital	NAO (%contribution)	#	Orbital	NAO (%contribution)	
54	BD(2)C12-C13	C12(50.00%) s(3.65%) p(96.19%) d(0.16%) C13(50.00%) s(3.65%) p(96.19%) d(0.16%)	59	LV(1)Cu1	LV(1)Cu1 s(96.96%) p(0.07%) d(2.98%)	91.37
23	LP(5)Cu1	Cu1 s(0.00%) p(0.03%) d(99.97%)	88	BD*(2)C12-C13	C12(50.00%) s(3.65%) p(96.19%) d(0.16%) C13(50.00%) s(3.65%) p(96.19%) d(0.16%)	28.84
53	BD(1)C12-C13	C12(50.00%) s(34.61%) p(65.31%) d(0.07%) C13(50.00%) s(34.61%) p(65.31%) d(0.07%)	59	LV(1)Cu1	LV(1)Cu1 s(96.96%) p(0.07%) d(2.98%)	2.29
23	LP(5)Cu1	Cu1 s(0.00%) p(0.03%) d(99.97%)	87	BD*(1)C12-C13	C12(50.00%) s(34.61%) p(65.31%) d(0.07%) C13(50.00%) s(34.61%) p(65.31%) d(0.07%)	0.25

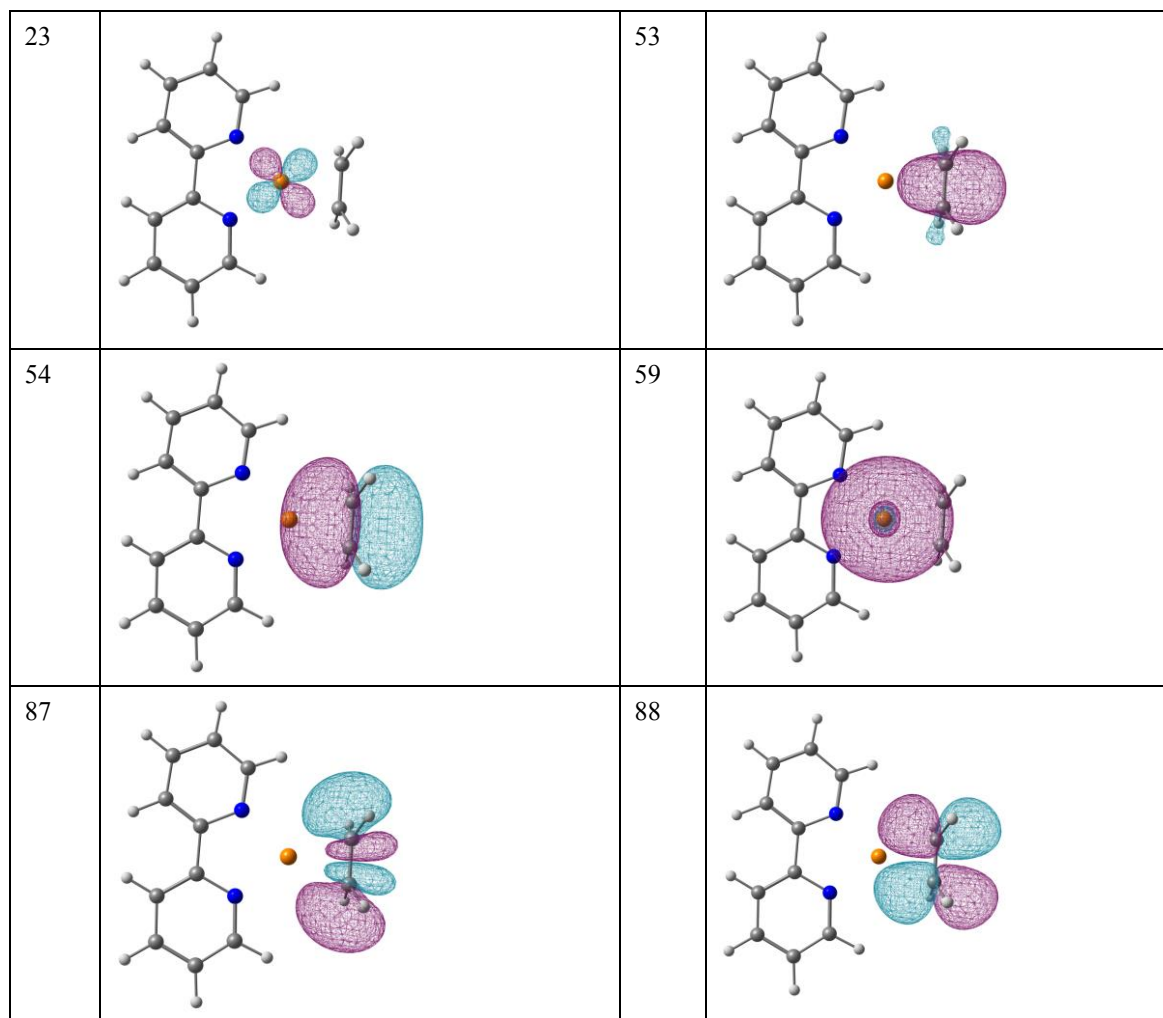


Figure S75. Orbital plots for complex E.

Table S24. Natural bond indices (NBI) corresponding to Cu(ethylene) motif in complex E.

	Cu1	C12	C13
Cu1	-	0.6054	0.6054
C12	0.6054	-	1.2670
C13	0.6054	1.2670	-

Table S25. Wiberg bond indices (WBI) corresponding to Cu(ethylene) motif in complex E.

	Cu1	C12	C13
Cu1	-	0.3666	0.3666
C12	0.3666	-	1.6053
C13	0.3666	1.6053	-

Complex [(phen)Cu(ethylene)]⁺ (complex **F** in Chart S1):

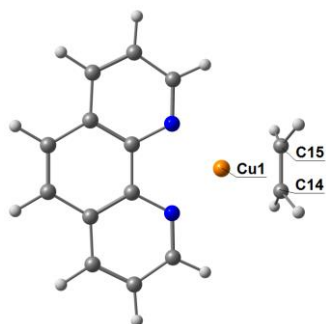


Figure S76. Atom numbering scheme in complex **F** used in NBO analysis.

Table S26. Key interactions in complex **F**.

Donor			Acceptor			E ⁽²⁾ , kcal/mol
#	Orbital	NAO (%contribution)	#	Orbital	NAO (%contribution)	
60	BD(2)C14-C15	C14(50.00%) s(3.59%) p(96.25%) d(0.16%) C15(50.00%) s(3.59%) p(96.25%) d(0.16%)	65	LV(1)Cu1	Cu1 s(97.01%) p(0.07%) d(2.92%)	89.50
25	LP(5)Cu1	Cu1 s(0.00%) p(0.03%) d(99.97%)	98	BD*(2)C14-C15	C14(50.00%) s(3.59%) p(96.25%) d(0.16%) C15(50.00%) s(3.59%) p(96.25%) d(0.16%)	28.67
59	BD(1)C14-C15	C14(50.00%) s(34.69%) p(65.24%) d(0.07%) C15(50.00%) s(34.69%) p(65.24%) d(0.07%)	65	LV(1)Cu1	Cu1 s(97.01%) p(0.07%) d(2.92%)	2.30
25	LP(5)Cu1	Cu1 s(0.00%) p(0.03%) d(99.97%)	97	BD*(1)C14-C15	C14(50.00%) s(34.69%) p(65.24%) d(0.07%) C15(50.00%) s(34.69%) p(65.24%) d(0.07%)	0.25

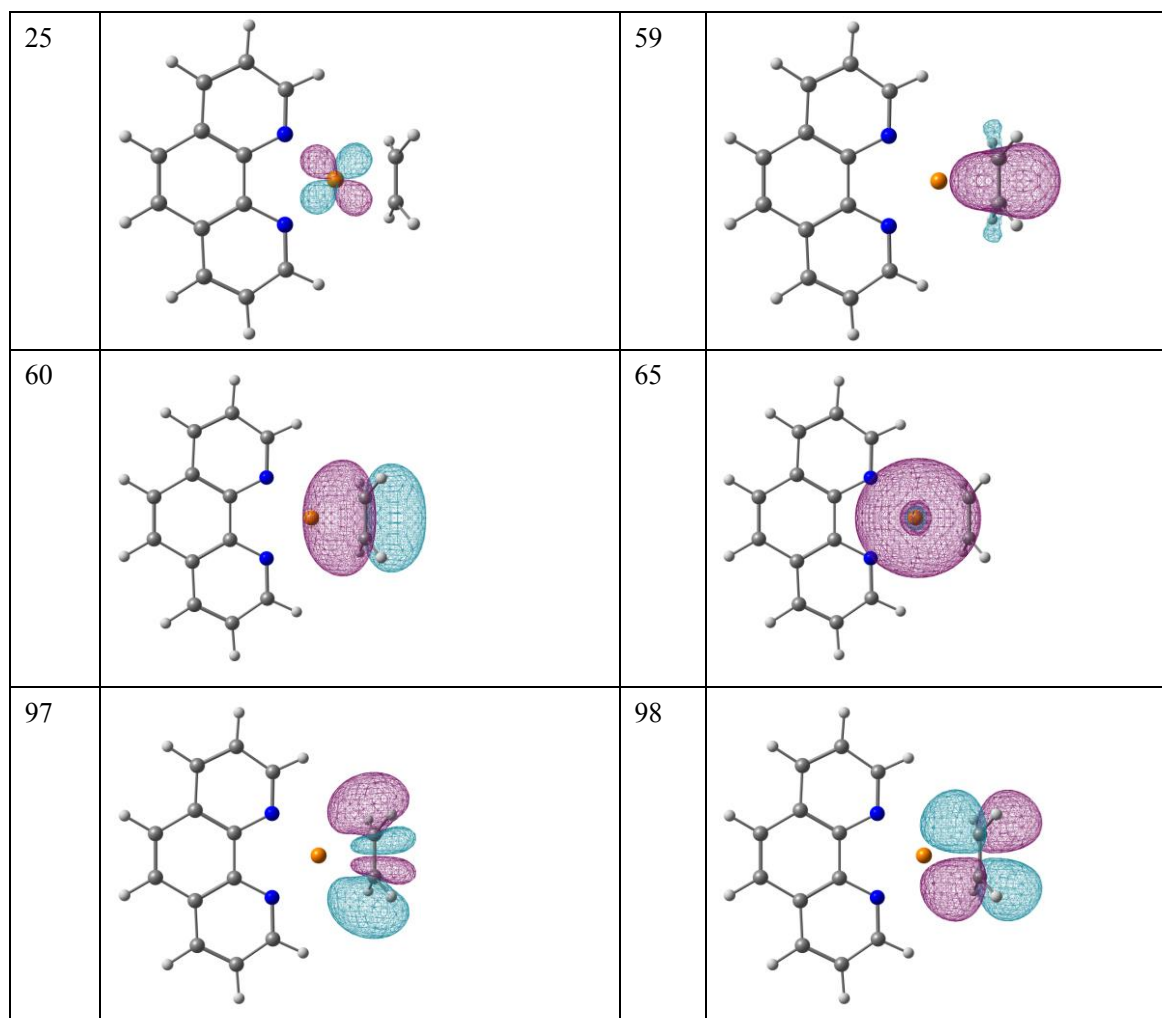


Figure S77. Orbital plots for complex **F**.

Table S27. Natural bond indices (NBI) corresponding to Cu(ethylene) motif in complex **F**.

	Cu1	C14	C15
Cu1	-	0.6032	0.6032
C14	0.6032	-	1.2689
C15	0.6032	1.2689	-

Table S28. Wiberg bond indices (WBI) corresponding to Cu(ethylene) motif in complex **F**.

	Cu1	C14	C15
Cu1	-	0.3639	0.3639
C14	0.3639	-	1.6102
C15	0.3639	1.6102	-

Complex [(tmen)Cu(ethylene)]⁺ (complex **P** in Chart S1):

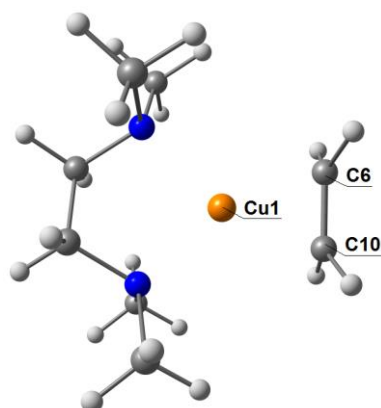


Figure S78. Atom numbering scheme in complex **P** used in NBO analysis.

Table S29. Key interactions in complex **P**.

Donor			Acceptor			E ⁽²⁾ , kcal/mol
#	Orbital	NAO (%contribution)	#	Orbital	NAO (%contribution)	
34	BD(2)C6-C10	C6(50.00%) s(3.58%) p(96.25%) d(0.16%) C10(50.00%) s(3.58%) p(96.25%) d(0.16%)	51	LV(1)Cu1	Cu1 s(96.89%) p(0.04%) d(3.06%)	88.47
19	LP(5)Cu1	Cu1 s(0.00%) p(0.04%) d(99.96%)	64	BD*(2)C6-C10	C6(50.00%) s(3.58%) p(96.25%) d(0.16%) C10(50.00%) s(3.58%) p(96.25%) d(0.16%)	29.34
33	BD(1)C6-C10	C6(50.00%) s(34.63%) p(65.30%) d(0.07%) C10(50.00%) s(34.63%) p(65.30%) d(0.07%)	51	LV(1)Cu1	Cu1 s(96.89%) p(0.04%) d(3.06%)	2.99
19	LP(5)Cu1	Cu1 s(0.00%) p(0.04%) d(99.96%)	63	BD*(1)C6-C10	C6(50.00%) s(34.63%) p(65.30%) d(0.07%) C10(50.00%) s(34.63%) p(65.30%) d(0.07%)	0.26

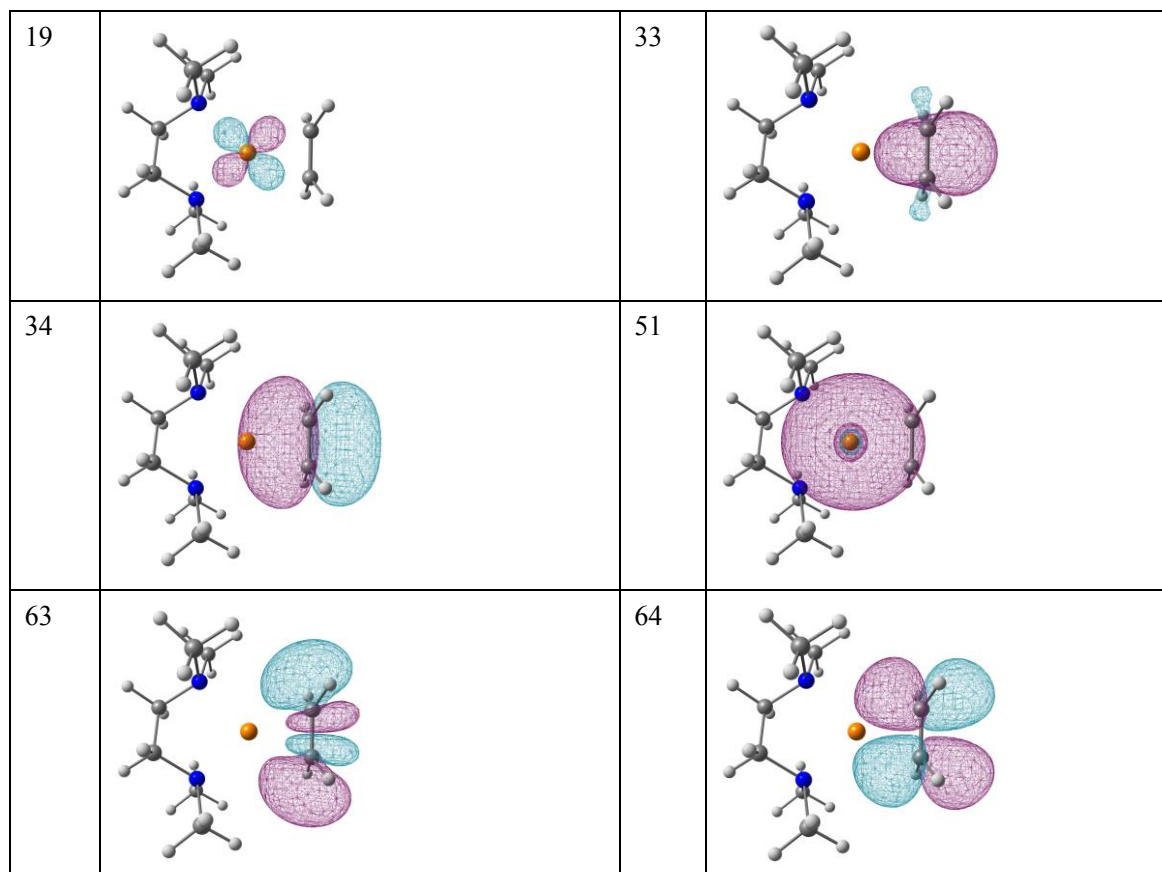


Figure S79. Orbital plots for complex **P**.

Table S30. Natural bond indices (NBI) corresponding to Cu(ethylene) motif in complex **P**.

	Cu1	C6	C10
Cu1	-	0.6071	0.6071
C6	0.6071	-	1.2633
C10	0.6071	1.2633	-

Table S31. Wiberg bond indices (WBI) corresponding to Cu(ethylene) motif in complex **P**.

	Cu1	C6	C10
Cu1	-	0.3685	0.3685
C6	0.3685	-	1.5959
C10	0.3685	1.5959	-

Complex (nacnac)Cu(ethylene) (complex **B** in Chart S1):

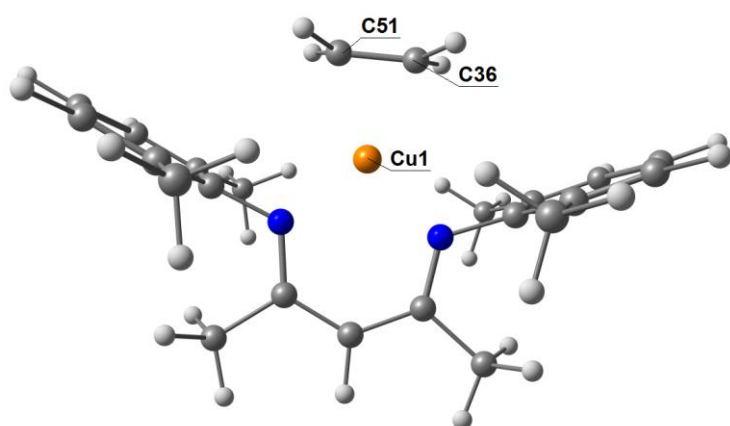


Figure S80. Atom numbering scheme in complex **B** used in NBO analysis.

Table S32. Key interactions in complex **B**.

Donor			Acceptor			$E^{(2)}$, kcal/mol
#	Orbital	NAO (%contribution)	#	Orbital	NAO (%contribution)	
84	BD(2)C36 -C51	C36(50.00%) s(4.26%) p(95.61%) d(0.14%) C51(50.00%) s(4.26%) p(95.61%) d(0.14%)	101	LV(1)Cu1	Cu1 s(97.37%) p(0.07%) d(2.55%)	82.47
34	LP(5)Cu1	Cu1 s(0.00%) p(0.02%) d(99.98%)	148	BD*(2)C36- C51	C36(50.00%) s(4.26%) p(95.61%) d(0.14%) C51(50.00%) s(4.26%) p(95.61%) d(0.14%)	31.50
83	BD(1)C36 -C51	C36(50.00%) s(34.34%) p(65.59%) d(0.07%) C51(50.00%) s(34.34%) p(65.59%) d(0.07%)	101	LV(1)Cu1	Cu1 s(97.37%) p(0.07%) d(2.55%)	1.60
34	LP(5)Cu1	Cu1 s(0.00%) p(0.02%) d(99.98%)	147	BD*(1)C36- C51	C36(50.00%) s(34.34%) p(65.59%) d(0.07%) C51(50.00%) s(34.34%) p(65.59%) d(0.07%)	0.26

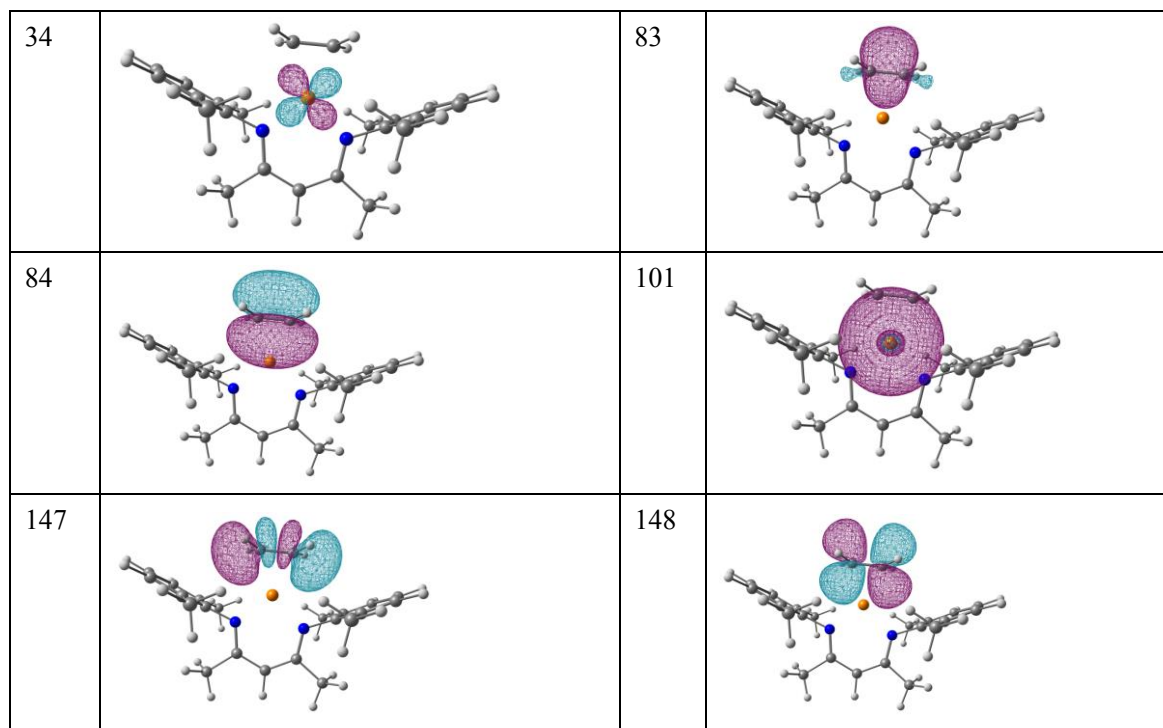


Figure S81. Orbital plots for complex **B**.

Table S33. Natural bond indices (NBI) corresponding to Cu(ethylene) motif in complex **B**.

	Cu1	C36	C51
Cu1	-	0.5954	0.5954
C36	0.5954	-	1.2548
C51	0.5954	1.2548	-

Table S34. Wiberg bond indices (WBI) corresponding to Cu(ethylene) motif in complex **B**.

	Cu1	C36	C51
Cu1	-	0.3545	0.3545
C36	0.3545	-	1.5745
C51	0.3545	1.5745	-

Complex (NPN)Cu(ethylene) (complex C in Chart S1):

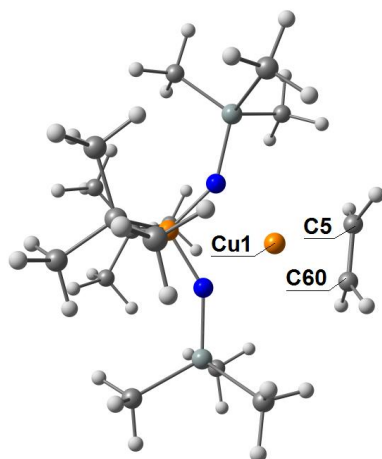


Figure S82. Atom numbering scheme in complex C used in NBO analysis.

Table S35. Key interactions in complex C.

Donor			Acceptor			E ⁽²⁾ , kcal/mol
#	Orbital	NAO (%contribution)	#	Orbital	NAO (%contribution)	
58	BD(2)C5-C60	C5(50.00%) s(4.47%) p(95.39%) d(0.14%) C60(50.00%) s(4.47%) p(95.39%) d(0.14%)	107	LV(1)Cu1	Cu1 s(96.96%) p(0.09%) d(2.95%)	78.85
42	LP(5)Cu1	Cu1 s(0.00%) p(0.04%) d(99.96%)	119	BD*(2)C5-C60	C5(50.00%) s(4.47%) p(95.39%) d(0.14%) C60(50.00%) s(4.47%) p(95.39%) d(0.14%)	32.87
57	BD(1)C5-C60	C5(50.00%) s(34.10%) p(65.83%) d(0.07%) C60(50.00%) s(34.10%) p(65.83%) d(0.07%)	107	LV(1)Cu1	Cu1 s(96.96%) p(0.09%) d(2.95%)	1.63
42	LP(5)Cu1	Cu1 s(0.00%) p(0.04%) d(99.96%)	118	BD*(1)C5-C60	C5(50.00%) s(34.10%) p(65.83%) d(0.07%) C60(50.00%) s(34.10%) p(65.83%) d(0.07%)	0.27

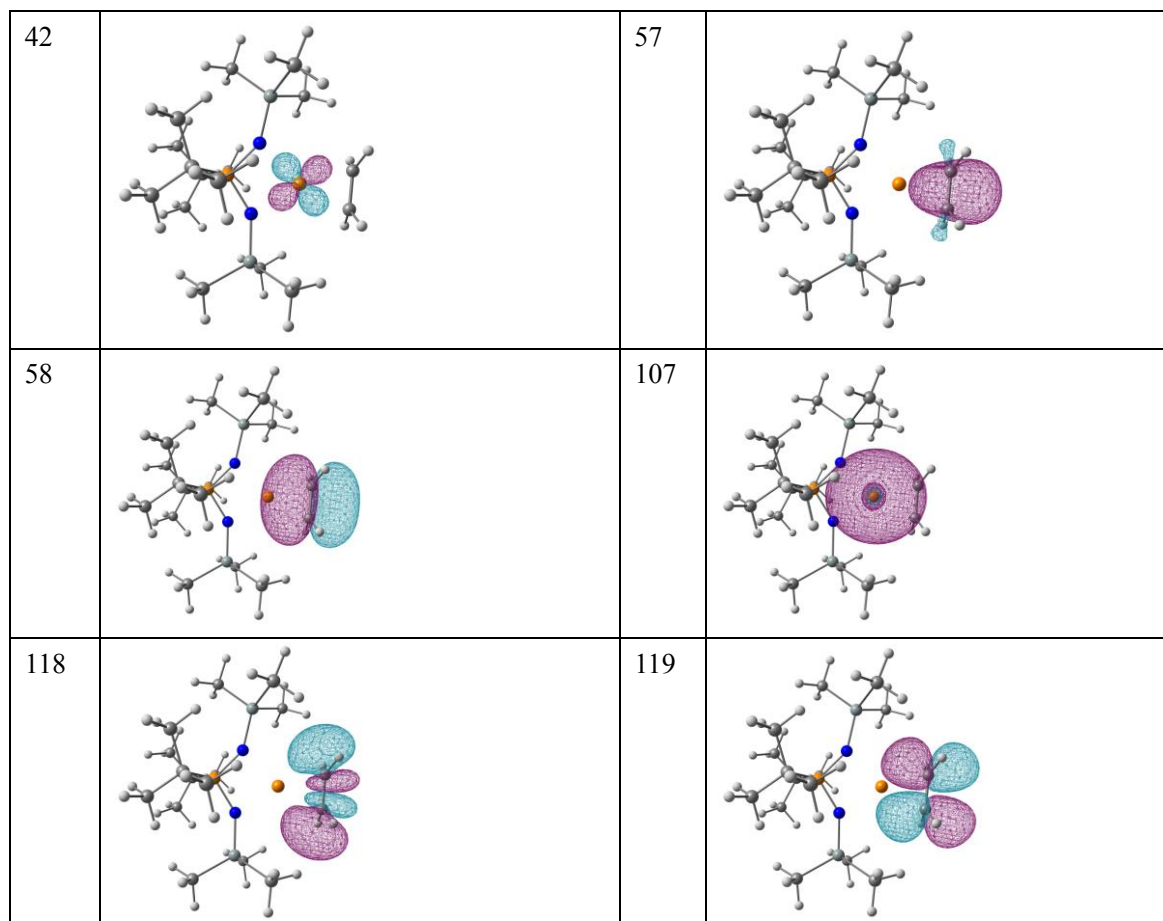


Figure S83. Orbital plots for complex C.

Table S36. Natural bond indices (NBI) corresponding to Cu(ethylene) motif in complex C.

	Cu1	C5	C60
Cu1	-	0.6155	0.6155
C5	0.6155	-	1.2455
C60	0.6155	1.2455	-

Table S37. Wiberg bond indices (WBI) corresponding to Cu(ethylene) motif in complex C.

	Cu1	C5	C60
Cu1	-	0.3789	0.3789
C5	0.3789	-	1.5512
C60	0.3789	1.5512	-

Complex (Tp^{Me2})Cu(ethylene) (complex **K** in Chart S1):

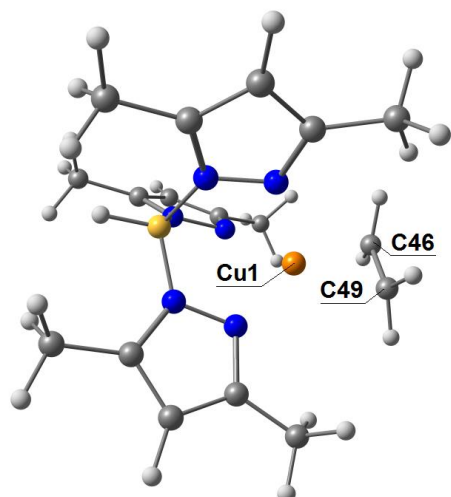


Figure S84. Atom numbering scheme in complex **K** used in NBO analysis.

Table S38. Key interactions in complex **K**.

Donor			Acceptor			E ⁽²⁾ , kcal/mol
#	Orbital	NAO (%contribution)	#	Orbital	NAO (%contribution)	
95	BD(2)C46 -C49	C46(50.11%) s(4.39%) p(95.47%) d(0.14%) C49(49.89%) s(4.38%) p(95.48%) d(0.14%)	98	LV(1)Cu1	Cu1 s(98.51%) p(0.02%) d(1.46%)	64.94
33	LP(5)Cu1	Cu1 s(0.00%) p(0.03%) d(99.97%)	154	BD*(2)C4 6-C49	C46(49.89%) s(4.39%) p(95.47%) d(0.14%) C49(50.11%) s(4.38%) p(95.48%) d(0.14%)	30.59
94	BD(1)C46 -C49	C46(50.02%) s(34.23%) p(65.70%) d(0.07%) C49(49.98%) s(34.23%) p(65.70%) d(0.07%)	98	LV(1)Cu1	Cu1 s(98.51%) p(0.02%) d(1.46%)	1.28
33	LP(5)Cu1	Cu1 s(0.00%) p(0.03%) d(99.97%)	153	BD*(1)C4 6-C49	C46(49.98%) s(34.23%) p(65.70%) d(0.07%) C49(50.02%) s(34.23%) p(65.70%) d(0.07%)	0.18

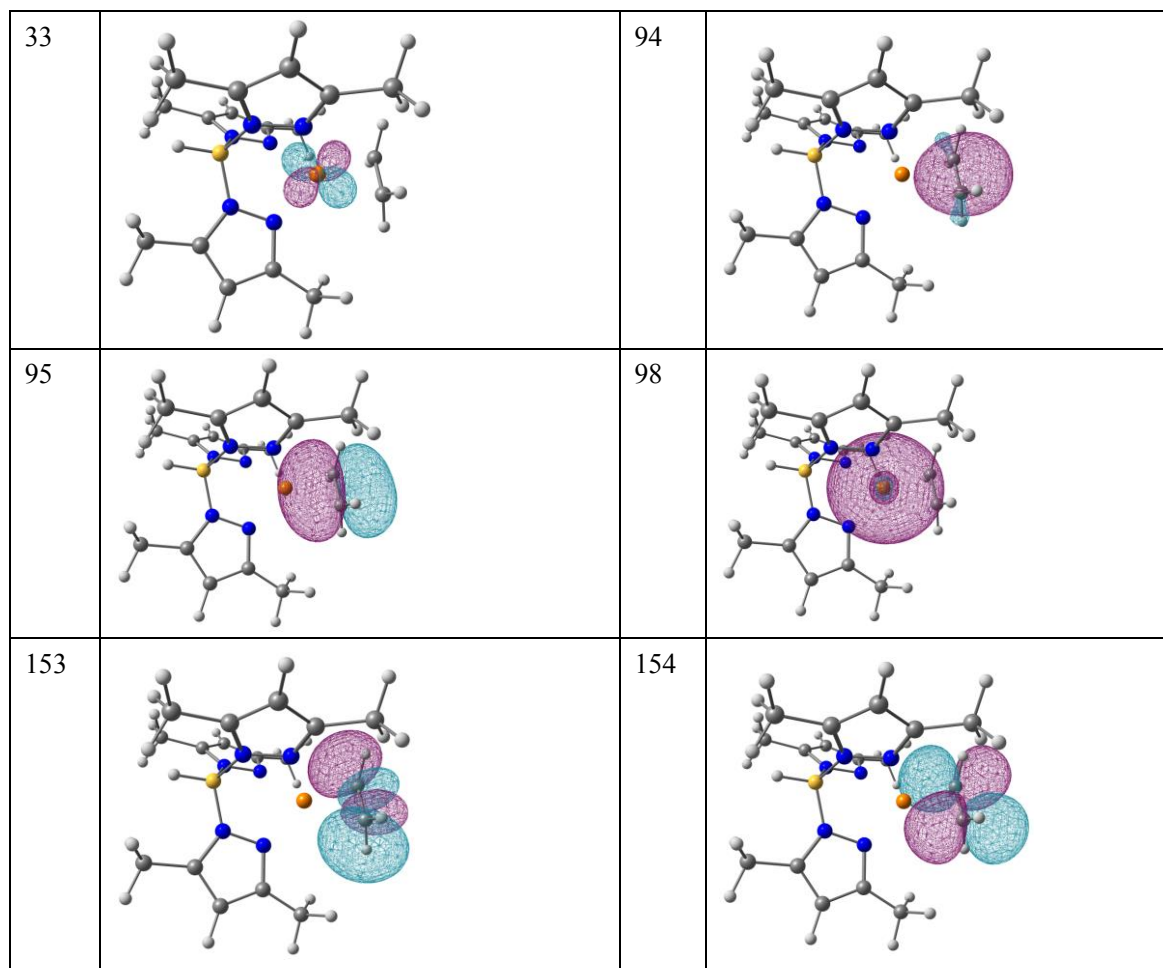


Figure S85. Orbital plots for complex **K**.

Table S39. Natural bond indices (NBI) corresponding to Cu(ethylene) motif in complex **K**.

	Cu1	C46	C49
Cu1	-	0.5895	0.5900
C46	0.5895	-	1.2681
C49	0.5900	1.2681	-

Table S40. Wiberg bond indices (WBI) corresponding to Cu(ethylene) motif in complex **K**.

	Cu1	C46	C49
Cu1	-	0.3475	0.3482
C46	0.3475	-	1.6081
C49	0.3482	1.6081	-

Comparison of bond lengths for geometry-optimized geometries

Among tested functional and basis set combinations, M06L tends to show C-C bonds in ethylene that are in better agreement with experimental X-ray structures and show the same trend in C-C bond length variation upon changing substitution at N4 ligand and ethylene coordination in mono- vs. binuclear complexes.

Table S41. Selected bond distances (Å) comparison in SC XRD structures and DFT-optimized geometries for cationic parts of corresponding complexes in gas phase.

Complex	X-ray	Functional/basis set			
		M06L/SDD(Cu)/6-31++g(d,p)	ω B97XD/SDD(Cu)/6-31++g(d,p)	ω B97XD/def2tzvp	B3LYP/lanl2dz(Cu)/6-31++g(d,p)
4					
C=C	1.371(2), 1.369(3) ^a	1.38511	1.37350	1.36511	1.36401
Cu-C	2.0039(15)- 2.0251(17) ^a	2.01672, 2.01672	2.05764, 2.05763	2.06298, 2.06299	2.14929, 2.14947
Cu-N _{amine}	2.3454(12)- 2.3858(13) ^a	2.41116, 2.41115	2.40590, 2.40588	2.41362, 2.41409	2.41250, 2.41268
Cu-N _{py}	2.0057(12)- 2.0334(12) ^a	2.09181, 2.09181	2.09801, 2.09803	2.09630, 2.09675	2.12111, 2.12086
Complex	X-ray	Functional/basis set			
5		M06L/SDD(Cu)/6-31++g(d,p)	ω B97XD/SDD(Cu)/6-31++g(d,p)	ω B97XD/def2tzvp	B3LYP/lanl2dz(Cu)/6-31++g(d,p)
C=C	1.359(7)	1.38511	1.37324	1.36482	1.36424
Cu-C	2.033(4)	2.01481, 2.01480	2.05403, 2.05402	2.05859, 2.05859	2.14224, 2.14224
Cu-N _{amine}	2.389(3)	2.43393, 2.43336	2.42439, 2.42437	2.43111, 2.43246	2.45355, 2.45359
Cu-N _{py}	2.0035(8)	2.09046, 2.09046	2.09865, 2.09866	2.09786, 2.09786	2.12114, 2.12115
Complex	X-ray	Functional/basis set			
6		M06L/SDD(Cu)/6-31++g(d,p)	ω B97XD/SDD(Cu)/6-31++g(d,p)	ω B97XD/def2tzvp	B3LYP/lanl2dz(Cu)/6-31++g(d,p)
C=C	1.382(3)	1.39091	1.37833	1.36998	1.36816
Cu-C	2.0197(11)	1.99985, 1.99985	2.03194, 2.03194	2.03667, 2.03667	2.11928, 2.11928
Cu-N _{amine}	2.5119(8)	2.53877, 2.53876	2.55773, 2.55774	2.56012, 2.56004	2.59499, 2.59498
Cu-N _{py}	2.0035(8)	2.04514, 2.04514	2.03921, 2.03921	2.03940, 2.03938	2.06906, 2.06904
Complex	X-ray	Functional/basis set			
7		M06L/SDD(Cu)/6-31++g(d,p)	ω B97XD/SDD(Cu)/6-31++g(d,p)	ω B97XD/def2tzvp	B3LYP/lanl2dz(Cu)/6-31++g(d,p)
C=C	1.444(8)	1.43699	1.40978	1.40081	1.39284
Cu-C	2.0907(15)	2.07096, 2.07096;	2.10779, 2.10779;	2.11567, 2.11567;	2.21560, 2.21560;

		2.07096, 2.07096	2.10779, 2.10779	2.11567, 2.11567	2.21560, 2.21560
Cu-N _{amine}	2.361(4)	2.40769, 2.40772; 2.40772, 2.40768	2.39888, 2.39887; 2.39887, 2.39888	2.40805, 2.40800; 2.40800, 2.40805	2.40423, 2.40412; 2.40410, 2.40425
Cu-N _{py}	2.063(2)	2.09246, 2.09246; 2.09246, 2.09246	2.09094, 2.09094; 2.09094, 2.09094	2.09389, 2.09389; 2.09389, 2.09389	2.11484, 2.11484; 2.11484, 2.11484

^aFor two independent molecules in a unit cell.

Cartesian coordinates for gas-phase optimized ethylene complexes and free ethylene using M06L/sdd/6-31++g(d,p)

Ethylene

C	0.000000	0.665100	0.000000
H	0.923600	1.237800	0.000000
H	-0.923600	1.237800	0.000000
C	-0.000000	-0.665100	0.000000
H	-0.923600	-1.237800	0.000000
H	0.923600	-1.237800	0.000000

[(^HN₄)Cu(ethylene)]⁺

Cu	1.512200	-0.000000	-0.000000
C	3.406200	-0.000100	-0.692600
H	3.552100	-0.920600	-1.254300
H	3.552100	0.920100	-1.254600
C	3.406300	0.000100	0.692500
H	3.552100	0.920600	1.254200
H	3.552100	-0.920100	1.254500
N	-0.070700	-0.000200	-1.367500
N	0.788500	2.300000	-0.000400
H	1.537400	2.981400	-0.000600
N	0.788500	-2.300000	0.000400
H	1.537300	-2.981400	0.000500
N	-0.070700	0.000200	1.367600
C	-0.704700	-1.162100	-1.610100
C	-0.704600	1.162100	1.610100
C	-0.704600	1.161500	-1.610500
C	0.023100	2.430700	-1.240400
H	0.738400	2.669300	-2.037400

H	-0.700800	3.260500	-1.208600
C	-1.976100	-1.197700	-2.177200
H	-2.459100	-2.153300	-2.359000
C	-1.976000	1.197000	-2.177600
H	-2.459100	2.152500	-2.359700
C	-1.976000	1.197700	2.177200
H	-2.459100	2.153300	2.359000
C	-2.614700	0.000500	2.480700
H	-3.608500	0.000600	2.917500
C	-0.704600	-1.161500	1.610500
C	-1.976000	-1.196900	2.177600
H	-2.459100	-2.152400	2.359700
C	0.023200	2.431100	1.239600
H	-0.700700	3.260900	1.207500
H	0.738500	2.669900	2.036400
C	0.023100	-2.431100	-1.239500
H	-0.700900	-3.260900	-1.207500
H	0.738300	-2.670000	-2.036400
C	0.023100	-2.430700	1.240400
H	0.738400	-2.669200	2.037400
H	-0.700800	-3.260500	1.208700
C	-2.614700	-0.000400	-2.480700
H	-3.608500	-0.000500	-2.917500

$[(^{\text{Me}}\text{N}_4)\text{Cu}(\text{ethylene})]^+$

Cu	0.042100	1.357800	0.000000
H	-0.812600	3.423600	1.254500
C	0.102700	3.248800	0.692600
H	1.027300	3.364500	-1.254600
C	0.102800	3.248800	-0.692600
H	1.027200	3.364500	1.254700
H	-0.812500	3.423600	-1.254600
N	-0.007800	-0.238700	1.348700
N	-2.311200	0.738800	0.000000
C	-2.426800	-0.055800	1.228700
H	-3.302900	-0.726700	1.206300
H	-2.601400	0.654200	2.047600

C	-1.189300	-0.850900	1.551100
C	-1.265600	-2.150400	2.045300
H	-2.236100	-2.612900	2.199000
C	-0.088800	-2.841800	2.312300
H	-0.120400	-3.858100	2.692900
C	-3.297100	1.819300	0.000000
H	-4.335700	1.452800	0.000000
H	-3.157100	2.443100	0.886700
N	2.352800	0.593300	-0.000000
C	2.418100	-0.206400	1.229200
H	3.250500	-0.930800	1.207800
H	2.636500	0.491900	2.047600
C	1.133400	-0.922700	1.552000
C	1.128700	-2.224500	2.046200
H	2.068600	-2.746300	2.200700
C	3.405400	1.609000	-0.000000
H	4.418500	1.177000	-0.000000
H	3.305400	2.240300	0.886600
N	-0.007800	-0.238600	-1.348700
C	-2.426800	-0.055700	-1.228700
H	-3.302900	-0.726600	-1.206400
H	-2.601400	0.654200	-2.047600
C	-1.189300	-0.850800	-1.551100
C	-1.265600	-2.150400	-2.045300
H	-2.236100	-2.612900	-2.199000
C	-0.088800	-2.841800	-2.312400
H	-0.120500	-3.858100	-2.692900
H	-3.157100	2.443100	-0.886600
C	2.418100	-0.206400	-1.229200
H	3.250500	-0.930800	-1.207800
H	2.636500	0.491800	-2.047600
C	1.133400	-0.922700	-1.552000
C	1.128700	-2.224500	-2.046300
H	2.068500	-2.746300	-2.200700
H	3.305400	2.240300	-0.886700

$[(^t\text{BuN}_4)\text{Cu}(\text{ethylene})]^+$

Cu	-0.000000	-0.000000	0.935600
C	-0.103900	0.687600	2.810600
H	-1.096000	1.105000	2.971100
H	0.718800	1.382200	2.971700
C	0.103900	-0.687700	2.810600
H	1.096000	-1.105100	2.971100
H	-0.718800	-1.382200	2.971700
N	-0.142700	1.394800	-0.553300
N	2.350600	0.350800	0.042900
C	2.211100	1.805600	-0.123600
H	3.044600	2.262800	-0.684300
H	2.224100	2.258200	0.874800
C	0.922800	2.174300	-0.816800
C	0.844300	3.213500	-1.739100
H	1.715700	3.829900	-1.938700
C	-0.359900	3.430200	-2.404100
H	-0.457300	4.250100	-3.109300
C	-1.415700	2.548500	-2.200700
H	-2.341500	2.644900	-2.761000
C	-1.263500	1.508900	-1.284200
C	-2.268600	0.377800	-1.227600
H	-3.245600	0.755500	-1.555100
H	-1.963900	-0.318500	-2.021100
C	3.548900	-0.064400	0.860600
C	4.871700	0.319200	0.190100
H	4.993100	-0.131900	-0.799300
H	5.711400	-0.024900	0.800300
H	4.974500	1.403700	0.085200
C	3.470200	-1.579800	1.043800
H	2.488300	-1.874800	1.430200
H	4.232000	-1.911600	1.753700
H	3.644700	-2.127400	0.112700
C	3.494300	0.594000	2.236500
H	3.658500	1.674400	2.199700
H	4.287300	0.180300	2.864600
H	2.543600	0.401500	2.737900
N	0.142700	-1.394800	-0.553300

N	-2.350600	-0.350800	0.042900
C	-2.211100	-1.805600	-0.123600
H	-3.044600	-2.262800	-0.684400
H	-2.224200	-2.258200	0.874800
C	-0.922800	-2.174300	-0.816800
C	-0.844300	-3.213500	-1.739100
H	-1.715700	-3.829900	-1.938700
C	0.359900	-3.430200	-2.404100
H	0.457300	-4.250100	-3.109300
C	1.415700	-2.548500	-2.200700
H	2.341500	-2.644900	-2.761000
C	1.263500	-1.508900	-1.284200
C	2.268600	-0.377800	-1.227600
H	3.245600	-0.755500	-1.555100
H	1.963900	0.318500	-2.021100
C	-3.548900	0.064400	0.860600
C	-4.871700	-0.319200	0.190100
H	-4.993100	0.131900	-0.799300
H	-5.711400	0.024900	0.800300
H	-4.974500	-1.403700	0.085200
C	-3.470200	1.579800	1.043800
H	-2.488300	1.874800	1.430200
H	-4.232000	1.911600	1.753700
H	-3.644700	2.127400	0.112700
C	-3.494300	-0.594000	2.236500
H	-3.658500	-1.674400	2.199700
H	-4.287300	-0.180200	2.864600
H	-2.543600	-0.401500	2.737900

$[(^1\text{H}^1\text{N})_2\text{Cu}_2(\text{ethylene})]^{2+}$

Cu	-1.942300	0.000000	-0.000000
C	-0.000000	0.000000	-0.718500
H	-0.000000	-0.924900	-1.292000
H	0.000000	0.924900	-1.292000
C	-0.000000	0.000000	0.718500
H	-0.000000	-0.924900	1.292000
H	0.000000	0.924900	1.292000

Cu	1.942300	-0.000100	-0.000000
N	-3.520300	0.000000	1.374200
N	-2.654400	2.300000	-0.000000
H	-1.940100	3.018600	-0.000000
N	-2.654300	-2.300000	-0.000000
H	-1.940000	-3.018500	-0.000000
C	-3.429700	2.429600	1.240300
H	-4.152200	3.258900	1.199800
H	-2.719300	2.672500	2.040700
C	-4.158800	1.161400	1.607400
C	-5.435400	1.197500	2.162000
H	-5.921600	2.152300	2.338600
C	-6.076100	-0.000000	2.461300
H	-7.073200	-0.000100	2.890400
C	-5.435300	-1.197500	2.162000
H	-5.921500	-2.152400	2.338600
C	-4.158700	-1.161400	1.607400
C	-3.429600	-2.429600	1.240300
H	-2.719200	-2.672500	2.040700
H	-4.152100	-3.258900	1.199800
N	-3.520300	0.000000	-1.374200
C	-3.429700	2.429600	-1.240300
H	-4.152200	3.258900	-1.199800
H	-2.719300	2.672500	-2.040700
C	-4.158800	1.161400	-1.607400
C	-5.435400	1.197500	-2.162000
H	-5.921600	2.152300	-2.338600
C	-6.076100	-0.000000	-2.461300
H	-7.073200	-0.000100	-2.890400
C	-5.435300	-1.197500	-2.162000
H	-5.921500	-2.152400	-2.338600
C	-4.158700	-1.161400	-1.607400
C	-3.429600	-2.429600	-1.240300
H	-2.719200	-2.672500	-2.040700
H	-4.152100	-3.258900	-1.199800
N	3.520300	-0.000000	1.374200
N	2.654400	-2.300000	-0.000000

H	1.940100	-3.018600	-0.000000
N	2.654300	2.300000	-0.000000
H	1.939900	3.018500	-0.000000
C	3.429700	-2.429600	1.240300
H	4.152200	-3.258900	1.199800
H	2.719300	-2.672500	2.040700
C	4.158800	-1.161400	1.607400
C	5.435400	-1.197500	2.162000
H	5.921600	-2.152300	2.338600
C	6.076100	0.000000	2.461300
H	7.073200	0.000100	2.890400
C	5.435300	1.197500	2.162000
H	5.921500	2.152400	2.338600
C	4.158700	1.161400	1.607400
C	3.429600	2.429600	1.240300
H	2.719200	2.672500	2.040700
H	4.152100	3.258900	1.199800
N	3.520300	-0.000000	-1.374200
C	3.429700	-2.429600	-1.240300
H	4.152200	-3.258900	-1.199800
H	2.719300	-2.672500	-2.040700
C	4.158800	-1.161400	-1.607300
C	5.435400	-1.197500	-2.162000
H	5.921600	-2.152300	-2.338600
C	6.076100	0.000100	-2.461300
H	7.073200	0.000100	-2.890400
C	5.435300	1.197500	-2.162000
H	5.921500	2.152400	-2.338600
C	4.158700	1.161400	-1.607400
C	3.429600	2.429600	-1.240300
H	2.719200	2.672500	-2.040700
H	4.152100	3.258900	-1.199800

[bpyCu(ethylene)]⁺ (complex E, Chart S1)

Cu	-0.000100	-1.488600	-0.000000
C	0.694900	-3.349100	-0.000100
C	-0.695100	-3.349000	0.000100

H	1.252600	-3.498900	0.922800
H	1.252400	-3.498900	-0.923000
H	-1.252800	-3.498800	-0.922800
H	-1.252600	-3.498800	0.923100
C	0.738300	1.255800	0.000000
C	1.508400	2.418300	0.000100
C	2.895300	2.318500	0.000100
C	3.485400	1.058900	0.000000
C	2.658800	-0.057600	-0.000000
C	-0.738300	1.255900	-0.000000
C	-1.508300	2.418400	-0.000100
C	-2.895200	2.318600	-0.000100
C	-3.485300	1.059100	0.000000
C	-2.658800	-0.057500	0.000000
N	1.321700	0.032500	-0.000000
N	-1.321700	0.032600	0.000000
H	3.069500	-1.063300	-0.000100
H	4.562500	0.936800	-0.000000
H	3.506000	3.215600	0.000100
H	-3.505800	3.215800	-0.000100
H	-4.562400	0.937000	0.000000
H	-3.069600	-1.063100	0.000100
H	1.035200	3.393800	0.000100
H	-1.035000	3.393800	-0.000100

[(phen)Cu(ethylene)]⁺ (complex F, Chart S1)

Cu	1.851900	-0.000000	-0.000000
C	3.714900	0.694700	-0.000100
C	3.714900	-0.694700	0.000100
H	3.863000	1.252700	0.922800
H	3.863000	1.252500	-0.923000
H	3.863000	-1.252700	-0.922700
H	3.862900	-1.252500	0.923100
C	-0.872500	0.716500	-0.000000
C	-2.098800	1.419500	0.000000
C	-2.033300	2.828200	0.000000
C	-0.803500	3.453700	0.000000

C	0.361600	2.673500	-0.000000
C	-0.872500	-0.716500	-0.000000
C	-2.098800	-1.419500	-0.000000
C	-2.033300	-2.828200	0.000000
C	-0.803500	-3.453700	-0.000000
C	0.361600	-2.673500	-0.000000
C	-3.323800	0.682000	0.000000
C	-3.323800	-0.682000	0.000000
N	0.334800	1.342700	-0.000000
N	0.334800	-1.342700	-0.000000
H	1.344500	3.136900	-0.000000
H	-0.721900	4.534700	0.000000
H	-2.952200	3.408200	0.000000
H	-4.260100	1.232300	0.000000
H	-4.260100	-1.232300	0.000000
H	-2.952200	-3.408200	0.000000
H	-0.721900	-4.534700	0.000000
H	1.344500	-3.136900	-0.000000

[(tmen)Cu(ethylene)]⁺ (complex P, Chart S1)

Cu	0.000000	0.786800	0.000000
C	0.695700	2.645700	0.023500
C	-0.695500	2.645800	-0.023500
H	1.222800	2.799600	0.963700
H	1.284600	2.801300	-0.879200
H	-1.222500	2.799800	-0.963800
H	-1.284300	2.801500	0.879200
N	-1.431300	-0.703800	-0.004300
N	1.431300	-0.703900	0.004300
C	-0.676500	-1.939000	-0.339700
C	0.676300	-1.939000	0.339800
C	-2.520200	-0.495600	-0.977600
C	2.008500	-0.798000	-1.352600
C	2.520200	-0.495800	0.977500
C	-2.008600	-0.797800	1.352600
H	-1.250500	-2.832800	-0.057900
H	-0.560900	-1.966600	-1.428300

H	1.250200	-2.832900	0.058000
H	0.560700	-1.966600	1.428300
H	-2.103100	-0.383100	-1.981000
H	-3.220200	-1.341700	-0.976600
H	-3.069500	0.412000	-0.719900
H	2.710300	-1.639900	-1.423300
H	1.220600	-0.934600	-2.096900
H	2.543600	0.125300	-1.583200
H	3.069500	0.411700	0.719900
H	2.103100	-0.383200	1.981000
H	3.220100	-1.341900	0.976600
H	-2.543600	0.125600	1.583100
H	-2.710500	-1.639600	1.423300
H	-1.220700	-0.934500	2.096900

(nacnac)Cu(ethylene) (complex B, Chart S1)

Cu	0.000000	-0.673300	0.039700
C	0.698200	-2.525800	0.153100
C	-0.698300	-2.525800	0.153100
H	1.263100	-2.622500	1.079300
H	-1.263200	-2.622400	1.079300
H	-1.263400	-2.732900	-0.754800
H	1.263400	-2.733000	-0.754800
N	-1.455700	0.605900	-0.040000
C	0.000000	2.528200	-0.173300
H	0.000000	3.610100	-0.250900
C	2.770900	0.075600	-0.001500
N	1.455700	0.605900	-0.040000
C	-3.398800	-0.127000	1.240700
C	4.663600	-0.719600	1.263300
H	5.155100	-0.876600	2.221600
C	-2.770900	0.075600	-0.001500
C	1.267600	1.921600	-0.132100
C	3.398800	-0.127000	1.240700
C	2.695400	0.268800	2.501600
H	3.282500	0.007000	3.385300
H	1.715800	-0.221600	2.578100

H	2.487400	1.344700	2.539500
C	2.470600	2.823400	-0.201500
H	3.108400	2.699900	0.680800
H	2.179600	3.872100	-0.275200
H	3.098900	2.574500	-1.064000
C	-1.267600	1.921600	-0.132100
C	4.650200	-0.921900	-1.136500
H	5.131200	-1.237200	-2.060600
C	-2.470600	2.823400	-0.201400
H	-3.098900	2.574500	-1.064000
H	-2.179600	3.872100	-0.275200
H	-3.108400	2.699900	0.680800
C	5.292300	-1.111800	0.084400
H	6.276000	-1.571600	0.117700
C	-3.385300	-0.332300	-1.199100
C	-2.667400	-0.151200	-2.500200
H	-3.248200	-0.549100	-3.336000
H	-1.691100	-0.654600	-2.486000
H	-2.449500	0.903000	-2.708900
C	3.385300	-0.332400	-1.199100
C	-4.663600	-0.719600	1.263300
H	-5.155000	-0.876700	2.221600
C	2.667300	-0.151200	-2.500200
H	1.691100	-0.654700	-2.485900
H	3.248200	-0.549300	-3.336000
H	2.449500	0.902900	-2.709000
C	-4.650300	-0.921800	-1.136500
H	-5.131300	-1.237100	-2.060600
C	-5.292300	-1.111800	0.084400
H	-6.276000	-1.571600	0.117700
C	-2.695300	0.268700	2.501600
H	-3.282400	0.006900	3.385400
H	-2.487400	1.344700	2.539600
H	-1.715700	-0.221700	2.578100

(NPN)Cu(ethylene) (complex C, Chart S1)

Cu	-0.000000	1.772200	-0.000000
----	-----------	----------	-----------

C	0.694700	3.617000	0.075300
H	1.147500	3.773000	1.052500
H	1.350900	3.784900	-0.777300
C	-0.694700	3.617000	-0.075300
H	-1.147500	3.773000	-1.052500
H	-1.350900	3.784900	0.777300
P	0.000000	-0.808700	-0.000000
Si	-2.975000	0.371100	-0.019900
N	-1.266100	0.192900	-0.048400
C	-0.068800	-1.866700	1.552600
C	-1.469400	-2.437800	1.777100
H	-1.782600	-3.125400	0.986800
H	-2.217900	-1.644300	1.854400
H	-1.485300	-2.996400	2.721300
C	0.254000	-0.915400	2.711100
H	0.125600	-1.444900	3.662800
H	-0.414000	-0.046200	2.714200
H	1.282800	-0.547600	2.657700
C	0.949400	-3.005800	1.541900
H	1.961000	-2.655100	1.318900
H	0.691100	-3.787600	0.820400
H	0.978100	-3.478500	2.531700
C	-3.461200	1.745700	-1.211000
H	-3.214300	2.736400	-0.817700
H	-4.540000	1.735100	-1.402400
H	-2.952500	1.638400	-2.175300
C	-3.551900	0.887200	1.698100
H	-3.421000	0.098300	2.446600
H	-4.611700	1.166300	1.700700
H	-2.982600	1.756500	2.046900
C	-3.955200	-1.150400	-0.548700
H	-3.785200	-1.395000	-1.603200
H	-5.026200	-0.942900	-0.439600
H	-3.739600	-2.046200	0.041600
Si	2.975000	0.371100	0.019900
N	1.266100	0.192900	0.048400
C	0.068800	-1.866700	-1.552600

C	1.469400	-2.437800	-1.777100
H	1.782600	-3.125400	-0.986800
H	2.217900	-1.644300	-1.854400
H	1.485300	-2.996400	-2.721200
C	-0.254000	-0.915400	-2.711100
H	-0.125600	-1.445000	-3.662800
H	0.414000	-0.046200	-2.714200
H	-1.282800	-0.547600	-2.657700
C	-0.949400	-3.005800	-1.541900
H	-1.961000	-2.655100	-1.318900
H	-0.691100	-3.787600	-0.820400
H	-0.978000	-3.478500	-2.531700
C	3.461100	1.745700	1.211000
H	3.214300	2.736400	0.817700
H	4.539900	1.735100	1.402400
H	2.952500	1.638400	2.175300
C	3.551900	0.887200	-1.698100
H	3.421000	0.098300	-2.446600
H	4.611700	1.166300	-1.700700
H	2.982600	1.756500	-2.046900
C	3.955200	-1.150400	0.548700
H	3.785200	-1.395000	1.603200
H	5.026200	-0.942900	0.439600
H	3.739600	-2.046200	-0.041600

(TpMe₂)Cu(ethylene) (complex K, Chart S1)

Cu	-1.578800	-0.035300	0.087500
C	-3.391900	0.433500	-0.622000
H	-3.898600	1.098400	0.074000
H	-3.230900	0.834500	-1.621300
C	-3.310800	-0.930400	-0.364300
H	-3.080600	-1.643800	-1.153800
H	-3.754400	-1.350000	0.535800
N	-0.489100	1.614000	0.524800
N	0.868400	1.468500	0.494500
N	-0.359800	-1.245200	1.166600
N	0.978300	-0.986600	1.083700

N	-0.167500	-0.368700	-1.694600
N	1.143300	-0.262500	-1.329700
C	-0.743700	2.889800	0.841500
C	0.462900	3.579800	1.018400
C	1.466500	2.647900	0.788700
C	-2.138700	3.391600	0.954800
C	2.942300	2.815000	0.831500
C	-0.514200	-2.257100	2.029800
C	0.738600	-2.660000	2.511100
C	1.664400	-1.832900	1.888500
C	-1.861900	-2.796400	2.352100
C	3.144500	-1.801700	2.015900
C	-0.175600	-0.723400	-2.983000
C	1.140900	-0.848900	-3.460700
C	1.955400	-0.549700	-2.379800
C	-1.457200	-0.942400	-3.706500
C	3.438800	-0.520800	-2.287300
B	1.507000	0.107300	0.121300
H	2.696400	0.185900	0.231700
H	0.592900	4.620100	1.282800
H	-2.626000	3.454000	-0.024600
H	-2.749500	2.732200	1.579600
H	-2.156900	4.389300	1.398400
H	3.193500	3.839900	1.111500
H	3.409700	2.140700	1.556200
H	3.404700	2.607400	-0.139000
H	0.947800	-3.447300	3.222000
H	-1.809200	-3.495900	3.188900
H	-2.297900	-3.329100	1.499700
H	-2.557200	-1.995800	2.624400
H	3.473500	-2.557100	2.732200
H	3.504300	-0.827100	2.361300
H	3.641800	-2.002600	1.061400
H	1.462400	-1.117100	-4.458200
H	-2.300500	-0.564700	-3.122600
H	-1.464700	-0.434400	-4.675600
H	-1.637900	-2.005700	-3.901000

H	3.814200	0.466800	-1.999600
H	3.817100	-1.231000	-1.544300
H	3.878700	-0.779500	-3.252500

References

1. B. Ke, L. Ma, T. Kang, W. He, X. Gou, D. Gong, L. Du and M. Li, *Anal. Chem.*, 2018, **90**, 4946-4950.
2. F. Bottino, M. Digrazia, P. Finocchiaro, F. R. Fronczek, A. Mamo and S. Pappalardo, *J. Org. Chem.*, 1988, **53**, 3521-3529.
3. H. M. Johnston, K. Pota, M. M. Barnett, O. Kinsinger, P. Braden, T. M. Schwartz, E. Hoffer, N. Sadagopan, N. Nguyen, Y. Yu, P. Gonzalez, G. Tircso, H. Wu, G. Akkaraju, M. J. Chumley and K. N. Green, *Inorg Chem*, 2019, **58**, 16771-16784.
4. C.-M. Che, Z.-Y. Li, K.-Y. Wong, C.-K. Poon, T. C. W. Mak and S.-M. Peng, *Polyhedron*, 1994, **13**, 771-776.
5. L. Ai, J. Xiao, X. Shen and C. Zhang, *Tetrahedron Lett.*, 2006, **47**, 2371-2375.
6. M. Fianchini, C. F. Campana, B. Chilukuri, T. R. Cundari, V. Petricek and H. V. R. Dias, *Organometallics*, 2013, **32**, 3034-3041.
7. X. Dai and T. H. Warren, *Chem. Commun.*, 2001, 1998-1999.
8. B. F. Straub, F. Eisenträger and P. Hofmann, *Chem. Commun.*, 1999, 2507-2508.
9. J. S. Thompson and J. F. Whitney, *Inorg. Chem.*, 1984, **23**, 2813-2819.
10. H. Masuda, N. Yamamoto, T. Taga, K. Machida, S. Kitagawa and M. Munakata, *J Organomet Chem*, 1987, **322**, 121-129.
11. M. Munakata, S. Kitagawa, S. Kosome and A. Asahara, *Inorg. Chem.*, 1986, **25**, 2622-2627.
12. P. Ebrahimpour, M. F. Haddow and D. F. Wass, *Inorg. Chem.*, 2013, **52**, 3765-3771.
13. K. Klimovica, K. Kirschbaum and O. Daugulis, *Organometallics*, 2016, **35**, 2938-2943.
14. H. V. R. Dias, X. Wang and H. V. K. Diyabalanage, *Inorg. Chem.*, 2005, **44**, 7322-7324.
15. R. M. Sullivan, H. Liu, D. S. Smith, J. C. Hanson, D. Osterhout, M. Ciruolo, C. P. Grey and J. D. Martin, *J. Am. Chem. Soc.*, 2003, **125**, 11065-11079.
16. J. S. Thompson, R. L. Harlow and J. F. Whitney, *J. Am. Chem. Soc.*, 1983, **105**, 3522-3527.
17. G. Santiso-Quiñones, A. Reisinger, J. Slattery and I. Krossing, *Chem. Commun.*, 2007, 5046-5048.
18. H. V. R. Dias, H.-L. Lu, H.-J. Kim, S. A. Polach, T. K. H. H. Goh, R. G. Browning and C. J. Lovely, *Organometallics*, 2002, **21**, 1466-1473.
19. J. Dai, M. Yamamoto, T. Kuroda-Sowa, M. Maekawa, Y. Suenaga and M. Munakata, *Inorg. Chem.*, 1997, **36**, 2688-2690.
20. V. A. K. Adiraju, J. A. Flores, M. Yousufuddin and H. V. R. Dias, *Organometallics*, 2012, **31**, 7926-7932.
21. Y. Suenaga, L. Ping Wu, T. Kuroda-sowa, M. Munakata and M. Maekawa, *Polyhedron*, 1997, **16**, 67-70.
22. G. Sheldrick, *Acta Crystallogr., Sect. A*, 2015, **71**, 3-8.
23. G. Sheldrick, *Acta Crystallogr., Sect. C*, 2015, **71**, 3-8.
24. L. J. Farrugia, *J. Appl. Crystallogr.*, 2012, **45**, 849-854.
25. Gaussian 16, Revision C.01, M. J. Frisch, G. W. Trucks, H. B. Schlegel, G. E. Scuseria, M. A. Robb, J. R. Cheeseman, G. Scalmani, V. Barone, G. A. Petersson, H. Nakatsuji, X. Li, M. Caricato, A. V. Marenich, J. Bloino, B. G. Janesko, R. Gomperts, B. Mennucci, H. P. Hratchian, J. V. Ortiz, A. F. Izmaylov, J. L. Sonnenberg, D. Williams-Young, F. Ding,

- F. Lipparini, F. Egidi, J. Goings, B. Peng, A. Petrone, T. Henderson, D. Ranasinghe, V. G. Zakrzewski, J. Gao, N. Rega, G. Zheng, W. Liang, M. Hada, M. Ehara, K. Toyota, R. Fukuda, J. Hasegawa, M. Ishida, T. Nakajima, Y. Honda, O. Kitao, H. Nakai, T. Vreven, K. Throssell, J. A. Montgomery, Jr., J. E. Peralta, F. Ogliaro, M. J. Bearpark, J. J. Heyd, E. N. Brothers, K. N. Kudin, V. N. Staroverov, T. A. Keith, R. Kobayashi, J. Normand, K. Raghavachari, A. P. Rendell, J. C. Burant, S. S. Iyengar, J. Tomasi, M. Cossi, J. M. Millam, M. Klene, C. Adamo, R. Cammi, J. W. Ochterski, R. L. Martin, K. Morokuma, O. Farkas, J. B. Foresman, and D. J. Fox, Gaussian, Inc., Wallingford CT, 2019.
26. Y. Zhao and D. G. Truhlar, *J. Chem. Phys.*, 2006, **125**, 194101.
 27. J.-D. Chai and M. Head-Gordon, *PCCP*, 2008, **10**, 6615-6620.
 28. D. Andrae, U. Haeussermann, M. Dolg, H. Stoll and H. Preuss, *Theor. Chim. Acta*, 1990, **77**, 123-141.
 29. P. C. Hariharan and J. A. Pople, *Mol. Phys.*, 1974, **27**, 209-214.
 30. P. C. Hariharan and J. A. Pople, *Theor. Chim. Acta*, 1973, **28**, 213-222.
 31. W. J. Hehre, R. Ditchfield and J. A. Pople, *J. Chem. Phys.*, 1972, **56**, 2257-2261.
 32. M. M. Francl, W. J. Pietro, W. J. Hehre, J. S. Binkley, M. S. Gordon, D. J. DeFrees and J. A. Pople, *J. Chem. Phys.*, 1982, **77**, 3654-3665.
 33. B. P. Pritchard, D. Altarawy, B. Didier, T. D. Gibson and T. L. Windus, *J. Chem. Inf. Model.*, 2019, **59**, 4814-4820.
 34. D. Feller, *J. Comput. Chem.*, 1996, **17**, 1571-1586.
 35. K. L. Schuchardt, B. T. Didier, T. Elsethagen, L. Sun, V. Gurumoorthi, J. Chase, J. Li and T. L. Windus, 2007, **47**, 1045-1052.
 36. P. J. Hay and W. R. Wadt, *J. Chem. Phys.*, 1985, **82**, 299-310.
 37. F. Weigend and R. Ahlrichs, *PCCP*, 2005, **7**, 3297-3305.
 38. AIMAll (Version 19.10.12), Todd A. Keith, TK Gristmill Software, Overland Park KS, USA, 2019 (aim.tkgristmill.com).
 39. R. F. W. Bader, *Chem. Rev.*, 1991, **91**, 893-928.
 40. C. Lepetit, P. Fau, K. Fajerweg, M. L. Kahn and B. Silvi, *Coord. Chem. Rev.*, 2017, **345**, 150-181.
 41. R. Bianchi, G. Gervasio and D. Marabello, *Inorg. Chem.*, 2000, **39**, 2360-2366.
 42. P. R. Varadwaj, A. Varadwaj and H. M. Marques, *J. Phys. Chem. A*, 2011, **115**, 5592-5601.
 43. P. R. Varadwaj, I. Cukrowski and H. M. Marques, *J. Phys. Chem. A*, 2008, **112**, 10657-10666.
 44. P. Macchi, D. M. Proserpio and A. Sironi, *J. Am. Chem. Soc.*, 1998, **120**, 13429-13435.
 45. G. Gervasio, R. Bianchi and D. Marabello, *Chem. Phys. Lett.*, 2004, **387**, 481-484.
 46. NBO 7.0. E. D. Glendening, J. K. Badenhoop, A. E. Reed, J. E. Carpenter, J. A. Bohmann, C. M. Morales, P. Karafiloglou, C. R. Landis, and F. Weinhold, Theoretical Chemistry Institute, University of Wisconsin, Madison, WI (2018).
 47. Chemcraft - graphical software for visualization of quantum chemistry computations. <https://www.chemcraftprog.com>.